République Algérienne Démocratique et Populaire

Ministère de l'Enseignement Supérieur et de la Recherche Scientifique

Université de Yahia FARES Médéa

Faculté de Technologie

Département de Génie des Procédés et de l'Environnement

Laboratoire des biomatériaux et des phénomènes de transport



Thèse Doctorat en Sciences

Étudiée par: Mr. Lakhdar ABOUDA

Spécialité: Génie des procédés

CONTRIBUTION A LA MODELISATION FRACTIONNELLE DE LA FILTRATION

Soutenue le 13/04/2024 devant le jury composé par :

Zakaria TRIKI	**Professeur, Université de Médéa**	**Président**
Radhia YOUS	**Maitre de conférences, Université de Médéa**	**Examinatrice**
Abdelhalim ZOUKEL	**Professeur, Université de Laghouat**	**Examinateur**
Yacine KERCHICH	**Professeur, ENP Alger**	**Examinateur**
Ahmed AZIZI	**Maitre de conférences, Université de Laghouat**	**Directeur de thèse**
Salah HANINI	**Professeur, Université de Médéa**	**Co-Directeur de thèse**

2023-2024

People's Democratic Republic of Algeria

Ministry of Higher Education and Scientific Research

University of Yahia FARES Medea

Faculty of Technology

Department of Process and Environment Engineering

Laboratory of Biomaterials and Transport Phenomena

Doctorate Thesis in Sciences

Studied by: Mr. Lakhdar ABOUDA

Specialty: Process Engineering

CONTRIBUTION TO THE FRACTIONAL MODELLING OF FILTRATION

Defended in 13/0/2024 in front of the jury composed by:

Zakaria TRIKI	**Full professor, University of Medea**	**Chair**
Radhia YOUS	**Associate professor, University of Medea**	**Reviewer**
Abdelhalim ZOUKEL	**Full Professor, University of Laghouat**	**Reviewer**
Yacine KERCHICH	**Full professor, ENP Alger**	**Reviewer**
Ahmed AZIZI	**Associate professor, University of Laghouat**	**Thesis director**
Salah HANINI	**Full professor, University of Medea**	**Thesis co-director**

2023-2024

Table of contents

Dedication vii

Acknowledgements viii

Abstract ix

ملخص x

Résumé xi

Graphical abstract xii

Nomenclatures & Abbreviations xiii

List of figures xv

List of tables xvii

Introduction 1

1. Literature review 5

1.1. Desalination by RO process 6

1.1.1. History of natural osmosis 6

1.1.2. History of reverse osmosis 7

1.1.3. RO process definition 11

1.1.4. Principle 11

1.1.5. Osmotic pressure 12

1.1.6. Description of RO desalination plant 12

1.2. RO membrane 13

1.2.1. Structure of RO membrane 13

1.2.1.1. Integral asymmetric membrane 14

1.2.1.2. Thin-film composite membrane 14

1.2.2. Material of RO membrane 15

1.2.2.1. Organic membrane 15

1.2.2.2. Inorganic membrane 18

1.2.3. Technical specifications of RO membrane 18

1.2.4. Module configuration of RO membrane 19

1.2.4.1. Hollow-Fiber module 19

1.2.4.2. Spiral-Wound module 21

1.2.4.3. Flat-Sheet (Plate-and-Frame) module 22

1.2.4.4. Tubular module 23
1.3. RO performance indicators 24
1.3.1. TDS rejection 24
1.3.2. Permeate flow rate & Recovery 24
1.3.3. Pressure drop 24
1.3.4. Energy consumption 24
1.4. Factors affecting RO performance 25
1.4.1. Effect of membrane properties 25
1.4.2. Effect of feedwater properties 25
1.4.2.1. Salt concentration 25
1.4.2.2. pH 25
1.4.2.3. Oxidizing reduction potential (ORP) 26
1.4.3. Effect of feed operational parameters 26
1.4.3.1. Feed pressure 26
1.4.3.2. Feed temperature 26
1.4.4. Effect of matter accumulation 27
1.4.4.1. Concentration polarization 27
1.4.4.2. Membrane fouling 28
1.5. Monitoring of RO performance by transport models 33
1.5.1. Phenomenological transport models 34
1.5.2. Mechanistic transport models 34
1.5.2.1. Solution diffusion model 36
1.5.2.2. Solution-diffusion-imperfection model 36
1.5.2.3. Extended solution diffusion model 36
1.5.2.4. Finely porous model 37
1.5.2.5. Preferential sorption-capillary flow model 37
1.5.2.6. Surface force-pore flow model 37
1.5.3. Scaling/fouling transport models 38
1.5.3.1. Constant pressure pore-blocking model 38
1.5.3.2. Scaling-based flux model 38
1.5.3.3. Pseudo N^{th} order model 38
1.6. Memory effect of physical phenomena 38
1.6.1. Notion of memory effect 39
1.6.2. Mathematical description of memory effect by fractional calculus 39

1.6.2.1. History of fractional calculus 39
1.6.2.2. Previous applications of fractional calculus 40
1.6.2.3. Mathematical definitions of fractional derivatives 45
2. Materials and methods 48
2.1. Experimental 49
2.1.1. Description of water treatment by the RO process 49
2.1.2. Construction of experimental data 50
2.2. Modelling 51
2.2.1. Model approach 51
2.2.2. Solution of the differential equation 53
2.2.2.1. Pseudo-zero order kinetics 53
2.2.2.2. Pseudo-first order kinetics 54
2.2.2.3. Pseudo-second order kinetics 55
2.2.2.4. Pseudo-n^{th} order kinetics 56
2.2.3. Transformation to dimensionless models 59
2.2.3.1. Pseudo-zero order kinetics 60
2.2.3.2. Pseudo-first order kinetics 61
2.2.3.3. Pseudo-second order kinetics 61
2.2.3.4. Pseudo-n^{th} order kinetics 62
2.3. Solving of the dimensionless models 64
2.4. Evaluation of the models accuracy by statistical criteria 64
3. Results and discussions 66
3.1. Models' reliability and accuracy 67
3.1.1. Alimentation compartment 67
3.1.1.1. Optimization of the kinetic constants of models 67
3.1.1.2. Calcul of dimensionless cumulative volume of alimentation 68
3.1.1.3. Evaluation of the models accuracy by statistical criteria 70
3.1.2. Permeate compartment 72
3.1.2.1. Optimization of the kinetic constants of models 72
3.1.2.2. Calcul of dimensionless cumulative volume of permeate 72
3.1.2.3. Evaluation of the models accuracy by statistical criteria 74
3.1.3. Rejection compartment 76
3.1.3.1. Optimization of the kinetic constants of models 76
3.1.3.2. Calcul of dimensionless cumulative volume of rejection 76

3.1.3.3. Evaluation of the models accuracy by statistical criteria 78

3.2. Comparison between the fractional dimensionless models and others models…. 80

Conclusion & Recommendation 82

References 85

Scientific production 101

Dedication

I dedicate this modest work to my very dear parents who have sacrificed and devoted themselves to my happiness. I also dedicate it to my family and all my friends. To everyone who has helped me in any way to build this work.

Lakhdar ABOUDA.

Acknowledgements

First of all, I thank Allah who has given me power and health to achieve this study.

This work was carried out under the supervision of Mr **Ahmed AZIZI**, **associate professor** at the University of Laghouat, who never ceased to show his confidence in me and to encourage me from the start of this work. I would like to express my sincere thanks to him. His highly distinguished contribution to the completion of this work will remain with me. His sense of scientific appreciation, his rigour for a job well done, his pertinent suggestions in the research and above all his availability to receive me without hesitation despite his busy schedule, have enabled me, on many occasions, to clarify my thoughts.

This work was done under the supervision of Mr. **Salah HANINI**, **full professor** at the University of Medea, who is greatly credited with initiating the research topic and guiding it. Despite his intense work program, he did not hesitate to give valuable corrections and observations that contributed to the completion of the research with high quality. I am very grateful and thankful to him for all these efforts.

I would like to thank all the professors who agreed to contribute to the enrichment and discussion of this research: Mr. **Zakaria TRIKI**, **full professor** at the University of Medea, Ms. **Radhia YOUS**, **associate professor** at the University of Medea, Mr. **Abdelhalim ZOUKEL**, **full professor** at the University of Laghouat, Mr. **Yassin KERCHICH**, **full professor** at the National Polytechnic School of Algers. Their valuable scientific input will undoubtedly improve the quality of this research.

Thanks also to Ms. **Hakima CHERIFI, full professor** at the University of Medea, Mr **Mohamed MOUSSAOUI**, **associate professor** at the University of Bouira, for all the scientific assistance that contributed to the completion of this research.

I would also like to thank Mr. **Mustafa DOUMIR**, Administrative Officer at the Faculty of Technology, for all the assistance and administrative facilities he provided during the completion of this research.

I would like to thank everyone who has contributed to the completion of this work.

Abstract: Contribution to the fractional modelling of filtration

In this thesis, new fractional dimensionless models (FDM) have been proposed to follow the performance of the RO desalination process using the dimensionless cumulative volumes of alimentation, permeate, and rejection. The proposed models were mathematically developed from the pseudo n^{th} order (PNO) equation and resolved by the establishment of a MATLAB software program. The FDMs were thoroughly tested using statistical criteria to assess their accuracy in representing the 2561 cumulative volumes of experimental data collected over the four years lifetime of the RO membranes. The fractional dimensionless models (FDM) with optimal kinetic constants provided an accurate result and perfect consistency with the experimental data. As such, the coefficient of determination (R2) values were 0.9975, 0.9750 and 0.9801, with lower average absolute relative deviation (AARD) around 8.03, 0.53 and 0.45, through lower root mean squared error (RMSE) about 1.452, 0.976 and 0.880 for alimentation, permeate and rejection, respectively.

Keywords: Fractional modelling, membrane transport models, dimensionless parameters, separation kinetic, desalination, reverse osmosis process performance.

ملخص : المساهمة في النمذجة الجزئية للترشيح

في هذه المذكرة ،تم اقتراح نماذج جديدة بدون أبعاد جزئية (FDM) لمتابعة أداء عملية تحلية المياه بالتناضح العكسي باستخدام الأحجام التراكمية بدون أبعاد للتغذية ،والتخلل ،والرفض. تم تطويرالنماذج المقترحة رياضيًا من معادلة الترتيب الزائف (PNO) وتم حلها عن طريق إنشاء خوارزمية على برنامج الماتلاب. تم اختبار دقة النماذج FDMs باستخدام معاييرإحصائية في تمثيل قاعدة بيانات تحوي 2561 نقطة من البيانات التجريبية التي تم جمعها على مدى اربع سنوات من عمرأغشية التناضح العكسي. قدمت النماذج الكسرية عديمة الأبعاد (FDM) ذات الثوابت الحركية المثلى نتيجة دقيقة واتساقًا تامًا مع البيانات التجريبية. على هذا النحو، كانت قيم معامل التحديد (R2) 0.9975 و0.9750 و0.9801، مع انخفاض متوسط الانحراف النسبي المطلق (AARD) حوالي 8.03 و0.53 و0.45، و كذا انخفاض متوسط جذر الخطأ التربيعي (RMSE) حوالي 1.452 و0.976 و0.880 للتغذية والتخلل والرفض، على التوالي.

الكلمات المفتاحية: النمذجة الجزئية، نماذج النقل الغشائي، المعلمات اللابعدية، حركية الفصل، تحلية المياه، أداء عملية التناضح العكسي.

Résumé : Contribution à la modélisation fractionnelle de la filtration

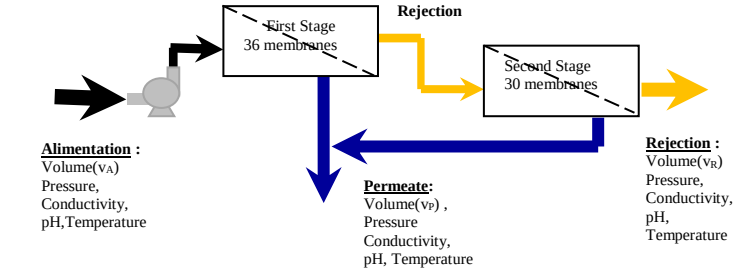
Dans cette thèse, de nouveaux modèles fractionnaires sans dimension (FDM) ont été proposés pour suivre les performances du procédé de dessalement par osmose inverse en utilisant les volumes cumulés sans dimension de l'alimentation, du perméat et du rejet. Les modèles proposés ont été développés mathématiquement à partir de l'équation du pseudo-n^{ième} ordre (PNO) et résolus par l'établissement d'un programme sur logiciel MATLAB. Les FDM ont été testés de manière approfondie à l'aide de critères statistiques afin d'évaluer leur précision dans la représentation des 2561 volumes cumulés de données expérimentales collectées au cours de quatre ans de durée de vie des membranes d'osmose inverse. Les modèles fractionnaires sans dimension (FDM) avec des constantes cinétiques optimales ont fourni un résultat précis et une cohérence parfaite avec les données expérimentales. Ainsi, les valeurs du coefficient de détermination (R2) étaient de 0,9975, 0,9750 et 0,9801, avec un écart relatif absolu moyen (AARD) inférieur d'environ 8,03, 0,53 et 0,45, et une erreur quadratique moyenne (RMSE) inférieure d'environ 1,452, 0,976 et 0,880 pour l'alimentation, le perméat et le rejet, respectivement.

Mots-clés : Modélisation fractionnelle, modèles de transport membranaire, paramètres adimensionnelles, cinétique de séparation, dessalement, performance du procédé d’osmose inverse.

Graphical abstract



(a)



(b)



(c)

The RO desalination process (a): Picture; (b): block flow diagram (c): Fractional modelling inputs and outputs to monitor the performance of the RO process.

Nomenclatures & Abbreviations

Nomenclatures

- C_b: the solute concentration of bulk feed (mg. L^{-1}).
- C_{in}: the initial mass concentration of solute in the feed suspension (mg L^{-1}).
- C_m: the solute concentration on membrane surface (mg. L^{-1}).
- C_p: the solute concentration of permeate flow (mg. L^{-1}).
- C_s: the saturated solute concentration (mg. L^{-1}).
- d: the thickness of boundary layer (mm).
- J_v: the permeate volume flux ($m^3 (m^2 s)^{-1}$).
- k'_n: the rate constant of adsorption reaction of the PNO equation ((mg $g^{-1})^{1-n}$ h^{-1}).
- k_0 *is* the constants of O-PZO model (-).
- K_0: the rate constant of filtration of the O-PZO equation (L h^{-1}).
- k_{0f} : the constant of F-PZO model (-).
- K_{0f} : the rate constant of filtration of the F-PZO equation (L $h^{-\alpha}$).
- k_1*:* the constants of O-PFO model (-).
- K_1: the rate constant of filtration for the O-PFO equation (h^{-1}).
- K_{1f} : the rate constant of filtration for the F-PFO equation ($h^{-\alpha}$).
- k_{1f}: the constant of F-PFO model (-).
- k_2: the constants of O-PSO model (-).
- K_2: the rate constant of filtration for the O-PSO equation (L^{-1} h^{-1}).
- K_{2f} : the rate constant of filtration for the F-PSO equation (L^{-1} $h^{-\alpha}$).
- k_{2f}: the constant of F-PSO model (-).
- k_n *:* the constants of O-PNO model (-).
- K_n: the rate constant of filtration of the O-PNO equation (L^{1-n} h^{-1}).
- k_{nf}: the constant of F-PNO model (-).
- K_{nf}: the rate constant of filtration for the F-PNO equation (L^{1-n} $h^{-\alpha}$).
- M : the mass of RO membrane (g).
- m_{ad}: the adsorbed mass of solute (mg).
- m_{in}: the initial mass of solute (mg).
- n: the order of adsorption reaction (-).
- $q(t)$: the adsorbed amount of solute per unit mass of the membrane (mg g^{-1}).
- q_{max}: the maximum adsorption capacity of the membrane per unit mass of the membrane (mg g^{-1}).

- R^2: Coefficient of Determination.
- t : the filtration time (h).
- t_m: the maximum filtration time (h).
- $v(t)$: the cumulative volume of the filtrate (m^3).
- V: the dimensionless cumulative volume of the filtrate (-).
- v_m : the maximum cumulative volume of the filtrate (m^3).

Greek letter

- α: the fractional order of time (-).
- Γ: the Gamma function.
- γ: the retention rate (-).
- τ: the dimensionless filtration time (-).

Abbreviations

- AARD: Average Absolute Relative Deviation.
- DF : Depth Filtration.
- DWRO: Dam Water Reverse Osmosis.
- FDE: Fractional Differential Equation.
- FDM: Fractional Dimensionless Models.
- F-PFO: Fractional Pseudo-First-Order.
- F-PNO: Fractional Pseudo-n^{th} -Order.
- F-PSO: Fractional Pseudo-Second-Order.
- F-PZO: Fractional Pseudo-Zero-Order.
- MAE: Mean Absolute Error.
- MF: Microfiltration.
- NF: Nanofiltration.
- ODE: Ordinary Differential Equation.
- ODM: Ordinary Dimensionless Models.
- O-PFO: Ordinary Pseudo-First-Order.
- O-PNO: Ordinary Pseudo-nth -Order.
- O-PSO: Ordinary Pseudo-Second-Order.
- O-PZO: Ordinary Pseudo-Zero-Order.
- PNO: Pseudo n^{th} Order
- RMSE: Root Mean Squared Error.
- RO: Reverse osmosis.
- SSE: Sum of Squares Error
- SSR: Sum of Squares Regression.
- TDS : Total Dissolved Salt.

List of figures

Figure 1.1. The development of asymmetric RO membrane 10
Figure 1.2. The development of thin film composite RO membrane 10
Figure 1.3. RO separation process. 11
Figure 1.4. Principle of RO separation 12
Figure 1.5. Schematic diagram of standard RO plant 13
Figure 1.6. Cross sectional diagrams of asymmetric membrane 14
Figure 1.7. Cross section of a thin-film composite membrane 14
Figure 1.8. Chemical structure of cellulose triacetate polymer of RO membrane 15
Figure 1.9. Chemical structure of polyamide polymer of RO membrane: (a) linear aromatic; (b) crosslinked aromatic 16
Figure 1.10. Structure of the synthesized polyamide RO membrane with the top and cross-sectional morphologies 17
Figure 1.11. Chemical structure of others polymer of RO membrane: (a) polypiperazineamide; (b) crosslinked polyether 17
Figure 1.12. Hollow-fiber membrane modules 20
Figure 1.13. Spiral-wound module 22
Figure 1.14. Plate-and-frame module 23
Figure 1.15. Tubular module 23
Figure 1.16. Concentration polarization phenomenon. 27
Figure 1.17. Scanning electron microscope of different fouling types 28
Figure 1.18. Biofouling formation on membrane surface 29
Figure 1.19. Main phases of inorganic fouling in an RO membrane 31
Figure 1.20. Schematic representation of colloidal fouling 32
Figure 2.1. The RO desalination process (a): Picture; (b): block flow diagram (c): Fractional modelling inputs and outputs to monitor the performance of the RO process. 49
Figure 3.1. The calculated and the experimental values of dimensionless cumulative volume of alimentation (V_A^{cal}, V_A^{exp}) plotted as function of dimensionless filtration time (τ): (a) O-PZO model, (b) O-PFO model, (c) O-PSO model, (d) O-PNO model, (e) F-PZO model, (f) F-PFO model, (g) F-PSO model, (h) F-PNO model. 69

Figure 3.2. Scatter plot of the calculated values ((V_A^{cal}), by the ODM and FDM, versus the experimental values (V_A^{exp}) of dimensionless cumulative volume for alimentation: (a) O-PZO model, (b) O-PFO model, (c) O-PSO model, (d) O-PNO model, (e) F-PZO model**,** (f) F-PFO model**,** (g) F-PSO model**,** (h) F-PNO model. 71

Figure 3.3. The calculated and the experimental values of dimensionless cumulative volume of permeate (V_P^{cal}, V_P^{exp}) plotted as function of dimensionless filtration time (τ): (a) O-PZO model, (b) O-PFO model, (c) O-PSO model, (d) O-PNO model, (e) F-PZO model, (f) F-PFO model, (g) F-PSO model, (h) F-PNO model. 73

Figure 3.4. Scatter plot of the calculated values (V_P^{cal}), by the ODM and FDM, versus the experimental values (V_P^{exp}) of dimensionless cumulative volume for permeate: (a) O-PZO model, (b) O-PFO model, (c) O-PSO model, (d) O-PNO model, (e) F-PZO model, (f) F-PFO model, (g) F-PSO model, (h) F-PNO model. 75

Figure 3.5. The calculated and the experimental values of dimensionless cumulative volume of rejection (V_R^{cal}, V_R^{exp}) plotted as function of dimensionless filtration time (τ): (a) O-PZO model, (b) O-PFO model, (c) O-PSO model, (d) O-PNO model, (e) F-PZO model, (f) F-PFO model, (g) F-PSO model, (h) F-PNO model. 77

Figure 3.6. Scatter plot of the calculated values (V_R^{cal}), by the ODM and FDM, versus the experimental values (V_R^{exp}) of dimensionless cumulative volume for rejection: (a) O-PZO model, (b) O-PFO model, (c) O-PSO model, (d) O-PNO model, (e) F-PZO model, (f) F-PFO model, (g) F-PSO model, (h) F-PNO model. 79

List of tables

Table 1.1. The Grünwald–Letnikov fractional derivative. 45
Table 1.2. The Riemann–Liouville fractional derivatives. 46
Table 1.3. The Caputo fractional derivatives. 47
Table 2.1. Technical specifications of the RO desalination process. 49
Table 2.2. Chemical cleaning cycles of the RO membranes. 50
Table 2.3. Maximum experimental values of cumulative volume and filtration time. 51
Table 2.4. The ordinary and fractional dimensional models developed in this work. 59
Table 2.5. The ordinary and fractional dimensionless models developed in this work. 63
Table 3.1. The kinetic constants of ODM and FDM for the calculated cumulative volume of alimentation (V_A^{cal}). 68
Table 3.2. The statistical criteria of ODM and FDM for the calculated cumulative volume of alimentation (V_A^{cal}). 70
Table 3.3. The kinetic constants of ODM and FDM for the calculated cumulative volume of permeate (V_P^{cal}). 72
Table 3.4. The statistical criteria of ODM and FDM for the calculated cumulative volume of permeate (V_P^{cal}). 74
Table 3.5. The kinetic constants of ODM and FDM for the calculated cumulative volume of rejection (V_R^{cal}). 76
Table 3.6. The statistical criteria of ODM and FDM for the calculated cumulative volume of rejection (V_R^{cal}). 78
Table 3.7. Comparison between the proposed fractional dimensionless models (FDM) and others models in the literature. 81

INTRODUCTION

Introduction

Membrane separation technology is considered one of the main filtration processes in the industrial sector, particularly in water treatment. The membrane process known as the reverse osmosis (RO) process is used in numerous industrial applications. RO process is considered one of the most important desalination technologies due to its advantages, including flexibility, high efficiency and ease of operation [Feria-Díaz *et al*., 2021]. It can be used to produce drinking water and process water for various industrial applications, such as food and pharmaceutical. Since its invention in the 1950s [Glater, 1998], the RO process has been extensively studied to enhance its development [Reid and Breton, 1959; Lonsdale *et al*., 1965; Riley *et al*., 1967; Anderson *et al*.; 1972; Jonsson and Boesen, 1975; Matsuura and Sourirajan, 1981; Košuti´c *et al*., 2000; Qin *et al*., 2005; Hoang *et al*., 2010; Abid *et al*., 2012; Albo *et al*., 2014; Alsarayreh *et al*., 2020].

The water desalination plant performance is greatly affected by the RO membranes efficiency, which it has prompted researchers and membrane manufacturers to study the transport of solvent (water) and solute (salts) through the RO membranes in order to improve its efficiency [Madaeni; 2001; Ozaki *et al*., 2002; Odabaşı *et al*., 2022]. Monitoring the performance of RO process is necessary to identify early symptoms of failure in order to improve maintenance and extend the process lifetime. However, one of the major limitations to adequately ensure its performance monitoring is the matter accumulation on the membrane, such as concentration polarization and fouling [Park *et al*., 2006; Hoek *et al*., 2008; Tong *et al*., 2020; Gu *et al*., 2021; Ling *et al*., 2021; Piekutin, 2021]. This limitation increases the difficulty of the supervision of RO membrane's performances and introduces multiple factors in the separation process. This difficulty can be attributed to its enormous complexity leading to the uncertainties in the prediction of the operating parameters (flow rate, pressure …etc.). Various techniques are used as indicators for fouling monitoring: pressure drop, salt passage and flow rate. Thus, mastering the monitoring and prediction of fouling kinetics using models has made it possible to improve filtration efficiency.

Mathematical modelling has been widely used to accurately describe the performance of the RO process [A1-Bastaki and Abbas, 1999; Kahdim *et al*., 2003; Jamal *et al*., 2004; Dimitriou *et al*., 2017; Haluch *et al*., 2017; Al-Obaidi *et al*., 2018; Mohammad *et al*., 2020; Puti´c *et al*., 2021; Wang *et al*., 2021a; Yokoyama *et al*., 2022; Azizi *et al*., 2022; Bchiti *et al*., 2022]. Developing an appropriate mathematical model that accounts the fouling is essential for optimizing design and improving efficiency, thus reducing the overall costs. However, a universal mathematical model expressing the kinetics of RO process is unavailable, until now, due to the difficulty to fully

elucidate and understand the physical principles of the complex phenomena that occurs during RO like diffusion and fouling. The kinetic of this complex phenomena can deviate from the classic description because they have nonlinear behavior, giving rise to so-called anomalous kinetic which introduce memory effects into the process.

Anomalous kinetics cannot be represented by classical models, but it can be described by fractional kinetics theory that uses fractional calculus, where fractional models have proven their performance for other processes [Kashchenko and Nikitin, 2014; Zhai *et al*., 2015; Padrino, 2017; Obembe *et al*., 2018; Kumar *et al*., 2019; Ramírez *et al*., 2017; De Souza Matias *et al*., 2019; Lemus-Mondaca *et al*., 2021; Mahdad *et al*., 2021a; Mahdad *et al*., 2021b; Friesen *et al*., 2015; Nikan *et al*., 2020; Mirza *et al*., 2021; El-Gazar *et al*., 2021]. On the other hand, The majority of previous modelling studies have relied on a limited range of experimental data, thus limiting their range of validity using a small database that could not evaluate the accuracy of the model [Ruth *et al*., 1933; Hermans and Bredée, 1935; Ho and Zydney, 2000; Jamal *et al*., 2004 ; Fouladitajar *et al*., 2013; Tien *et al*., 2014; Heidari *et al*., 2017; Goldrick *et al*., 2017; Debnath *et al*., 2019; Tong *et al*., 2020; Xu *et al*., 2020; Heidari *et al*., 2021; Bchiti *et al*., 2022].

In this study, new approach has been adopted to describe the performance of reverse osmosis desalination using the pseudo n^{th} order equation with a fractional solution to establish dimensionless cumulative volumes models for alimentation, permeate, and rejection. The study has been structured into three chapters: literature review, materials and methods and results and discussions.

The first chapter includes a literature review on various aspects of the subject, including: reverse osmosis water desalination, membranes and reverse osmosis process performance, mathematical models of membrane transport and fractional calculus.

The second chapter is devoted to the materials and methods used in this study. This chapter includes: a brief presentation of the studied reverse osmosis process and the operational data collected for performance monitoring, a modelling study using the pseudo n^{th} order model. The various steps that have been followed to complete the fractional modelling can be resumed in two phases: mathematical preparation of models and selection of the best models. The first phase was constituted by mathematical preparation of models according to the following tasks:

- development of differential equation, from the pseudo n^{th} order (PNO) equation, to express the variation of the cumulative volume over the filtration time,
- solving of the differential equation using ordinary and fractional methods to obtain the dimensional models,
- Transformation of the dimensional models into dimensionless models.

The second phase was constituted by selection of the best models, among the established models, that can better fit the 2561 data point of experimental cumulative volumes collected over four year's period of the lifespan of RO membranes for the three compartments according to the following tasks:

- Optimization the kinetic constants of the models (n, α, k_i and k_{if}) by establishing an algorithm on MATLAB software.
- Calculation of the dimensionless cumulative volumes using the ordinary (ODM) and fractional (FDM) models while using the optimized values of kinetic constants.
- Evaluation of the accuracy of established models (ODM, FDM) using statistical criteria (R^2, RMSE, AARD, MAE, SSR and SSE) and linear regression.
- Comparison between the proposed models and other models in the literature based on statistical criteria, the number of experimental data points and the number of compartments.

The third chapter presents and discusses the results of ordinary and fractional modelling of the reverse osmosis process.

Finally, this work will be concluded with a conclusion and review the various findings. Then offer some suggestions for further research will be proposed.

1. Literature review

1. Literature review

1.1. Desalination by RO process

Desalination is a process that purifies salt water by removing the dissolved mineral salts that were originally in water. The most commonly used desalination method includes the thermal-based and membrane-based separation methods. Multistage flash distillation (MSF), multi-effect distillation (MED), and vapor compression (VC) are the most utilized thermal desalination processes in large and medium scale. Although there are various membrane-based desalination techniques available, reverse osmosis (RO) and electro-dialysis (ED) are the most prevalent from them. The advantages of RO process over thermal process include greater mitigation of the effects of environmental pollution, wider availability of suitable site, for desalination plant construction, less complex plant design, lower maintenance costs, and lower operating costs. The RO desalination process was developed from the natural osmosis phenomenon.

1.1.1. History of natural osmosis

The natural osmosis phenomenon was first discovered by *Nollet* in 1748. In his experience, he noted that when water and alcohol were separated using an animal bladder, the water passed into the alcohol but never vice versa [Nollet, 1748].

In 1828, *Dutrochet* proposed the terms "endosmosis" and "exosmosis" to describe the osmosis phenomenon. His classic work about endosmosis and exosmosis described the process by which water passes through a semi-permeable membrane from one side to another [Dutrochet, 1828]. In 1854, *Graham* explicitly distinguished between diffusion when two solutions are carefully layered upon one another and what occurs when the two solutions are separated by semi-permeable membrane. He measured the osmotic pressure generated by a variety of solutes and solutions. He rejected Dutrochet's hypothesis that suppose the osmotic pressure was due to the capillarity of the tube in which it was measured [Graham, 1854]. In 1855, *Fick* worked on dialysis of solutions through artificial membranes formed from collodion [Fick, 1855]. In 1867, *Traube* prepared the first inorganic semi-permeable membrane. This gelatinous film of copper ferrocyanide supported on a porous clay frit displayed remarkable selectivity to dilute solutions of electrolytes. He observed that a cupric ferrocyanide membrane would allow water to diffuse through it, but that sugar molecules were restrained

from diffusing. *Traube* speculated that the membrane amounted to a molecular sieve, and that it contained holes or pores large enough to allow passage of a water molecule, but too small to permit diffusion of larger molecules such as sugar [Traube, 1867]. In 1877, *Pfeffer* developed a semi-porous membrane to study the phenomena of osmosis. He precipitated copper ferrocyanide in a porous material, producing a membrane with good mechanical strength. The eponymous "Pfeffer cell" is named for the osmometric device he constructed for determining the osmotic pressure of a solution. He developed a method for measuring osmotic pressure and showed that pressure depended on the size of the molecules too large to pass through the membrane [Pfeffer, 1877]. In 1887, *van't Hoff* published an analogy between dilute aqueous solutions and perfect gases and applied the second law of thermodynamics to osmosis. He established a law, similar in form to the law of perfect gases, and proposed the adjective "semi-permeable" to designate membranes [Van't Hoff, 1887].

In 1907, *Bechold* published the most carefully documented use of pressure as a driving force for membrane filtration. These "ultrafiltration" (UF) studies were carried out by forcing solutions at pressures up to several atmospheres through membranes prepared by impregnating filter paper with acetic acid collodion. *Bechold* was successful in developing membranes with graded porosities and designing the first ultrafilter [Bechold, 1907].

1.1.2. History of reverse osmosis

In 1931, *Horvath* invented a new method of water-softening using the reverse osmosis [Horvath, 1931]. After the Second World War, the California's rapidly growing population was matched by a diminishing supply of fresh water in this semi-arid region. This made 'saltwater conversion' a high-priority research area in the US, especially at the University of California, which was actively involved in desalination [Glater, 1998]. The first considerations of water desalination at University of California date to the early 1950's and described in two School of Engineering Reports authored by *Hassler*. In 1949, he started the membrane desalination research where the possibility of transporting vapor through cellophane sheets was mentioned [Hassler, 1949]. In 1950, he described the concept of "salt repelling osmotic membrane" [Hassler, 1950].

In the mid-1950s, *Reid's* team, funded by The Office of Saline Water, undertook research on "*Osmotic Membranes for Demineralization of Saline Water"* at the University of Florida. They evaluated the performance of a variety of available commercial polymeric films for the

first time to verify the concept of pressure driven reverse osmosis membrane desalination. The most promising of these membrane materials was cellulose acetate which displayed very high salt rejection but disappointing levels of product water flux [Reid, 1958]. In 1959, *Reid and Breton w*ere successfully fabricated an active cellulose acetate (CA) membrane to remove salt from water. The membrane could retain salt effectively, but the permeate flux through the membrane was significantly low. They also proposed an interesting mechanism for membrane transport. It was postulated that passage of water took place via hydrogen bonding to carbonyl oxygen in cellulose acetate thereby filling membrane voids with bound water. Ions and molecules, not capable of hydrogen bonding, could then pass through the membrane by "hole type diffusion" only. Resistance to ion transport would occur when such holes became filled with bound water. These postulates are indeed innovative and among the first proposed models for membrane perm-selectivity. In an effort to support these ideas, cellulose acetate membrane samples were subjected to a variety of physical measurements including electrical resistance and dielectric constant [Reid and Breton, 1959].

In 1963, the breakthrough discovery was made by *Loeb and Sourirajan* to improve the membrane performance. They developed an anisotropic cellulose acetate membrane for demineralizing saline brines such as sea water. The membrane is fabricated from a casting solution of cellulose acetate and acetone, to which is added an aqueous magnesium perchlorate solution. Key operations in the membrane fabrication process include immersion of the membrane in ice water within a prescribed period after casting, and subsequent heating of the membrane. The major attractions of the process from an economic standpoint are its simplicity and relatively low energy consumption. The membrane is capable of producing a flux of 5 to 11 gallons/day/ft^2 of 0.05% NaCl water from a brine containing 5.25% NaCl, under a pressure of 1500 to 2000 psi.g [Loeb and Sourirajan, 1963].

After the development of the *Loeb-Sourirajan* RO membrane, further research on cellulose acetate materials was focused on the improvement of the membrane transport properties and simplification of manufacturing to bring the technology to industrial application. Research in membrane casting solution optimization continued to develop an all-organic formulation. Contributions involved the use of formamide ($HCONH_2$) as a swelling agent in place of magnesium perchlorate [Manjikian, 1965], the development of methods for casting tubular membranes [Loeb, 1966].

In 1965, the world's first commercial RO plant was built in Coalinga, California based on the L–S membrane. The plant consisted of an array of one-inch tubular cellulose acetate membranes inserted into titanium support tubes [Loeb and Selover, 1967]. This newly developed RO membrane plant provided a breakthrough in desalination technology by demonstrating the first large-scale production of potable water by reverse osmosis. The Research Group of California University collected data and supervised operation of this facility for 3½ years [[Johnson *et al*., 1969].

In the 1970s, research into cellulose membrane development continued. For example, a blend of cellulose diacetate and cellulose triacetate provided higher permeability and selectivity than cellulose acetate membranes, as well as offering great resistance to compaction [King *et al.*, 1970]. More studies have been performed, such as control degree of mixed ester substitution for the hydroxyl groups found in cellulose to monitor the performance of the cellulose acetate membranes [Cannon and Cantor, 1971].

In 1971, the desalination group at university of California was assigned the task of designing a reverse osmosis pilot plant to be installed at *Firebaugh*, California [Antoniuk and McCutchan, 1973]. A one-inch tubular plant, similar in design to the Coalinga facility, operated for a period of four months with continuing involvement in the analysis and optimization of the facility [Speight and McCutchan, 1979]. It is important to note that prior to the installation of the desalination plant at Firebaugh, efforts were made by several industrial companies, including DuPont, Aeroget- General and Ionics.

In 1971, *Richter and Hoehn* developed the first aromatic polyamide (PA) asymmetric hollow-fibre membrane [Richter and Hoehn, 1971]. The presence of the sulphonic and phenyl groups in sulfonated polysulfone was expected to enhance permeability, mechanical, chemical and biological stability however the salt rejection was below the acceptable level necessary for commercialization [Brousse *et al*., 1975]. This was subsequently commercialized by Du Pont under the trade name of B-9 Permasep®, for application in brackish water desalination [Shields, 1979]. However the susceptibility of polyamides to attack by disinfectants (chlorine and ozone) was observed after the prolonged use of the B-9 Permasep® membrane.

Figure 1.1 shows the different developments of RO membranes from the end of the 1950s to the beginning of the 1990s, taking into account the salt rejection rate and normalized water permeability.

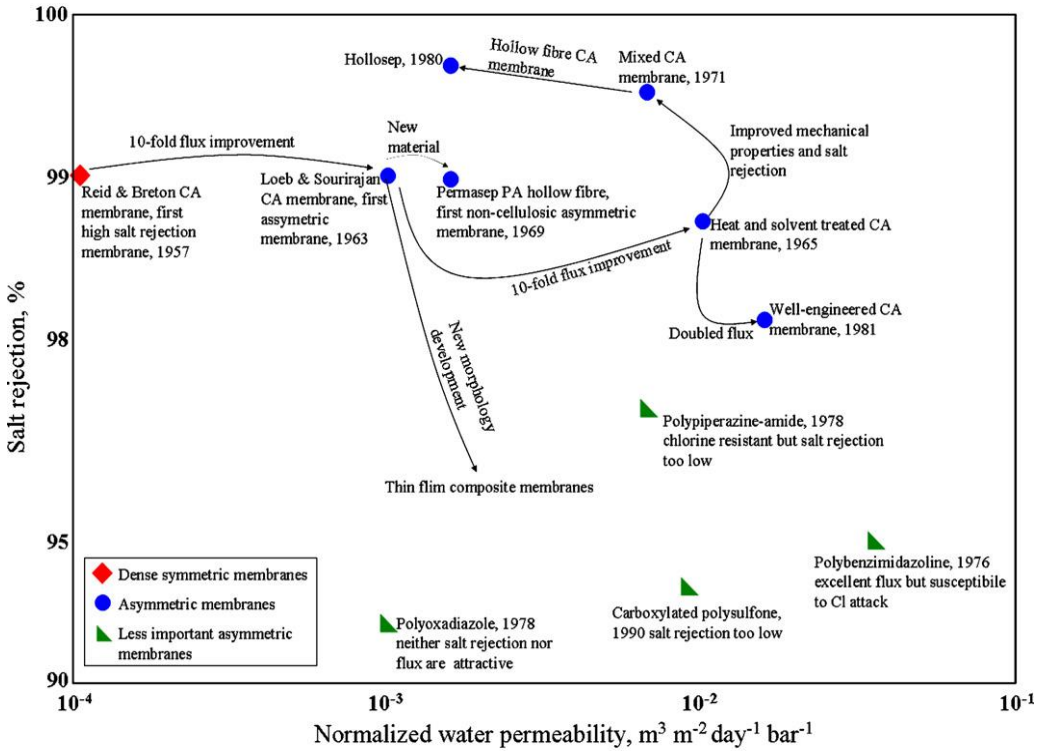


Figure 1.1. The development of asymmetric RO membrane [Lee *et al.*, 2011].

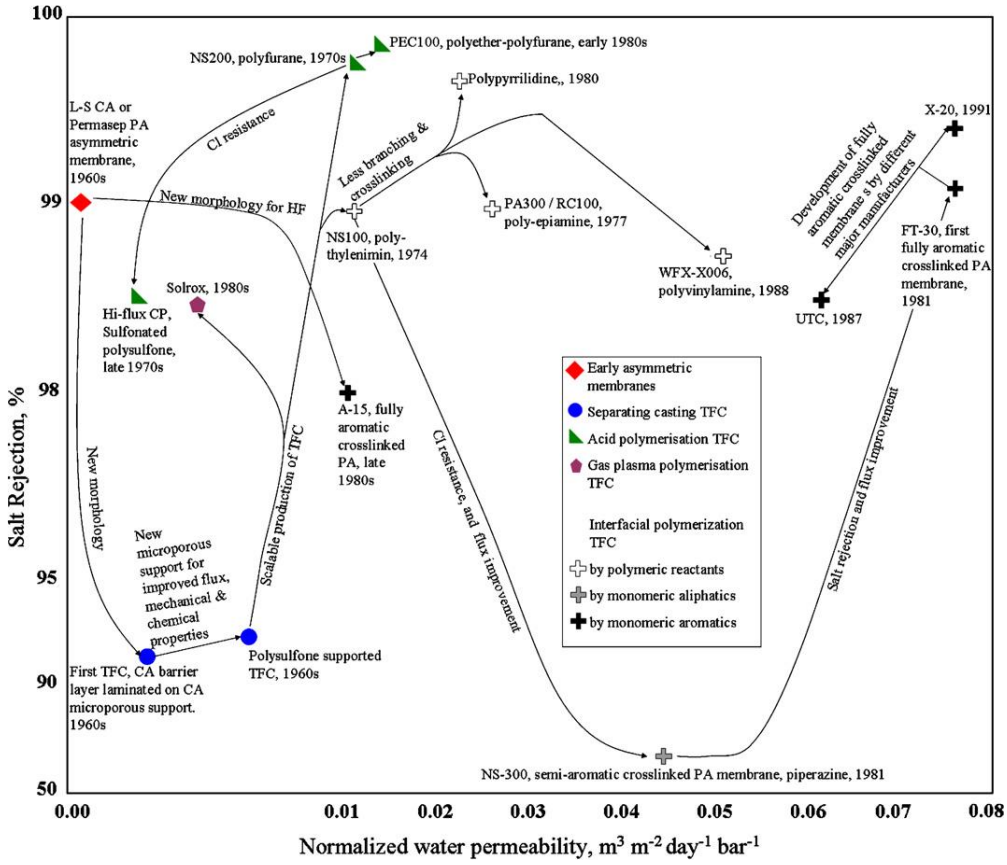


Figure 1.2. The development of thin film composite RO membrane [Lee *et al.*, 2011].

1.1.3. RO process definition

RO process is a technique that can be used to separate, under the pressure action, solvent and solute mixture (feed) using a semi-permeable membrane that allow the passage of solvent (permeate) and retain solute (rejection).

Many industrial applications uses RO process such as water purification processes (desalination, industrial production and wastewater treatment units) and food processes (concentration of fruit juice, sugar, coffee and milk, solvents).

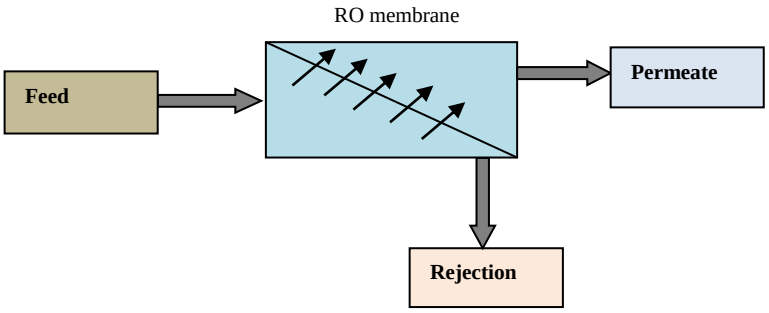


Figure 1.3. RO separation process.

1.1.4. Principle

The RO desalination process was developed from the natural osmosis phenomenon. This occurs when a semi-permeable membrane is placed between two water compartments with different salinity. The water molecules pass from the less salty water compartment to the more salty water compartment until the same concentration of salts is reached in both compartments (Figure 1.4a).

A difference in solution level is observed between the two compartments (Figure 1.4b), where it will increase until the pressure of the more saline water column is so high as to stop the flow of the less saline water. The equilibrium point of this water column height in terms of water pressure against the membrane is called the osmotic pressure.

RO is therefore created by applying a pressure to the salt water column that is greater than the osmotic pressure, forcing the water molecules to flow through the semi-permeable membrane towards the less salty water compartment (Figure 1.4c).

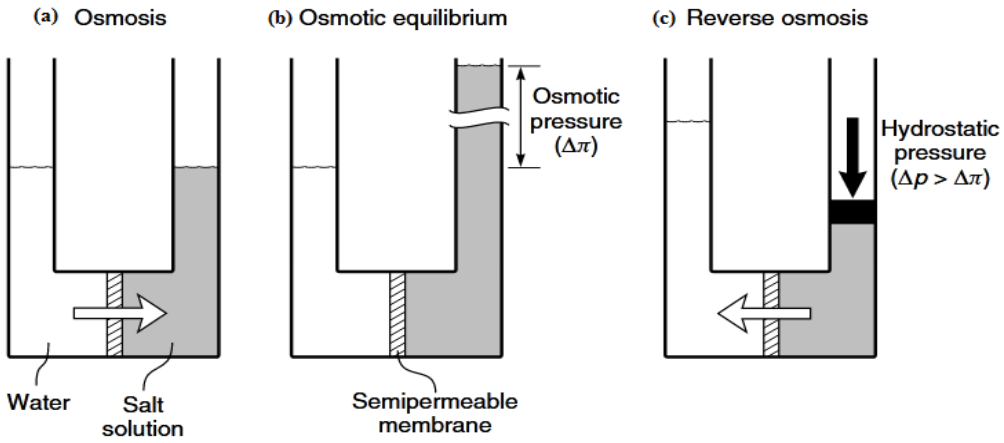


Figure 1.4. Principle of RO separation [Baker, 2004].

1.1.5. Osmotic pressure

Osmotic pressure is a thermodynamic property of a solution. It can be calculated using *Van't Hoff's* law [Van't Hoff, 1887]: the osmotic pressure exerted by a solute is equal to the pressure that this body would have exerted in the perfect gaseous state in the same volume and at the same temperature. If the solute is dissociated into i ions, the osmotic pressure will be i times greater. The osmotic pressure of a solution is proportional to the concentration of solutes:

$$\Pi = i\ C\ R\ T$$

With : Π is the osmotic pressure (bar), i is the Van't Hoff factor which is the number of particles into which the solute separates in solution, C is the molar concentration of salt ($mol.L^{-1}$), R is the perfect gas constant (equal to 0.082 $L.bar^{-1}.mol^{-1}.K^{-1}$), T is the temperature in Kelvin (K).

1.1.4. Description of RO desalination plant

RO desalination is the most technologically advanced method of purifying water (Figure 1.5). Water is taken from the sea and receives a first treatment to eliminate impurities, oil, seaweed, rubbish, and so on. Once free of organic substances, the saltwater can be subjected to RO separation, which after filtering, there are two streams: one is brine and the other is fresh water. The brine solution is diluted before being returned to the sea, avoiding high concentrations of salt which could harm the ecosystem. The fresh water passes through a re-mineralization and chlorination process, after which it is stored in tanks and then sent to the distribution network for consumption.

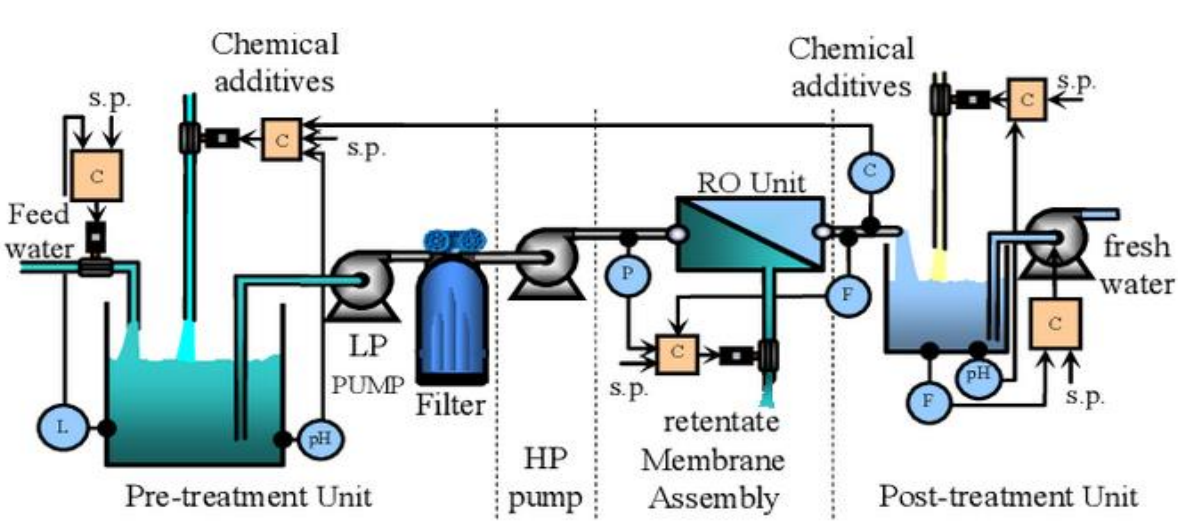


Figure 1.5. Schematic diagram of standard RO plant [Goh *et al*., 2021].

Using this property, a large proportion of the impurities in salt water (dissolved salts, particles, colloids, organic matter, micro-organisms) can be eliminated, enabling water to be produced for different uses. The separation of impurities by a RO membrane is based on some criteria such as size, chemical nature, physical state and ionic charge [Annane, 2015]. For example, RO membranes cannot remove gases (CO_2, O_2) because they have a very low molecular weight and are weakly ionized in solution.

1.2. RO membrane

1.2.1. Structure of RO membrane

Most RO membranes have an asymmetric structure with a thin dense top layer supported by a porous sublayer, the resistance towards transport being determined mainly by the dense top layer. Salt rejection takes place at the surface of the top skin layer with the permeate passing into the porous sublayer. The porosity in an asymmetric membrane is not uniform and the porosity distribution depends on thickness orientation in the membrane; this is especially evident in the high-density surface layer, which is called the dense layer, as it has a selectivity function; the other layer, composed of porous material, is called the support layer. Commercially used RO membranes with asymmetric structures are of basically two types: integral asymmetric and thin-film composite. In the asymmetric membrane, the dense and support layers are usually composed of the same material; if the material composition differs between these two layers, the asymmetric membrane is called a composite membrane [Kumano, 2013].

1.2.1.1. Integral asymmetric membrane

In integral asymmetric membranes, both the top layer and the sublayer consist of the same material. These membranes are prepared using phase inversion techniques. For this reason it is essential that the polymeric material from which the membrane is to be prepared is soluble in a solvent or a solvent mixture [Kumano, 2013].

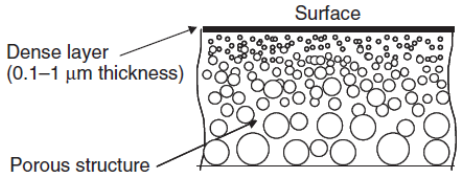


Figure 1.6. Cross sectional diagrams of asymmetric membrane [Kumano, 2013].

1.2.1.2. Thin-film composite membrane

The thin-film composite (TFC) membrane, proposed by Cadotte in 1980, exhibited improved water flux with high salt rejection and demonstrated improved chemical resistance with a wide range of pH [Cadotte *et al*., 1980]. It consists of three layers: the first bottom layer is the nonwoven polyester fabric; the second middle layer is a substrate layer, which is usually polysulfone; and the third top layer is the polyamide (PA) selective layer. The substrate and the nonwoven polyester fabric layers act as a support layer. The top PA layer is formed via the IP reaction between amine and acid chloride and controls the membrane water flux and solute rejection [Rahaman *et al*., 2014]. In addition, the performance of the TFC membrane can be easily altered by doing some minor changes in the chemical structure and morphology of the PA layer and surface properties of the substrate. Therefore, it can be considered as one of the major advantages of TFC RO membrane over cellulosic RO membranes. In recent literatures, sufficient amount of research work in terms of the selection of monomer, substrate and their modification, incorporation of different additives, and optimization of IP reaction time has been done to improve the TFC membrane performances [Ibrahim *et al*., 2020].

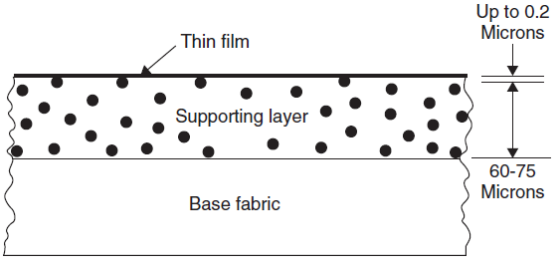


Figure 1.7. Cross section of a thin-film composite membrane [Kumano, 2013].

1.2.2. Material of RO membrane

The RO membranes can be prepared from different materials such as organic polymers and inorganic materials.

1.2.2.1. Organic membrane

The widely organic polymers those can be used in RO membranes are the cellulose-derived (cellulose acetate and cellulose triacetate) for the integral asymmetric membrane and aromatic polyamides for the thin composite membranes.

Loeb and Sourirajan proposed the first asymmetric cellulose membrane [Loeb and Sourirajan, 1963]. Furthermore, the membrane performance was improved by using cellulose diacetate (CDA), cellulose triacetate (CTA), and their blend [Kim *et al.*, 2019]. While the CTA membrane exhibited improved performances, the CDA and CTA blend membrane demonstrated superior performance than the CTA membrane. In addition, the cellulose acetate membrane shows better chlorine resistance (up to 1ppm) property. Nevertheless, the acetate group present in these membranes is susceptible to hydrolysis under high acidic or basic medium, and these membranes are also vulnerable to microbial attack, according. To avoid hydrolysis of the acetate group, the operating pH for this membrane is 4–6 [Ibrahim *et al.*, 2020].

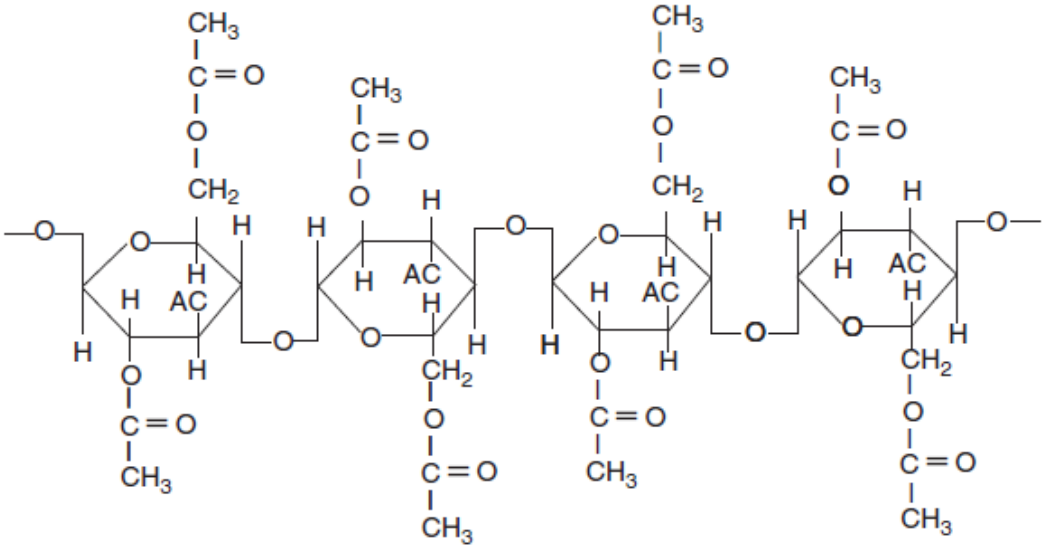


Figure 1.8. Chemical structure of cellulose triacetate polymer of RO membrane [Kumano, 2013].

The polyamide materials, proposed by *Richter and Hoehn*, are described as aromatic polymers with substantially linear condensation. Although the water permeability from this membrane was found to be lesser than the cellulose acetate membranes, it exhibited a comparable NaCl rejection (99%) [Richter and Hoehn, 1971].

Later in 1979, a major milestone was achieved when *Cadotte* introduced polyamide thin film composite (TFC) membranes. The polyamide membrane was produced from the interfacial polymerization of m-phenylenediamine (MPD) and trimesoyl chloride (TMC) on a microporous polysulfone (Psf) support, which was supported by a non-woven polyester fabric. Compared to the cellulose acetate membranes, the fabricated polyamide membrane showed a higher water permeance (0.73 LMH/bar) and a similar NaCl rejection (99%). This membrane also had better stability in acidic and alkaline environments [Cadotte *et al*., 1980].

Polyamides can be used over a wider pH range, approximately from 5-9. The single greatest disadvantage of these membranes is their susceptibility to oxidants and free chlorine in particular. This is because of the structure of the polyamide which contains residual diamines. It is these residual linkages that cause its sensitivity to chlorine [Kumano, 2013].

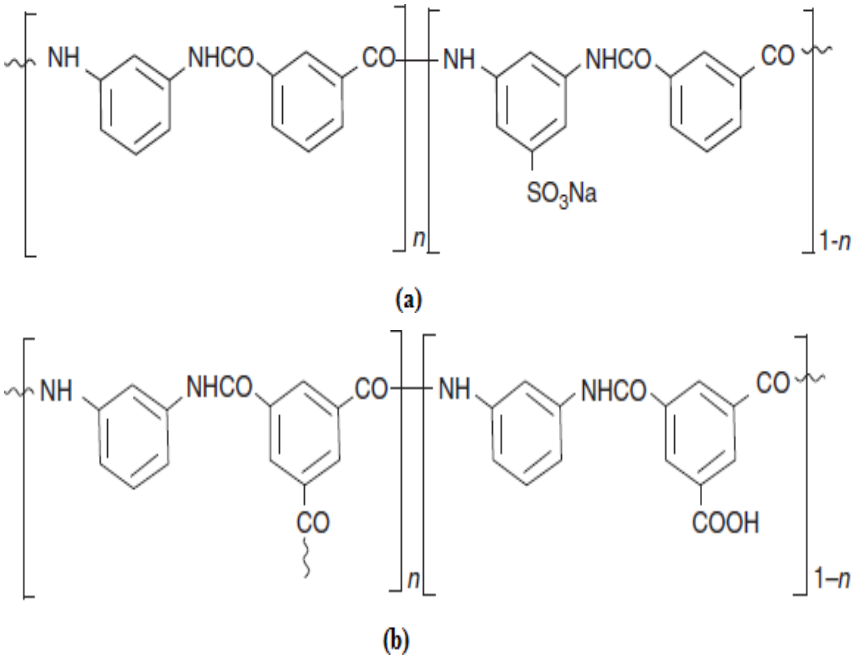


Figure 1.9. Chemical structure of polyamide polymer of RO membrane: (a) linear aromatic; (b) crosslinked aromatic [Kumano, 2013].

Figure 1.10 Structure of the synthesized polyamide RO membrane with the top and cross-sectional morphologies.

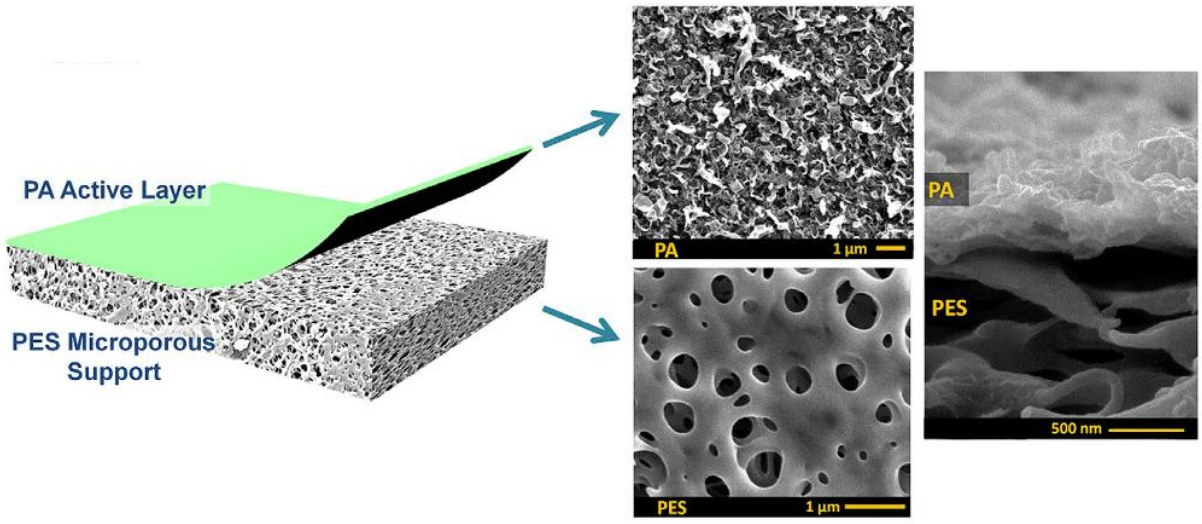


Figure 1.10. Structure of the synthesized polyamide RO membrane with the top and cross-sectional morphologies [Khorshidi *et al*., 2016].

Some other RO membrane materials are shown in Figure 1.11. Polypiperazineamide is used for low-pressure RO membranes and also for nanofiltration membranes at present. A composite membrane using polyether was developed in 1982.

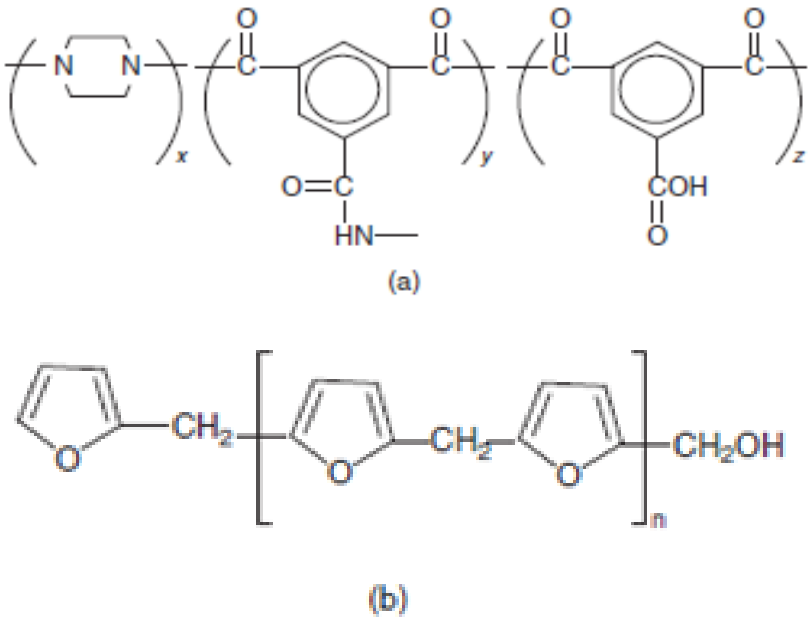


Figure 1.11. Chemical structure of others polymer of RO membrane: (a) polypiperazineamide; (b) crosslinked polyether [Kumano, 2013].

1.2.2.2. Inorganic membrane

These membranes, which are made from ceramics (aluminium, zirconium or titanium oxides), are chemically, mechanically and thermally more stable than organic membranes [Hamlaoui *et al.*, 2002]. Inorganic membranes are resistant to chlorine and other disinfectants and can withstand steam treatments making them less vulnerable to biofouling with a very long lifetime in water treatment. Unfortunately, the high fabrication cost and the poor process ability (it is hard to make flexible flat sheet or hollow fibers.) prevent them from becoming as popular membrane material as organic polymers. Yet, inorganic membranes "deserve more attention" as they require much smaller foot print and the process becomes more energy efficient, which results in a life-cycle cost less than the existing membrane systems. Particularly, for the treatment of organic liquids, inorganic membranes seem more desirable, since swelling of the polymeric membranes causes deterioration of separation performances. There are different inorganic membranes but not many show RO membrane performance. Zeolites are capable of providing the required desalination properties while being potentially tolerant to feed waters which readily foul polymer membranes, and/or can withstand more cost-effective cleaning methods [Duke, 2009].

1.2.3. Technical specifications of RO membrane

The reverse osmosis membrane has many technical specifications where each type has well-defined values for these specifications that distinguish it from other types:

- Material.
- Effective membrane area.
- pH.
- Temperature.
- Resistance to bacterial attack.
- Resistance to damage by chlorine.
- Typical rejection of salts.
- Typical rejection of nitrate.
- Typical treated water production.
- Turbidity allowed in feed water.
- Iron allowed in feed water.
- Relative cost.

1.2.4. Module configuration of RO membrane

In literature, four different types of RO membrane modules such as plate and frame, tubular, spiral wound, and hollow-fiber **(**HF) can be found. Among the modules reported, the plate- and frame and spiral wound modules are composed of flat sheet membranes. In the industrial point of view, the RO membrane module should have high resistance to fouling, low cost, and ease of cleaning. Furthermore, membrane module with high packing density such that a large area of the membrane can be packed in a small volume will be more preferable as it improves the compactness of the module, easy installation, and cleaning. Thus, plate and- frame and tubular modules became outdated as these suffer from low packing density. The state of the art RO membrane modules are based on the spiral wound and HF modules [Ibrahim *et al*., 2020].

1.2.4.1. Hollow-Fiber module

The HF modules (Figure 1.12), developed by Mahon at Dow, were fabricated using cellulose acetate as the membrane material. The available polymers in hollow-fiber elements for RO are cellulose triacetate, cellulose diacetate, and aromatic polyamide [Ibrahim *et al*., 2020].

The outer and the inner diameters of the hollow fibers are very fine, respectively about 0.04–0.12 mm and 0.1–0.3 mm. The outer-inner diameter ratio is >2 because the fiber requires a thick-walled cylinder to provide the compressive strength necessary to withstand the operating pressure. In general, HF membranes exhibit high surface area when compared with the flat sheet membranes and do not need any support. Also, because of their high packing density, hollow-fiber membranes also provide considerably lower flux than do flat-sheet and spiral-wound membranes **[**Kumano, 2013; Ibrahim *et al*., 2020**]**.

A continuous hollow fiber is wound into a bundle around a core tube as a feedwater distributor. The core tube pipe is sealed at the product-water end and is positioned in the center of the hollow-fiber bundle. Both ends of the fiber bundle are embedded in an adhesive material as a resin layer. The resin layer is cut to open the fibers at each end.

The hollow-fiber membrane module consists of a pressure vessel and an element containing the hollow-fiber bundle. The hollow-fiber bundle is then installed in a pressure vessel and an O-ring seal is placed in the product-water end of the tube sheet, against the pressure vessel wall, to prevent the high-pressure brine water flow from entering the pressure vessel and

mixing with the product-water flow. The feedwater flow enters the hollow-fiber element from a perforated feed tube placed in the center of the membrane bundle. The feedwater stream then flows radially outward from the center core tube to the brine collection channel at the outside of the element.

When the feedwater stream attains maximum velocity, it enters into the module; at minimum velocity, it approaches the outer edge of the membrane bundle. The rate of recovery from a hollow-fiber element ranges from 40% to 75% for feedwater and brackish-water, respectively, and between 25% and 60% for seawater. The recovery rate is typically higher in hollow-fiber than in spiral-elements wound elements [Kumano, 2013].

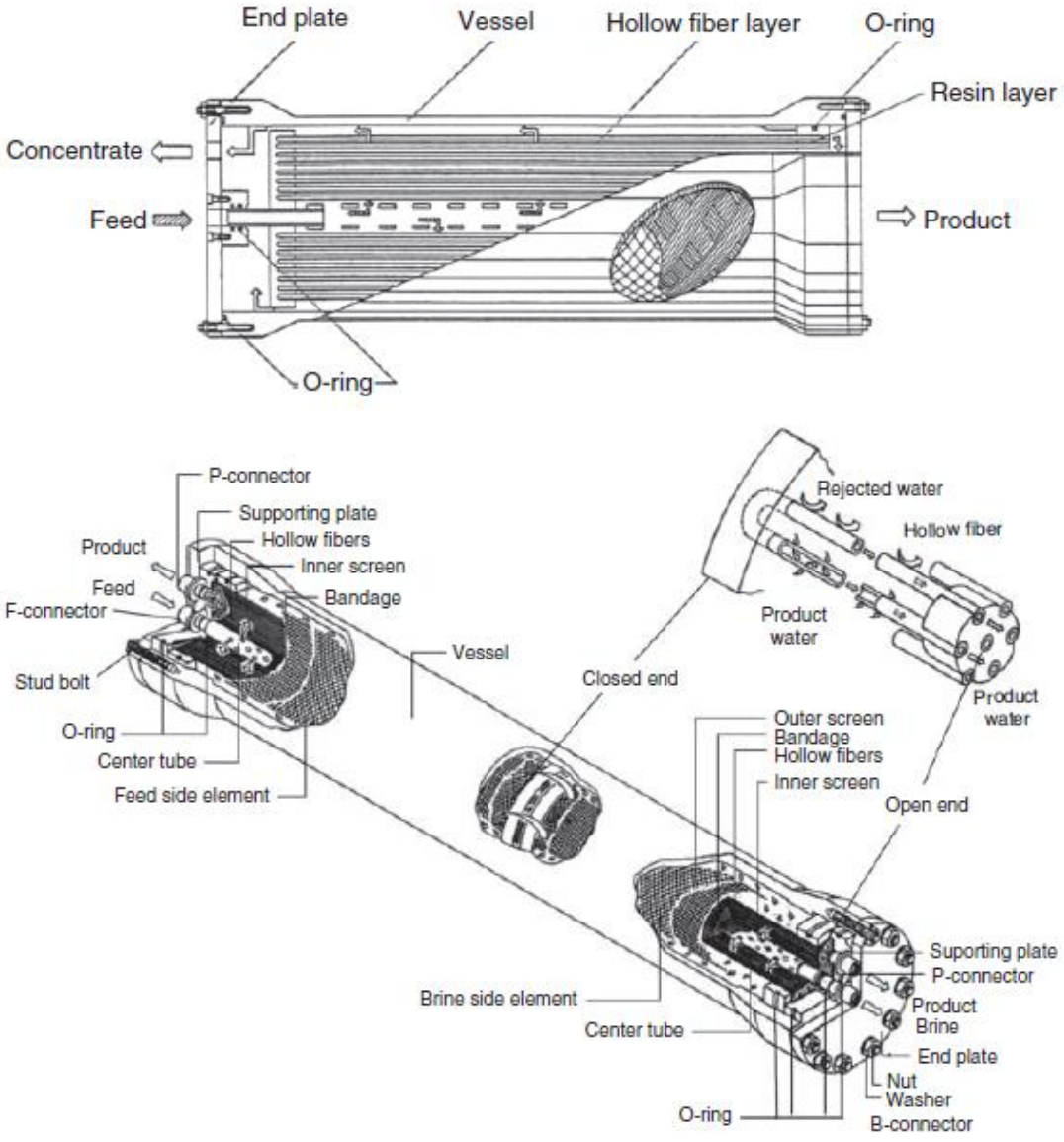


Figure 1.12. Hollow-fiber membrane modules [Kumano, 2013].

1.2.4.2. Spiral-Wound module

The spiral-wound module (Figure 1.13) is made up of flat sheet RO membranes and currently used membranes for RO desalination in commercial scale. Most of the commercial spiral wound modules consist of TFC membranes [Ibrahim *et al*., 2020]. This technology was developed, in 1968, by Gulf General Atomic under the sponsorship of OSW [Westmoreland; 1968].

The spiral-wound configuration consists of two sheets of membrane separated by fabric material. This fabric material both supports the membrane against the operating pressure and provides a flow path for withdrawal of the permeate water. The membrane envelope is sealed with an adhesive on three sides to prevent contamination of the permeate water. The fourth side is attached to a permeate-water tube that has holes within the edge seal to allow for removal of permeate water from the porous product-water spacer. The membrane envelope is rolled up around the central permeate-water tube, with a plastic mesh spacer positioned between the facing membrane surfaces, in a spiral pattern. The mesh spacer not only separates the membrane surfaces but also provides a flow path for and turbulence in the feed/reject water flow of each element. The elements are equipped with an outer wrap to contain the feed/reject water flow in the mesh passageway and brine seal to ensure that the feed/reject water flow passes through, around, the element and not. Spiral-wound elements are installed in a pressure vessel that is usually fabricated from fiberglass-reinforced plastic. The pressure vessel inside diameter is sized to match the outside diameter of the element's brine seal. Pressure vessels are designed and fabricated to accommodate one to eight elements and operating pressures ranging from 60 to 90 bar in seawater desalination applications.

Feedwater enters on one side of the pressure vessel and flows through the first element and then through the permeate-water spacer into the permeate-water tube. The reject water from the first element flows to the second element, and the reject from this second element becomes the feed to the next element. The reject water from the last element flows out from the pressure vessel. The element permeate-water tubes in the pressure vessel are interconnected by filaments that contain O-ring seals to prevent permeate-water contamination. The permeate water can flow out the pressure vessel from either end of the pressure vessel. The minimum brine (reject) water flow rate in an element is limited and therefore is used in low-recovery elements. In high-recovery systems, a arrangement of pressure vessels are arranged in a multistage configuration [Kumano, 2013].

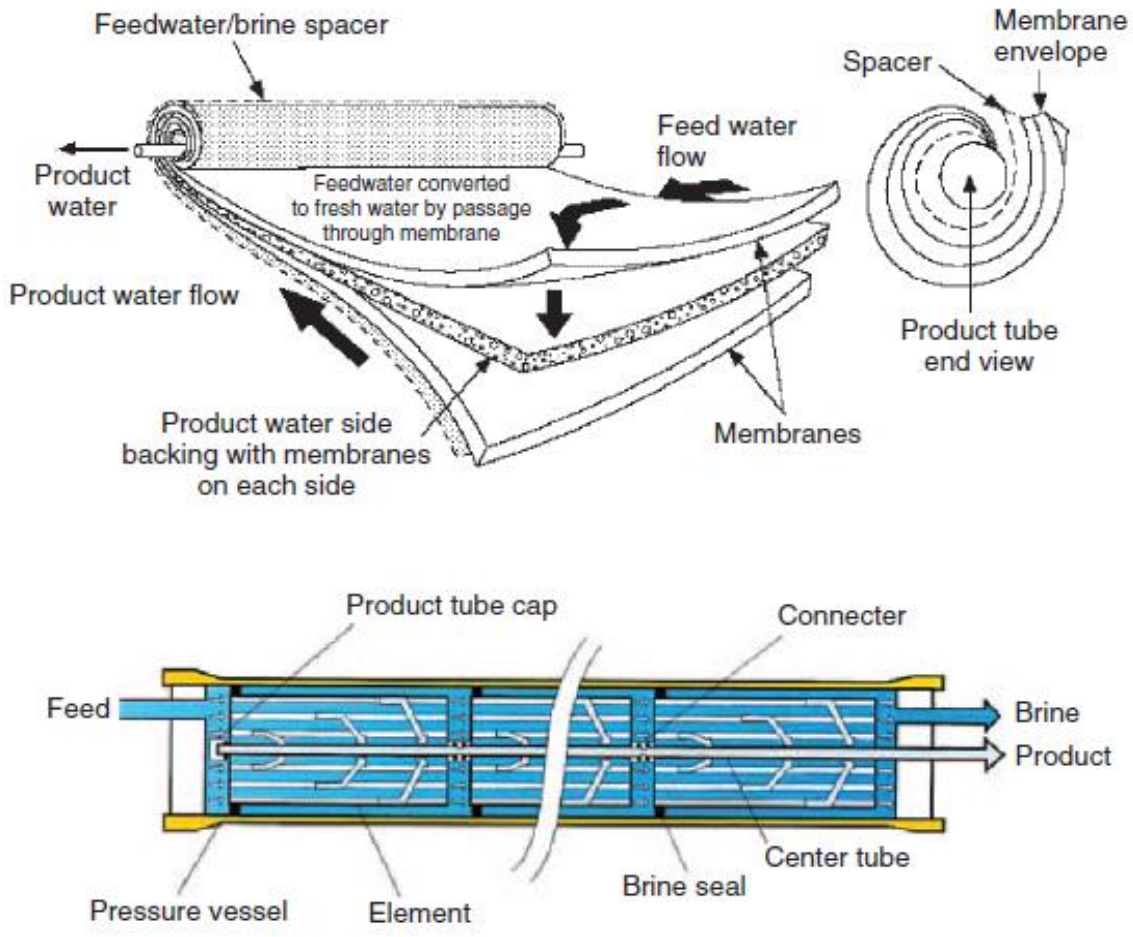


Figure 1.13. Spiral-wound module [Kumano, 2013].

1.2.4.3. Flat-Sheet (Plate-and-Frame) module

In the plate-and-frame configuration (Figure 1.14), circular sheets of membrane are sealed to molded plates. These plates provide protective support against operating pressure and in flow channels against permeate water. The plate-and-frame configuration is conceptually similar to the conventional plate-and-frame format used in gas separation and low-pressure applications, for example, except that a typical higher fluid operation pressure is applied, especially in RO applications. The membrane package is installed in a pressure vessel designed and fabricated to withstand operating pressure ranging from 30 to 200 bar. A stack of parallel porous plates is used to support the membrane on each side of the porous plate. Pressurized feedwater enters the top of the pressure vessel and flows between the parallel stacks of membranes and porous plates. Permeate water passes through the membrane and into the porous plate to be routed to the product water collection system and then out of pressure vessel. As the feed/reject water stream passes across the membrane, it becomes concentrated and eventually leaves the pressure vessel as a concentrate or reject [Kumano, 2013].

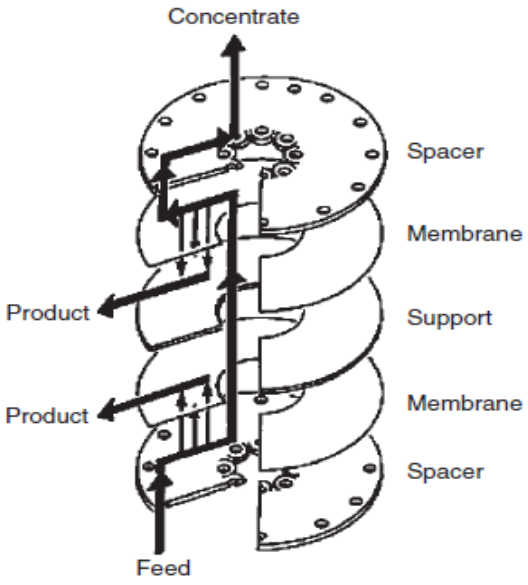


Figure 1.14. Plate-and-frame module [Kumano, 2013].

1.2.4.4. Tubular module

The tubular membrane module (Figure 1.15) consists of a tube-type membrane that is similar in structure to the hollow-fiber membrane. The perm-selective (i.e., permeate-water selective) membrane is installed inside the tube, which serves as the pressure vessel. Its inner diameter is 0.5–1 in. Feedwater enters through one end of the tube, where the membrane is sealed to the tube to prevent contamination of the product water. The brine water flows through the other end of tube and is routed to additional tubes in series or to wastewater. The main advantages of the tubular RO membrane module are (1) tolerance to high concentrations of turbidity and suspended solids in feedwater and (2) contamination resistance mechanical cleaning. The main disadvantage is the design complexity, with a large number of components (tubes, O-ring sealing devices, etc., in the membrane area of the pressure vessel.

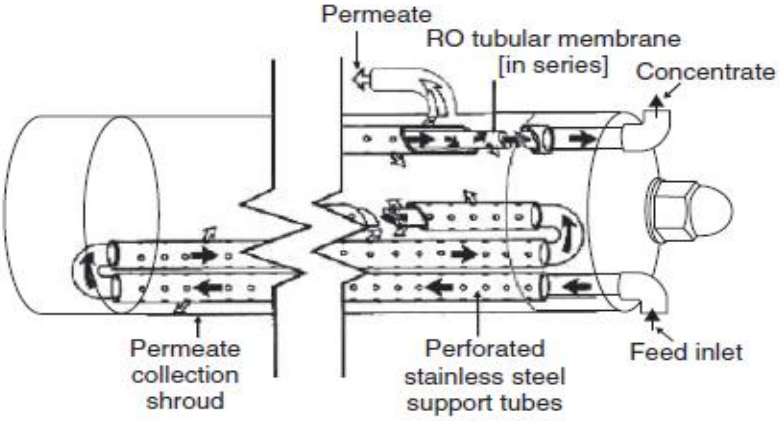


Figure 1.15. Tubular module [Kumano, 2013].

1.3. RO performance indicators

The performance indicators help to evaluate the performance of RO process, identify anomalies and assist with troubleshooting. With these indicators, the customer can be advised on maintenance, cleaning or membrane replacement. The main performance indicators of RO system are cited bellow.

1.3.1. TDS rejection

TDS rejection rate measures the total dissolved solids that RO membrane removes from feed water. It is used to describe the capacity of RO membrane in removing impurities from feedwater stream and is generally expressed in percentage. If TDS rejection drops below 80%, the RO membrane is performing poorly and should be replaced.

1.3.2. Permeate flow rate & Recovery

Permeate flow rate is an indicator that reflects the volume of pure water produced by RO membrane per unit time under certain test conditions. Recovery is used to describe the percentage of RO feedwater that is converted into permeate. Ideally, the rate of recovery should always be at least 20%. If it has more and more wastewater and less pure water, it's a sign that RO membrane is clogged.

1.3.3. Pressure drop

Pressure drop involves measuring water pressure before and after the RO membrane. The pressure drop will remain constant if there are no obstructions within the membrane.

1.3.4. Energy consumption

The energy consumption is an RO system represents between 50 and 60 % of the total cost of the process; with this value it being the key factor for the use of RO technology. Initially, the energy consumption exceeded 15kWh/m^3; today, and with new advances in general, the consumption is in the order of 2,5 kWh/m^3.The energy consumption in an RO system was reduced by 80 %, between 1970 and 2022, due to lower energy consumption in each of the components of the RO plant. Such is the case for the pretreatment system, high-pressure pumps, the materials and configuration of the membrane, energy recovery devices and post treatment [Ahmed *et al*., 2019, Zarzo *et al*., 2018].

1.4. Factors affecting RO performance

Several factors can affect the RO performance which the understanding of the factors effects is very crucial. We provide a brief overview of those factors which can be investigated in three groups; membrane properties, feedwater characteristics and feed operational parameters.

1.4.1. Effect of membrane properties

Separation performance can be affected by many RO membranes properties, such as membrane material, porosity (pore size, pore size distribution and effective number of pores) and surface characteristics (hydrophobicity, roughness, and charge) [Madaeni *et al*., 2001, K. Košuti´c *et al*., 2000].

1.4.2. Effect of feedwater properties

Feedwater properties have a considerable effect on the RO performance. Those properties are salt concentration, pH, oxidizing reduction potential, total suspended solid, turbidity and chemical oxygen demand [Odabaşı *et al*., 2022; Lipp *et al*., 1994].

1.4.2.1. Salt concentration

High salt concentration affects the permeability of different molecules across the membrane, because it increases the surface charge of the RO membrane which may reduce the ability of molecules to diffuse across it. However, a higher salt concentration will also increase the amount of salt passing through the membrane, which results in lower water quality for two reasons: first, less water is produced; Second, more salt is dispersed and dissolved in less water. Ultimately, high salt concentrations can cause scaling and decreasing the net driver pressure (NDP) (by increase osmotic pressure) which can decrease the permeate flow.

1.4.2.2. pH

The indicators of RO performance are influenced by pH as well as the composition of the feed water [Hoang *et al*., 2010; Qin *et al*., 2005; Wang *et al*., 2021]. Changes to the feed pH may alter the nature of the membrane surface charge, which can subsequently affect the membrane performance. Water flux was independent of feed pH, but salt rejection decreased at extreme pH values (i.e., below pH 5 and above pH 11). Over this pH range, the pH effects were reversible, indicating no permanent change in membrane structure. A fairly linear relationship

was reported between sodium chloride salt rejection and feed pH for their RO membranes due to the increasingly negative charge of the polyamide membrane surface [Van Wagner *et al*., 2009]. Other study has reported that the RO membrane had a high rejection capacity of heavy metals (Ni, Cu and Cr), which was influenced by pH and the presence of divalent cations such as Ca^{2+} and Mg^{2+} [Ozaki *et al*., 2002].

1.4.2.3. Oxidizing reduction potential (ORP)

The ORP may be used to determine the activity of an oxidizer such as chlorine, bromine, ozone and hydrogen peroxide, which the oxidizer can attack the RO membrane. A high ORP value may trigger the oxidation of membrane pores and affects membrane permeability. Maintaining the right ORP leveles helps ensure th effecient removal of conaminants [Xie *et al*., 2009].

1.4.3. Effect of feed operational parameters

1.4.3.1. Feed pressure

The applied pressure to feedwater is a critical performance component which it has a direct effect on pressure difference across membranes and an indirect effect on permeate flow rate and salt passage [Jiang *et al*., 2017]. In order to understand the impact of changing the feed pressure on an RO system, one must first consider the concept of net driving pressure (NDP) that represents the sum of all of the forces acting on the RO membrane. These may include pump or feed pressure; back pressure from line restrictions and storage tank; and osmotic pressure of the feed and permeate water. The productivity and salt rejection of the RO membrane increase as the feed pressure rises. The pressure should not be too high, which could cause the membrane to degrade over time.

1.4.3.2. Feed temperature

The permeate flow and the salt passage are strongly dependent on the operating temperature. As the feedwater temperature increases, the productivity of the RO membrane increases due to lower viscosity and higher diffusion rate of water at higher temperatures, which makes it easier for the water to permeate the RO membrane. The higher temperature of feedwater increases the temperature of the RO membrane, which the membrane pores allow the diffusion of salt more quickly [Lee and Ghaffour, 2019].

1.4.4. Effect of matter accumulation

RO membranes are subject to the matter accumulation, which leads to lower performances: permeate flow decreases for a constant applied pressure or pressure increases for a constant permeable flow. The accumulation of matter on the RO membranes can occur through two phenomena: concentration polarization and fouling. Despite sharing some similarities, they are two distinct phenomena. In summary, concentration polarization is a result of high-solutes concentration at the membrane surface, while fouling is the accumulation of particulate matter on the membrane surface.

1.4.4.1. Concentration polarization

Concentration polarization occurs when solutes are accumulated near the upstream face of the RO membrane surface because they are not able to pass through it. This results in a higher concentration of solutes at the membrane surface than in the solution which it can reduces permeability by generating an anti-osmotic pressure, lead to a considerable decrease in permeate flow, creates an additional resistance to mass transfer, cause fouling and/or scaling, poses a mass transfer resistance. A schematic of the concentration polarization phenomenon demonstrating the increased concentration in the feed boundary layer due to the retention of solute is shown in Figure 1.16 [Yokoyama *et al.*, 2022].

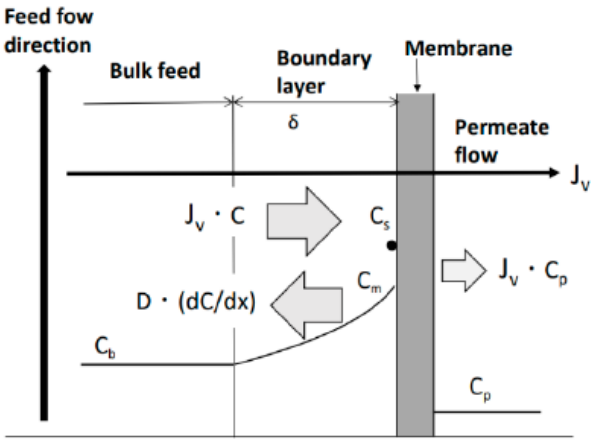


Figure 1.16. Concentration polarization phenomenon. J_v: permeate flux; $J_v C$: migration of solute with permeate flux; $D(dC/dx)$: diffusion of solute; C_m: solute concentration on membrane surface; C_s: saturated solute concentration; C_b: solute concentration of bulk feed; C_p: solute concentration of permeate flow; and *d*: thickness of boundary layer, [Yokoyama *et al.*, 2022].

1.4.4.2. Membrane fouling

Membrane fouling is a process whereby a solute is deposited on a membrane surface or in membrane pores. It can degrade the membrane's performance which it cause severe flux decline and affect the quality of the produced water. Severe fouling may require intense chemical cleaning or membrane replacement which this increases the operating costs of a treatment plant.

According to the type of the foulant substance accumulated onto the membrane surface, fouling can be categorized into biofouling organic, inorganic and colloidal. However, membrane fouling usually occurs in a combined pattern, where the four types of membrane fouling cannot be clearly distinguished. Figure 1.17 outlines scanning electron microscopy (SEM) images of different fouling types on membrane surfaces.

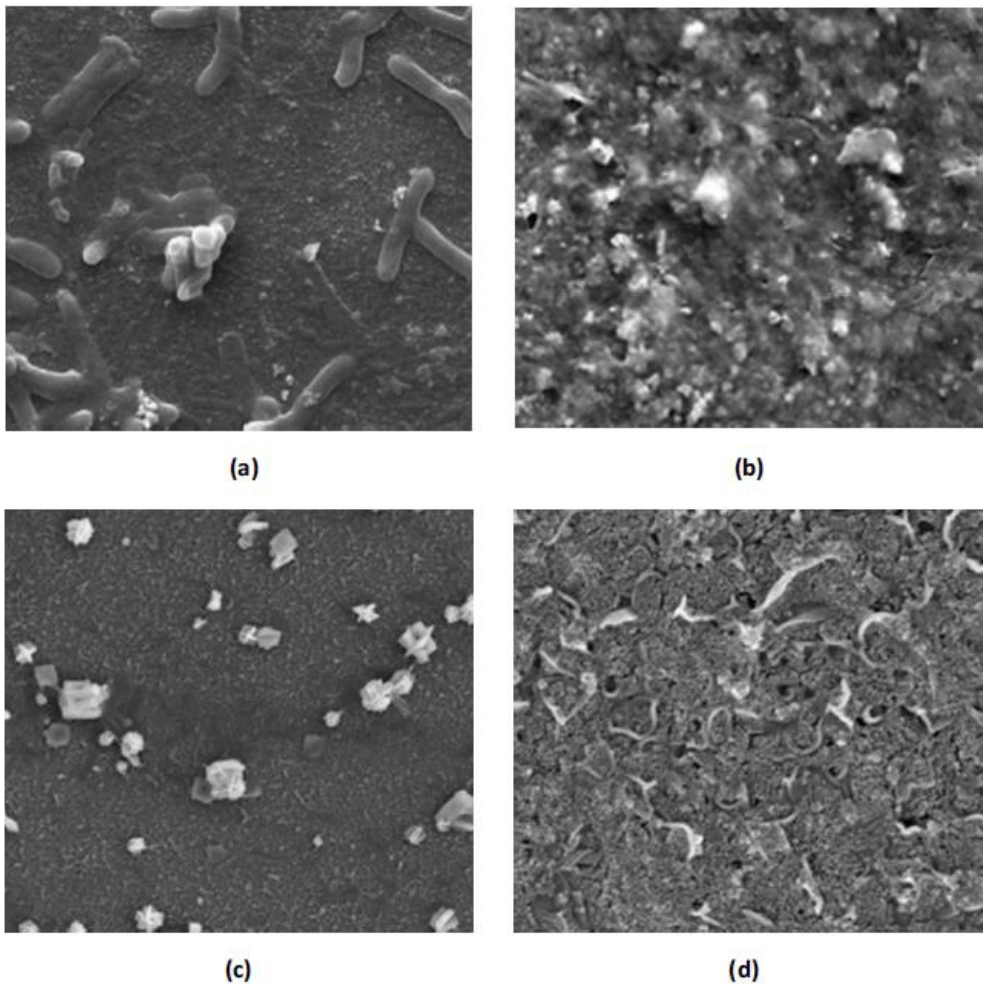


Figure 1.17. Scanning electron microscope of different fouling types [Jiang *et al*., 2017]. (a) Biofouling, (b) organic fouling, (c) inorganic fouling, and (d) colloidal fouling.

Biofouling

Biofouling is the formation of biofilm to an unacceptable degree which could cause huge operational costs. It can be occurs by the irreversible process of microorganism (bacterial cells, viruses, fungi, and algae) adhesion and proliferation on membrane surface resulting in forming a glutinous slime layer. This layer is formed when microorganisms grow at appropriate conditions of temperature and nutrients in water treatment utilities [Jiang *el al.*, 2017; Zheng *et al*., 2018; Qrenawi *et al.*, 2020]. There are two key components of biofilms, namely the bacteria and the extracellular polymeric substances (EPS) which are excreted by bacteria during the metabolism process [Yu *et al*., 2016]. In terms of bacteria activity and mobility, the biofilm can be formed in three successive stages: bacteria attachment, reproduction, and detachment (Figure 1.18).

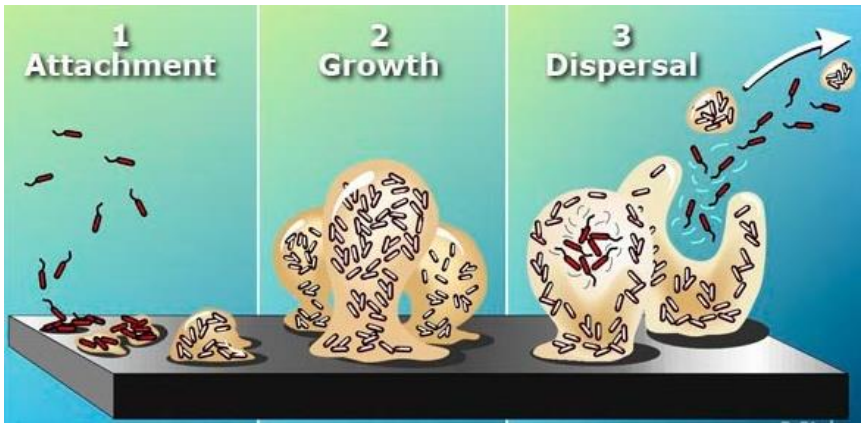


Figure 1.18. Biofouling formation on membrane surface [Cunningham *et al*., 2011].

Bacteria attachment is a dynamic process consisting of bacteria approaching and then adhering to the membrane surface, which is expected to be the most important stage in biofilm formation [Jiang *el al.*, 2017]. The next stage is bacteria reproduction, and during this period the attached microorganisms consume nutrients in the water and undergo proliferation and meanwhile excrete EPS [Matin *et al*., 2011]. The final stage is the bacteria detachment, and during this period the bacteria leave the mature biofilm due to lack of nutrients as well as the increase of population density. The bacteria find new sites to grow and the process repeats and new biofilm forms [Jiang *el al.*, 2017]. This phase is mainly controlled by nutrient concentration and the resultant growth rate, the mechanical stability of the biofilm, and the effective shear forces. Original surface properties of the membrane are masked by the biofilm [Flemming H.C., 1997]. Later stage of biofouling is more difficult to be controlled compared to earlier stage [Creber *et al*., 2010].

For SWRO plant, biofouling is controlled by the surrounding environment as well as the pretreatment of feed water. The population of bacteria in seawater is dependent on various environmental factors such as light, temperature, tides, currents, turbidity, and nutrients. SWRO module is more vulnerable to biofouling in hot climatic conditions. For example, the degradation of humic acid is much easier and greater at a temperature of 35°C than 18°C. The degraded small molecules are a source of nutrition for bacterial growth, so, the biofouling potential is expected at the increased temperatures. For the case of the Middle East and the Gulf Region, about 70% of the seawater RO plants suffer from biofouling problems which can be resolved by the application of several physical and chemical disinfection techniques [Qrenawi *et al.*, 2020].

Organic fouling

Organic fouling describes the attachment of the organic matters onto the external membrane layer. It results from various types of materials that are dissolved within the feedwater with the ability to be attached to the membrane surface. These organic matters usually consist of humic substances, polysaccharides, proteins, lipids, nucleic acids and amino acids, organic acids, and cell components. The previously mentioned materials will enhance forming an organic gel layer onto the membrane surface or inside the pores [Jeong *et al.*, 2016; Qrenawi *et al.*, 2020].

Adsorption is responsible for the first accumulation of the foulant onto the surface of the membrane. Organic fouling can results from interaction between different foulant species (electrostatic attraction, hydrophobic effect, and hydrogen bonding) and form aggregations in feeds. The removing organic foulants sedimented onto the membrane is commonly difficult, but possibly easy when using chemical substances [Myat *et al.*, 2014; Wang *et al.*, 2015; Lee *et al.*, 2017]. However, feed water chemistry, foulant-surface interactions as well as foulant–foulant interactions are three important factors affecting organic fouling.

Among RO membrane organic foulants that have received a strong research interests there are bovine serum albumin (BSA), alginate and humic acid. BSA is a type of protein while alginate is a typical representative of polysaccharide [Jiang *el al.*, 2017]. For example, the aggregation of BSA and humic acids could be formed by the bond between the amide groups of BSA and the hydroxyl groups of humic acids [Shao *et al.*, 2019].

Inorganic fouling (scaling)

Inorganic fouling also known as scaling consists of crystallization and deposition of sparingly soluble salts within the feed spacer of RO membranes under conditions where the solubility of the salts is exceeded and kinetics are favorable for crystal formation [Henthorne and Boysen, 2015]. The scale forming mechanisms (Figure 1.19) have been well detailed by *Antony* [Antony *et al*., 2011].

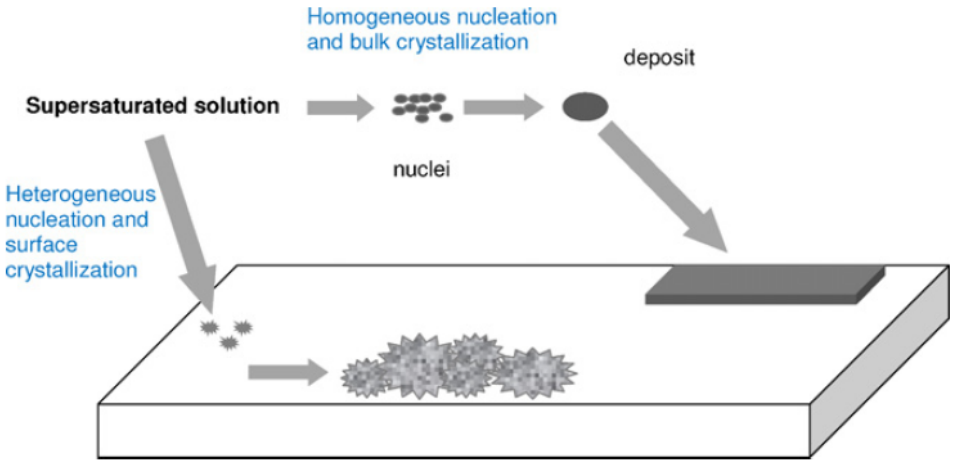


Figure 1.19. Main phases of inorganic fouling in an RO membrane [Antony *et al*., 2011].

The main inorganic fouling constituents are calcium carbonate ($CaCO_3$), calcium sulfate ($CaSO_4$), calcium phosphate $Ca_3(PO_4)_2$, sodium chloride (NaCl), magnesium sulfate ($MgSO_4$), magnesium carbonate ($MgCO_3$), magnesium bicarbonate $Mg(HCO_3)_2$, barium sulfate ($BaSO_4$), iron oxides (Fe_2O_3), aluminum oxide (Al_2O_3), and aluminum silicate in the form of kaolinite ($Al_2Si_2O_5(OH)_4$). Additionally, inorganic colloidal matter and residues including silica, silt, clays, and corrosion causing products, are greatly contributing to inorganic fouling [Lisdonk *et al*., 2000; Gabelich *et al*., 2005; Qrenawi *et al*., 2020]. When scaling occurs the permeability of the membranes decreases and the head-loss in the feed-brine channel increases. A higher feed pressure should be applied to maintain the de- sired flux causing an increase in energy consumption. In addition, the membranes should be cleaned more frequently, which can result in a shorter membrane life expectancy [Van de Lisdonk *et al*., 2000].

Scaling is mitigated primarily through the use of chemical addition during pretreatment and appropriate RO design to minimize super saturation. The basic science of crystal formation has been developed, but there is still room for significant research in crystal formation

kinetics, seeding and formation. However, there is a strong body of applied research in the mitigation of scaling using techniques such as pH adjustment, design of the RO system water recovery, use of dispersants and crystallization inhibitors. Consequently, scaling of RO membranes is usually easily mitigated once the predominant sparingly soluble salts are identified, through one or a combination of the above techniques [Henthorne and Boysen, 2015].

Colloidal fouling

Colloidal fouling of RO membrane is refers to the deposition and accumulation of colloids or particles on the membrane surface or into its pores; which results in forming a cake layer. Figure 1.20 shows a probable schematic illustration of colloidal fouling [Jiang *el al.*, 2017; Qrenawi *et al.*, 2020].

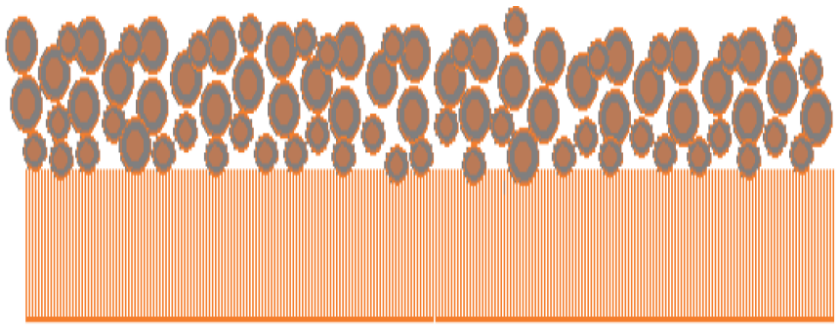


Figure 1.20. Schematic representation of colloidal fouling [Qrenawi *et al.*, 2020].

The cake layer formed by deposition of colloids on the membrane surface could lead to an additional hydraulic resistance and a serious concentration polarization, which could cause decrease of permeate flux and increase of operating pressure [Jiang *el al.*, 2017].

The colloidal aggregation rate could be determined by the frequency of particle collision and the attachment coefficient, while the coefficient is the reflect of the energy barrier that results from the summation of the van der Waals force and the electrostatic interaction force [Tang *et al.*, 2011].

The formation of a colloidal cake layer on RO membrane could also be affected by many factors such as feedwater characteristics (the concentrations of the foulants and the physiochemical characteristics) and membranes properties (operational conditions) [Ning *et al.*, 2005; Ju and Hong, 2014; Kim *et al.*, 2014].

1.5. Monitoring of RO performance by transport models

Monitoring of RO performance is necessary to identify early symptoms of failure in order to improve maintenance and extend the membrane lifetime. Several approaches have been used to monitor the RO performance, such as the measurement and the mathematical models. To monitor the performance indicator and the operating parameters, the RO systems should be equipped with the necessary instrumentation (sensors, flow meter and thermocouple…ect). For analyzing a RO membrane performance by mathematical models, there are three different approaches: physics-based, data-driven and hybrid models [An *et al*., 2015].

Physics-based models describe the behavior of a system. For example, in scope of RO membranes, Fick's law for solution-diffusion transport mechanism, Van't Hoff or Pitzer equation for osmotic pressure and film theory model for concentration polarization equation can be employed as physical models [Ang and Mohammad, 2015].

Due to complexity of membrane processes, it is difficult to express the whole system with physics-based models which are based on assumptions and apply generalized equations to every system [Solomatine and Ostfeld, 2008]. For this reason, data driven models are gaining much more attention for industrial plants since these models can extract nonlinear relationships between input and output without using complex physical models [Del Rio-Chanona *et al*., 2019]. In addition, huge amounts of data can be collected from industrial processes to monitor plant performance.

Hybrid models are defined as a combination of physics-based and data-driven models, however, the application of these models in the membrane field is not mature yet [An *et al*., 2015].

Mathematical models can be used to predict energy consumption (energy models), pressure drop (pressure models) and solution transport (transport models). Monitoring the energy consumption can help optimize the process, reduce energy costs, and improve sustainability. Monitoring pressure drop and solution transport can help optimize the process and prevent fouling and scaling.

Membrane transport models are theories that used to describe solution (solvent and solute) movement through the RO membranes in order to establish mathematical relationships that express separation characteristics as function of applied operating parameters and thus predict

the membrane performance. The success of transport model can be measured in terms of its ability to describe mathematically the experimental or operational data with the coefficients that are reasonably constant over the range of the operating conditions. However, the transport mechanism within RO systems is quite complex to understand, as many researchers have attempted to model such systems using various assumptions that simplify the overall transport models attained. There are three types of transport models that can used to describe the performance of an RO system such as phenomenological, mechanistic and scaling/fouling models.

1.5.1. Phenomenological transport models

Phenomenological transport models are based on the principles of non-equilibrium or irreversible thermodynamics which they assume that the membrane is not far from equilibrium and so fluxes can be described by phenomenological relationships [Kedem and Katchalsky, 1958; Spiegler and Kedem, 1966; Jonsson, 1980; Soltanieh and Gill, 1981].

As a result, phenomenological models assume that the membrane is simply a black box; hence no insight into the exact transport mechanism can be deduced. These models don't require information on mechanism of transport. Hence, they are independent of the transport mechanism in the membrane, as well as the membrane structure. It should also be noted that phenomenological models, derived from real time plant data, are useful for the calculation of permeate and rejection characteristics that also incorporate concentration polarization [Subramani and Panda, 2014].

1.5.2. Mechanistic transport models

Mechanistic transport models take into consideration the membrane transport mechanism, the physiochemical properties of membrane and solution. If all of the information on the membrane and solution are available, then one can predict the membrane performance without having experimental data under actual operating conditions.

Mechanistic transport models were classified according to the assumptions made about the RO membrane porosity which there are two approaches (porous and nonporous) to explain water purification mechanism. A fundamental difference exists between the assumptions of the porous and nonporous membrane models. While both mechanistic models had some

success in predicting RO separations, the controversy of whether a RO membrane is or porous or no porous is still a point of debate.

Non porous models assume that the membrane is nonporous; that is, transport takes place between the interstitial spaces of the polymer chains or polymer nodules, usually by diffusion. For such membranes called perfect membranes, a study has calculated defined theoretical levels of solute separations in RO from solubility measurements.

According to the solution-diffusion mechanism, membranes offering solute separation levels lower than these theoretical levels are qualified as imperfect and RO is only limited to perfect membranes [Riley *et al*., 1967]. Other research has explained RO separation on the basis of solute partition coefficients between water and the cellulose acetate material of the membrane [Anderson *et al*., 1972].Some studies have explained the selectivity of membranes for different ions on the basis of the relative free energy of the interaction between water and the membrane sites [Eisenman, 1962]. Among the porous models found in the literature are: solution diffusion model, solution-diffusion-imperfection model and extended solution diffusion model.

Porous models assume that the membrane is porous [Chen *et al*., 2011; Albo *et al*., 2014; Hagihara *et al*., 2014] and transport takes place through pores that run the length of the membrane barrier layer; as a result, transport can occur by both diffusion and convection through the pores. The most force driving force for water-solute separation is the pressure difference applied across the membrane.

One hypothesis holds that water molecules wet the membrane surface by hydrogen bonding to the polymer polar groups [Reid and Breton, 1959]. Under the influence of the applied pressure, water molecules manage a passage way through the interstitial polymeric spacing's. Therefore the hydrophilic nature of the polymer is a factor. The more hydrophilic the polymer, the greater the density of its polar substituent; and therefore less pressure may be required to intrude water, as into the pores of the hydrophilic filters. The water molecules thus permeate the RO membrane. However the hydrated ions are too large to pass through the RO membrane pores.

According to *Dytnerskii* [Dytnerskii *et al*., 1972], the surface of RO membrane is assumed to contain capillary pores of various sizes. When a hydrophilic RO membrane is in contact with

an aqueous solution of an electrolyte, an equilibrium layer of bound water forms both the membrane surface and the walls of the capillaries. The hydrated ions, because of their size, are not transmitted through most of the capillaries. On application of pressure, liquid flows through the capillaries disrupting the initial equilibrium and decreasing the thickness of the bound water layer on the membrane surface; simultaneously, the bound water equilibrium is reestablished by the interaction of the membrane with the hydrated envelopes of close-by ions which are thus partially dehydrated and reduced in size so as to be able to pass through the membrane capillaries. Among the porous models found in the literature are: preferential sorption-capillary flow model, surface force-pore flow model, finely porous model.

1.5.2.1. Solution diffusion model

The solution diffusion model assumes that the membrane is homogenous, nonporous and has no imperfections that affect its efficiency. According to this model, solvent and solute molecules dissolve in the membrane on the high-pressure side, diffuse through the non-porous surface layer of the membrane independently, and emerge on the low-pressure side. This results in separation because the diffusion rates of the solvent and solute are different [Lonsdale *et al*., 1965].

1.5.2.2. Solution-diffusion-imperfection model

The solution-diffusion-imperfection model was an early modification of the solution diffusion model to include pore flow in addition to diffusion of solvent and solute through the membrane as the mechanisms of transport. This model assumes that there may be small imperfections or defects (pores) on the surface of membranes through which transport of solvent and solute can occur during the separation process. The coefficients in the solution-diffusion and solution-diffusion-imperfection models were defined to be functions of both pressure and concentration [Sherwood *et al*., 1967].

1.5.2.3. Extended solution diffusion model

The extended-solution-diffusion model was proposed because it was assumed that the solution diffusion model did not explain the negative solute rejections found for some organics. They pointed out that the solution diffusion model does not take into account possible pressure dependence of the solute chemical potential which, while negligible for inorganic salt solutions, can be important for organic solutes [Burghoff *et al*., 1980].

1.5.2.4. Finely porous model

The finely-porous model, proposed by Merten [Merten, ,1966] and modified by Jonnson and Boesen [Jonnson and Boesen, 1975], assumes that transport of water takes place by viscous flow through uniform membrane pores and that transport of solute occurs by both diffusion and convection in these pores. In this model, the friction between solute and solvent molecules, as well as the thickness of the membrane material was taken into account when studying solute and solvent transport across the membrane.

1.5.2.5. Preferential sorption-capillary flow model

This preferential sorption-capillary flow model hypothesized that the transfer of solute and solvent across the membrane will take place only through the microscopic pores of the membrane, but the "preferential sorption" will be for the water that will be adsorbed on the walls of the pores, while the salts will be sequestered and rejected from passing through for physical and chemical reasons [Sourirajan, 1970].

1.5.2.6. Surface force-pore flow model

The surface force-pore flow (SFPF) model is a two-dimensional extension of the finely porous model. While the finely-porous model considers only axial solute concentration gradients, the SFPF model recognizes that the solute concentration in a RO membrane pore may be a function of radial as well as axial position. The SFPF model assumptions are [Matsuura and Sourirajan, 1981; Sourirajan and Matsuura, 1985; Dickson, 1988; Bhattacharyya and Williams, 1992c]:

- Water transport through the membrane occurs in pores by viscous flow;
- Solute transport takes place by diffusion and convection in the membrane pores;
- Transport of both water and solute through the membrane pores is determined by interaction forces, friction forces, and chemical potential gradients of the water and solute;
- The pores of the membrane are cylindrical and run the length of the membrane barrier layer;
- A molecular layer of pure water is preferentially sorbed on the pore wall;
- A potential field controls the solute distribution of the membrane pore.

1.5.3. Scaling/fouling transport models

Mathematical models can be used to predict the scaling potential and fouling rate of RO membranes under different operating conditions. Monitoring these parameters can help prevent fouling, scaling, and other issues.

1.5.3.1. Constant pressure pore-blocking model (Hermia Model)

The Hermia model is one of the equations found in the literature that allows determination of the mechanism of membrane blockage during filtration under constant pressure [Hermia, 1982]. The model describes the change in the efficiency of the filtration process using a two-parameter differential equation. To identify the fouling mechanism during the reverse osmosis process, a mathematical model describing the drop in flux over time can be used [Piekutin, 2021].

1.5.3.2. Scaling-based flux model

Three types off scales precipitation mechanisms related to the decline in permeate flux in RO membranes are proposed: cake formation, surface blockage, and mixed crystallization. The convergent values of decline in permeate flux by each mechanism were studied using a newly proposed scaling-based flux model [Matin *et al*, 2019; Yokoyama *et al*., 2022].

1.5.3.3. Pseudo N^{th} order model

The PNO equation was originally proposed for expressing solid-liquid adsorption [Lagergren, 1898; Blanchard *et al*., 1984; Morais *et al*., 2007; Özer, 2007; Morais *et al*., 2008; Leyva-Ramos *et al*., 2010; Tseng *et al*., 2014]. This adsorption mechanism is considered one of the mechanisms leading to RO membranes fouling and, consequently, to the reduction of permeate flow [Lee and Elimelech, 2006; Fritzmann *et al*., 2007; Qrenawi and Abuhabib, 2020; Ahmed *et al*., 2023]. It is assumed that, during the flow of solute-rich water through an RO membrane, a portion of this solute will be adsorbed on the membrane, while the remaining portion will be removed.

1.6. Memory effect of physical phenomena

Many transport models have been proposed to describe solute and solvent transport through the RO membrane. But, since the memory effect plays a key role in the kinetic of physical

phenomena, so a possible generalization of the classic desalination model would be a system with fractional order derivative which it is able to provide an accurate description of different nonlinear phenomena [Belhamiti and Absar, 2017].

1.6.1. Notion of memory effect

The memory means an existence of output at the present time that depends on the history of the change of the input (impact) on a finite (or infinite) time interval [Tarasov, 2018]. The memory effect has a considerable influence on the kinetic of dynamic systems witch this kinetic has nonlinear behavior giving rise to so-called anomalous kinetic. It is important to take into account this memory effect in order to better predict the outputs evolution of dynamic systems over time, and this will enable good control of the dynamic system (effective monitoring, optimal design).The anomalous kinetic of dynamic systems, caused by the memory effect, can be mathematically described by fractional calculus.

1.6.2. Mathematical description of memory effect by fractional calculus

The memory can be described by the function that is called the memory function, which is a kernel of the integro-differential operator [Tarasov, 2018]. The quantity of the memory can be described by the fractional order α [Du *et al*., 2013]. Higher fractional orders indicate a stronger memory effect, where past events or inputs have a more significant influence on the system's current state.

1.6.2.1. History of fractional calculus

Fractional derivative has a history as long as that of classical calculus. Machado [Machado, 2011] has stated that fractional calculus (FC) can be considered an old and yet new subject. It is an old subject because it began with some speculations by Leibniz (1695, 1697) and Euler (1730), and has developed gradually up to the present day. However, it can also be considered a new subject because it is only since the 1970s that fractional calculus has been the subject of conferences and specialized treatises.

Fractional calculus dates its inception in 1695, where *l'Hospital* wrote a letter to *Leibniz* asking how to interpret the newly invented derivative when n was not a natural number. Leibniz's response essentially told l'Hospital that it would be a problem for future generations of mathematicians. The concepts of fractional differentiation and fractional integration

attracted the attention of mathematical giants such as Liouville [Liouville, 1832], Riemann [Riemann, 1876], Abel [Abel, 1881], Laurent [Laurent, 1884], and Hardy and Littlewood [Hardy and Littlewood, 1928; Hardy and Littlewood, 1932]. The first description of physical system with memory was suggested by *Ludwig Boltzmann* in 1874 and 1876 [Boltzmann, 1874; Boltzmann, 1876].

The year 1974 saw two important events in the development of fractional calculus, the organization of the first conference on fractional calculus and its applications [Ross, 1974] and the publication of a book devoted to fractional calculus which dealt with mass and heat transfer problems in terms of semi-derivatives and semi-integrals [Oldham and Spanier, 1974]. In 1987, a book on fractional calculus was published first in Russian [Samko, Kilbas and Marichev, 1987], and then with an English edition in 1993.

1.6.2.2. Previous applications of fractional calculus

In recent decades, fractional calculus has received considerable attention in many scientific fields including physics, engineering, biology, mechanics, thermodynamics, finance and others.

Kashchenko and Nikitin [Kashchenko and Nikitin, 2014] have proposed a drainage system filtration model that takes into account the anomalous diffusion moisture transfer in soil caused by the fractal properties of a medium. It is shown that use of the fractal filtration model for soil leads to better agreement between the results of computations of groundwater profiles and the experimental data.

Zhai et al. [Zhai *et al*., 2015] have proposed a novel high-order alternating direction implicit (ADI) method for the three dimensional (3D) fractional convection–diffusion equations with a temporal fractional-derivative $\alpha \in (0, 1)$. In order to keep the fourth order accuracy to approximate the second order derivatives and the desirable tri diagonal nature of the finite difference equations, first a transformation have been proposed to eliminate the convection terms. Then the Riemann–Liouville fractional integral operator is used to eliminate the temporal fractional-derivative. Finally, two ADI schemes with convergence order are established respectively, where τ and h are the temporal and spatial step sizes. Numerical experiments are presented to show the high accuracy of the new method in comparison with the related works.

Padrino [Padrino, 2017] has used elements of fractional calculus to cast the small-time leading order diffusion equation in (x,t) space into a form for which an analytical solution has been obtained in the literature for the same boundary and initial conditions. For ease of computation, he has expressed the solution in terms of the Meijer G-function. He has compared the exact solution with previous numerical predictions, resulting in excellent agreement, thereby validating their numerical approach.

Ramírez et al. [Ramírez *et al*., 2017] have evaluated the diffusion mechanism based on Fick's second law and anomalous diffusion modifying the drying operating conditions temperature (T) and relative humidity (RH) on apple slices (cv. Granny smith). Drying was performed at 30 8C, 40 8C, 50 8C and 30%, 50%, 70%RH based on a 3^2 experimental design. The drying curves were analyzed to determine the effective diffusion (Deff) using two methods: Fick's second law and anomalous diffusion model based on fractional calculus approach. The results showed that the anomalous diffusion mechanism fit the experimental data better and revealed a super-diffusive behavior ($\alpha>1$). Therefore, Deff values were estimated using the anomalous diffusion model with $\alpha=1.735$. With respect to the use of anomalous diffusion model solution based on fractional calculus at different operations conditions allow to get better fitting of drying data than second Fick's law model, even keeping the Arrhenius behavior of Deff with temperature.

Obembe et al. [Obembe *et al*., 2018] have employed a temporal fractional flux relationship as a constitutive equation to relate the volumetric flow rate to the gradient of the pore pressure. The novelty of this paper entails interpreting the time fractional derivative operator in the flux relationship by the Grunwald-Letnikov (G-L) definition as opposed to the Caputo interpretation which has been widely considered. Subsequently, a numerical scheme based on the block-centered finite-difference discretization is formulated to handle the resulting nonlinear fractional diffusion model. In addition, a linear stability analysis is successfully performed to establish the stability criterion of the developed numerical scheme. An expression for the modified incremental material balance index was derived to assess the effectiveness of the numerical discretization process. Finally, numerical experiments were performed to provide qualitative insights into the nature of pressure evolution in a hydrocarbon reservoir under the influence subdiffusion. In summary, the results establish that subdiffusion regime results in the development of higher pressure drop in the reservoir.

Chamgoué et al. [Chamgoué *et al.*, 2018] have investigated birhythmicity in an enzymatic-substrate reaction described by a fractional-order extended van der Pol equation. The fractional derivatives are introduced in the system equations in order to model the memory property of the biological system. The residue harmonic balance scheme is used to study the periodic motions of the considered fractional-order van der Pol equations. It is shown that depending on system parameters and the fractional derivative order, the bistability area strongly in- creased. This fractional oscillator is analytically mapped, onto an ordinary bistable system with two stables amplitude. The obtained results clearly show an interesting collapse and revival of birhythmicity with the variation of the fractional derivative order. The amplitude and frequency of the fractional order van der Pol oscillator are derived. The analysis of amplitude equation corroborates with the results obtained by numerical simulations of the fractional-order differential equations describing the system.

De Souza Matias et al. [De Souza Matias *et al.*, 2018] introduced a new kinetic semi-empirical model for drying. The model was developed by arbitrary-order generalization of Lewis's kinetic equation that was obtained using the Laplace transform and Laplace's Inverse Transform. Kinetic data on soybean drying at 50, 60, 70, and 80 _C were retrieved to test the model which was compared to first-order Lewis's model and to Page's model by quantitative criteria. Results show that the process is best described by the fractional-order model and that arbitrary-order equation may be employed to adjust experimental data on drying, with better results among other models analyzed.

Kumar et al. [Kumar *et al.*, 2019] have studied the exothermic reactions model having constant heat source in the porous media with strong memory effects. The Caputo, Caputo-Fabrizio and Atangana-Baleanu fractional operators are used to induce memory effects in the mathematical modeling of exothermic reactions. The patterns of heat flow profiles are very essential for heat transfer in every kind of the thermal insulation. They have focused on the driving force problem due to the fact that temperature gradient is assumed. The mathematical equation of the problem is confined in a fractional energy balance equation (FEBE), which furnishes the temperature portrayal in conduction state having uniform heat source on steady state. The fractional Laplace decomposition technique is utilized to obtain the numerical solution of the corresponding FEBE describing the exothermic reactions. Some numerical results for the fractional exothermic reactions model are presented through graphs and tables.

Nikan et al [Nikan *et al*., 2020] have developed an efficient computational technique, stemming from the radial basis function-generated finite difference (RBF-FD), to solve the fractal mobile-immobile transport model (FMTM). The time fractional derivative of the FMTM is discretized via the shifted Grunwald-Letnikov formula with second-order accuracy. On the other hand, the spatial derivative is approximated using the local RBF-FD method. The stability and convergence analysis of the proposed method are proven via the energy method in the L2 space. The numerical results for the FMTM on regular and irregular domains confirm the theoretical formulation and efficiency of the proposed scheme.

Lemus-Mondaca et al. [Lemus-Mondaca *et al*., 2021] have demonstrated that the anomalous diffusion model based on fractional calculus can be used to model rehydration process and simultaneously provide a phenomenological understanding of the process. The food matrices assessed were aloe vera, apple, Chilean papaya, and bell peppers rehydrated at 20, 40, and 60 $^{\circ}$C. The results showed that the anomalous diffusion model was not only able to improve the goodness of fit of rehydration data (R^2>0.99), but also that Deff can be used under different temperatures given the goodness of fit of the Arrhenius model (R^2>0.88) compared with empirical and Fick's models. Finally, an anomalous diffusion model based on fractional calculus can be successfully used to model the rehydration process in food materials.

Mahdad et al. [Mahdad *et al*., 2021a] have conducted a comparative study between analytical and fractional solution of Fick's first- and second-order of diffusion to model the solar drying process of different products and dryers under different operating parameters. Laplace and Laplace's inverse transform have been used to obtain the solution in function with two parameters: the order index n and the fractional time index α of the above Fick's laws, and their parameters have been non-linearly optimized using a grey wolf optimization (GWO) algorithm. The results showed that the anomalous diffusion phenomenon during the drying process is best described by the fractional order model. Values obtained using the model MR12 were in better agreement with the experimental data than the values obtained using the other selected models with very acceptable statistical parameters.

Mahdad et al. [Mahdad *et al*., 2021b] have proposed two novel models based on semi-empirical and factional calculus incorporating non-integer time derivatives in the Fick's first law of anomalous diffusion. The experimental data has been collected from literature of fifteen kinetics investigated in a convective dryer under the effect of temperatures ranging from 40 to 80 °C at 10 °C interval, and thickness of the slices of 2 to 6 mm at 2 mm interval.

The collected experimental dataset was of apple slices (Golab variety). Results from this study were compared with a set of 64 thin-layer drying models previously published in the literature. The fitting capability of the models was compared using the mean of root mean square error MRMSE (%) of all kinetics and the global determination coefficient R^2. All models' constants and coefficients were optimized by dragonfly algorithm programmed in MATLAB software. Results showed that the fractional model is highly capable of describing the drying curve of the apple slices with a determination coefficient (R^2) of 0.99981, and average root mean square error (MRMSE) of 0.43 % in comparison to the best empirical models with R^2 of 0.99968 and MRMSE of 0.61 %.

Mirza et al. [Mirza *et al*., 2021] have studied the soil contamination transport phenomenon using fractional calculus. Specifically, a variant of non-integer fractional derivative known as Antangana–Baleanu fractional derivative is applied on one-dimensional advection diffusion equation to obtain a fractional model for the contaminant transport in soils. This fractional model is examined under the hypothesis of initial and generalized Robin type boundary conditions. The analytical expression of solution for contaminant transport in soil is derived for the fractional initial-boundary value problem for partial differential equation (PDE) of mixed type using integral transforms, namely, Laplace and finite sine–cosine Fourier transforms. The solution of the ordinary advection diffusion equation arises as a case of the obtained solution. The numerical results are obtained for initial concentrated loading and Heaviside unit step function as boundary conditions, from the analytical solution for various parameters of interest, and the corresponding graphs are plotted with the help of software MATHCAD. The graphs illustrate that the memory effects are remarkable for small values of time and ordinary for large values of the time.

El-Gazar et al. [El-Gazar *et al*., 2021] have presented a novel fractional model based on the *Riemann Liouville* fractional derivative to simulate the thermal performance of conventional solar still and show the effect of using hybrid nanofluid on the desalination system. The results of the fractional model are compared with the results obtained from the classical model, then compared to real experimental data under various climate conditions of Upper Egypt. The theoretical results reveal a perfect agreement between the proposed fractional model and the experimental data of the still with a percentage of error reached 1.486% in summer and 3.243% in winter compared to an error percentage of 24.1% and 20.08%, in case of applying the classical. Moreover, the performance of the modified solar still after adding

hybrid nanoparticles is also compared with the conventional solar still. The model is implemented using a hybrid nanofluid of alumina and copper oxide (Al_2O_3-CuO) with a concentration of 0.025% for each nanoparticle. The results show that using hybrid nanofluid raises the still daily productivity to 5.5239 kg/m^2/day in summer and 3.1079 kg/m^2/day in winter of an enhancement in the still output yield of 27.2% and 21.7% compared with still without nanoparticles. The average energy efficiency of the still in summer is also increased to 49.54% and 23.212% in summer and winter, respectively, with an augmentation of 12.6% and 11.85% in hot and cold climate conditions, respectively. In addition, the average exergy efficiency is raised by 22.5% in summer and 13.4% in winter by using hybrid nano.

1.6.2.3. Mathematical definitions of fractional derivatives

The definitions of the fractional order derivative are not unique which there exist several definitions, including: Grünwald–Letnikov, Riemann-Liouville, and the Caputo representation for fractional order derivative.

The Grünwald–Letnikov fractional derivative can be defined by the equations presented in the Table 1.1.

Table 1.1. The Grünwald–Letnikov fractional derivative.

Formula	Reference
$${}_{GL}D_{a,t}^{\alpha}y(t)=\lim_{n\to\infty}\left\{\frac{\left(\frac{t-a}{N}\right)^{-\alpha}}{\Gamma(-\alpha)}\sum_{j=0}^{N-1}\frac{\Gamma(j-\alpha)}{\Gamma(j+1)}y\left(t-j\left(\frac{t-a}{N}\right)\right)\right\}$$	[Li *et al.*, 2011]
$${}_{a}D_{t}^{\alpha}f(t)=\lim_{\substack{h\to 0\\ nh=t-a}}h^{-P}\sum_{r=0}^{n}(-1)^{r}\binom{p}{r}f(t-rh)$$	[Gupta and Ray, 2014]
$${}_{\alpha}D_{t}^{p}f(t)=\lim_{h\to 0}\sum_{j=0}^{\left[\frac{t-\alpha}{h}\right]}(-1)^{j}\binom{p}{j}f(t-jh)$$	[Chamgoué *et al.*, 2018]

The Riemann–Liouville fractional derivative can be defined by the equations presented in the Table 1.2.

Table 1.2. The Riemann–Liouville fractional derivatives.

Formula	Reference
${}_{RL}D_{a,t}^{\alpha}y(t)=\frac{1}{\Gamma(n-\alpha)}\frac{d^n}{dx^n}\int_0^t(t-\tau)^{n-\alpha-1}y(\tau)d\tau$	[Li *et al.*, 2011]
$D_x^{\alpha}(f(t))=\frac{1}{\Gamma(n-\alpha)}\frac{d^n}{dx^n}\int_0^x(x-t)^{n-\alpha-1}f(t)dt$	[Atangana and Secer, 2013]
${}_0D_t^{\alpha}\varepsilon(t)=\frac{1}{\Gamma(m-\alpha)}\frac{d^m}{dt^m}\int_0^t\frac{\varepsilon(\tau)}{(t-\tau)^{\alpha+1-m}}d\tau$	[Du *et al.*, 2013]
$D_a^{\alpha}(f)(t)=\frac{1}{\Gamma(n-\alpha)}\frac{d^n}{dt^n}\int_a^t\frac{f(x)}{(t-x)^{\alpha-n+1}}dx$	[Khalil *et al.*, 2014]
The left Riemann–Liouville fractional derivatives of order p. $${}_aD_t^p f(t)=\frac{1}{\Gamma(n-p)}\frac{d^n}{dt^n}\int_a^t\frac{f(\tau)}{(t-\tau)^{p-n+1}}d\tau$$	[Chamgoué *et al.*, 2018]
The right Riemann–Liouville fractional derivatives of order p. $${}_tD_b^p f(t)=\frac{1}{\Gamma(n-p)}\frac{d^n}{dt^n}\int_t^b\frac{f(\tau)}{(t-\tau)^{p-n+1}}d\tau$$	
${}_aD_x^{\alpha}(f(x))=\frac{1}{\Gamma(m-\alpha)}\left(\frac{d}{dx}\right)^m\int_a^x(x-\xi)^{(m-\alpha-1)}f(\xi)d\xi$	[Pakhira *et al.*, 2018]

The Caputo fractional derivative can be defined by the equations presented in the Table 1.3.

Table 1.3. The Caputo fractional derivatives.

Formula	Reference
$${}_{C}D_{a,t}^{\alpha}y(t)=\frac{1}{\Gamma(n-\alpha)}\int_{a}^{t}(t-\tau)^{n-\alpha-1}y^{(n)}\tau d\tau$$	[Li *et al.*, 2011]
$${}_{0}^{c}D_{x}^{\alpha}(f(x))=\frac{1}{\Gamma(n-\alpha)}\int_{0}^{x}(x-t)^{n-\alpha-1}\frac{d^{n}f(t)}{dt^{n}}dt$$	[Atangana and Secer, 2013]
$${}_{0}^{C}D_{t}^{\gamma}f(t)=\frac{1}{\Gamma(n-\gamma)}\int_{0}^{t}\frac{f^{(n)}(\eta)}{(t-\eta)^{\gamma-n+1}}d\eta$$	[Gómez-Aguilar et *al.*, 2014]
$${}_{0}D_{t}^{\alpha}f(t)=\frac{1}{\Gamma(n-\alpha)}\int_{0}^{t}\frac{f^{n}(\tau)}{(t-\tau)^{\alpha-n+1}}d\tau$$	[Gupta and Ray, 2014]
$$D_{a}^{\alpha}(f)(t)=\frac{1}{\Gamma(n-\alpha)}\int_{0}^{t}\frac{f^{(n)}(x)}{(t-x)^{\alpha-n+1}}dx$$	[Khalil *et al.*, 2014]
$${}_{a}D_{t}^{p}f(t)=\frac{1}{\Gamma(n-p)}\int_{a}^{t}\frac{f^{(n)}(\tau)}{(t-\tau)^{p-n+1}}d\tau$$	[Chamgoué *et al.*, 2018]
$${}_{a}^{C}D_{x}^{\alpha}(f(x))=\frac{1}{\Gamma(m-\alpha)}\int_{a}^{x}(x-\zeta)^{m-\alpha-1}f^{m}(\zeta)d\zeta$$	[Pakhira *et al.*, 2018]

2. Materials and methods

2. Materials and methods

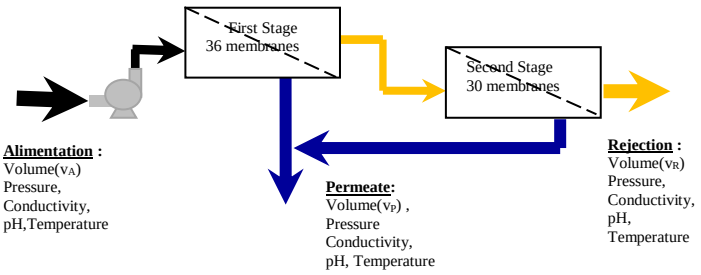
2.1. Experimental

2.1.1 Description of water treatment by RO process

The RO process was carried out at the antibiotic complex of Medea (North Algeria) for the production of ultra-pure water. The water stream, coming from the pre-treatment unit, is processed in the RO plant operating according to the scheme illustrated in Figure 2.1. The RO plant comprises eleven modules, each containing six membranes. They are arranged in two consecutive stages, where the first one includes six modules and the second consists of five modules. Each pressure vessel of the RO plant contains a spiral wound polyamide membrane. The technical specifications of the studied RO unit are summarized in Table 2.1.



(a)



(b)



(c)

Figure 2.1. The RO desalination process (a): Picture; (b): block flow diagram (c): Fractional modelling inputs and outputs to monitor the performance of the RO process.

Table 2.1. Technical specifications of the RO desalination process.

Specification	Parameter	Value
Membrane	Membrane type	ROGA® - HR 8.5" "spirale-wound"
	Number of modules (-)	11
	Number of membranes (-)	66
	Total surface area (m^2)	38.6
	Efficiency (%)	75
	Total treated water flow ($m^3.h^{-1}$)	92
	Permeate flow ($m^3\ h^{-1}$)	69
Alimentation	TDS ($mg.L^{-1}$)	1960 –30120
	Salinity (%)	≤1.3
	Turbidity (JTU)	≤0.19
	Total hardness ($mg.\ L^{-1}$)	≤1100
Operating conditions	Operating pressure (Bars)	35– 41
	Operating temperature (°C)	20 – 40
	Operating pH (-)	4 – 6

2.1.2. Construction of experimental data

The RO desalination system operates for only 8 hours per day during normal operation. As well, it will be completely stopped during some period for maintenance or when there is no need to produce water. Therefore, during the 4 years (35040 h) of monitoring, the experimental data points (2561) were only recorded during the operation time (5122 h). The experimental data were collected at the alimentation, permeate and rejection of the RO unit every 2 hours over a span of 4 years covering the lifespan of the RO membranes. Throughout the monitoring period, the RO membranes were not replaced but underwent 22 chemical cleaning operations, whose cleaning periods are presented in Table 2.2.

Table 2.2. Chemical cleaning cycles of the RO membranes.

Cleaning cycle	1	2	3	4	5	6	7	8
t (h)	3126	3414	3798	3942	4086	4566	5262	5766
τ (-)	0.09	0.10	0.11	0.11	0.11	0.13	0.15	0.16
Cleaning cycle	9	10	11	12	13	14	15	16
t (h)	6438	6606	6966	11142	11382	11526	11838	11886
τ (-)	0.18	0.18	0.19	0.31	0.32	0.32	0.33	0.33
Cleaning cycle	17	18	19	20	21	22		
t (h)	11982	12462	12822	13182	13734	15534		
τ (-)	0.33	0.35	0.36	0.37	0.38	0.43		

The experimental data of the studied RO desalination process were constructed through the following steps:

01 • Regular monitoring of instantaneous feed, permeate and rejection flows (Q^{inst}) as a function of filtration time (t), which are recorded using a flow-meter.

02 • Calculation of instantaneous volume values (v^{inst}) using the following relationship: $\mathbf{v^{inst} = Q^{inst} * t}$

03 • Calculation of the cumulative volume (v^{cum}) using the following relationship: $\mathbf{v^{cum}_i = v^{cum}_{i-1} + v^{inst}}$

04 • Calculation of the dimensionless cumulative volume (V) using the following relationships : $\mathbf{V = v^{cum} / v^{cum}_{max}}$

05 • Calculation of the dimensionless time (τ) using the relationship: $\mathbf{\tau = t/t_{max}}$

The experimental values of *v(t)* and *t* were transformed to dimensionless values by relating them to the maximum experimental value v_m and t_m, respectively. The maximum experimental values are presented by Table 2.3.

Table 2.3. Maximum experimental values of cumulative volume and filtration time.

Parameter	Alimentation	Permeate	Rejection
v_m (10^{+3} .m^3)	3603.78	2144.07	1496.72
t_m (10^{+3} .h)	51.22	51.22	51.22

The sum of permeability and rejection volumes should be equal to the feed volume, but the values presented in Table 2.3 show that there is a difference between them. This difference can be explained by the failure of the measuring instruments during the four-year study period.

2.2. Modelling

2.2.1. Model approach

The fractional models, established in this study for the RO process, were developed from the PNO equation that was originally proposed for expressing solid-liquid adsorption [Lagergren, 1898; Blanchard *et al*., 1984; Morais*et al*., 2007; Özer, 2007; Morais *et al*., 2008; Leyva-Ramos *et al*., 2010; Tseng *et al*., 2014]. This adsorption mechanism is considered one of the mechanisms leading to RO membranes fouling and, consequently, to the reduction of permeate flow [Lee and Elimelech, 2006; Fritzmann *et al*., 2007; Qrenawi and Abuhabib, 2020; Ahmed *et al*., 2023]. It is assumed that, during the flow of solute-rich water through an RO membrane, a portion of this solute will be adsorbed on the membrane, while the remaining portion will be removed. The adsorption kinetics of the solute can be expressed by equation (1) [Adda *et al*., 2020; Mesli *et al*., 2022]:

$$\frac{dq(t)}{dt} = k_n^{'}\left(q_{max} - q_t\right)^n \quad (1)$$

Where:

- *q(t)* is the adsorbed amount of solute per unit mass of the membrane (mg g^{-1}).
- q_{max} is the maximum adsorption capacity of the membrane per unit mass of the membrane (mg g^{-1}).
- *t* is the filtration time (h).
- $k_n^{'}$ is the rate constant of adsorption reaction of the PNO equation ((mg g^{-1})$^{1-n}$ h^{-1}).
- *n* is the order of adsorption reaction (-).

On the other hand, membrane fouling can be characterized by the retention rate (γ) which represents the ratio between the adsorbed mass (m_{ad}) and the initial mass (m_{in}) of solute. It can be expressed according to equation (2):

$$\gamma = \frac{m_{ad}}{m_{in}} \tag{2}$$

The m_{ad} and m_{in} can be expressed by equation (3) and equation (4), respectively:

$$m_{ad} = q(t).M \tag{3}$$

$$m_{in} = v(t).C_{in} \tag{4}$$

Where:

- C_{in} is the initial mass concentration of solute in the feed suspension (mg L^{-1}).
- M is the mass of RO membrane (g).
- $v(t)$ is the cumulative volume of the filtrate (m^3).

By replacing equation (3) and equation (4) in equation (2), the adsorbed amount of solute can be expressed according to the equation (5):

$$q(t). = \frac{\gamma.v(t).C_{in}}{M} \tag{5}$$

By replacing equation (5) in equation (1) and simplification, we obtain the equation (6):

$$\frac{dv(t)}{dt} = k_n^{'}.\left(\frac{\gamma.C_{in}}{M}\right)^{n-1}\left(v_m - v(t)\right)^n \tag{6}$$

Assuming that $K_n = k_n.\left(\frac{\gamma.C_{in}}{M}\right)^{n-1}$, the equation (6) can be written as the equation (7) [Adda *et al.*, 2020; Mesli *et al.*, 2022]:

$$\left.\begin{aligned}\frac{dv(t)}{dt} &= K_n.\left(v_m - v(t)\right)^n \\ v_{t=0} &= v(0) = 0\end{aligned}\right\} \tag{7}$$

Where:

- v_m is the maximum cumulative volume of the filtrate (m^3).
- K_n is the rate constant of filtration of the O-PNO equation (L^{1-n} h^{-1}).

2.2.2. Solution of the differential equation

The differential equation (7), which expresses the variation of cumulative volume, has been resolved using ordinary and fractional methods (Caputo derivative, Laplace Transform) for the different order of *n* (0, 1, 2 and *n*).

2.2.2.1. Pseudo-zero order kinetics

For the pseudo-zero order kinetics (n=0), the equation (7) can be expressed by the equation (8):

$$\left.\begin{array}{l} \dfrac{dv(t)}{dt} = K_0 \\ v(0) = 0 \end{array}\right\} \tag{8}$$

- **Ordinary solution**

Adopting the ordinary solution, the equation (8) can be expressed as the equation (9):

$$\int_0^{v_t} dv(t) = \int_0^t K_0 d(t) \tag{9}$$

By integration of equation (9) we get the equation (10):

$$v(t) = K_0.t \tag{10}$$

Where:

- K_0 is the rate constant of filtration of the O-PZO equation (L h^{-1}).

- **Fractional solution**

Adopting the fractional solution, the equation (8) can be expressed as the equation (11):

$$\left.\begin{array}{l} {}_o D_t^{\alpha} v(t) = K_{0f} \\ v(0) = 0 \end{array}\right\} \tag{11}$$

Using Laplace's direct and reverse transformation, equation (11) can be expressed as equation (12):

$$v(t) = \frac{K_{0f}.t^{\alpha}}{\Gamma(\alpha+1)} \tag{12}$$

Where:

- K_{0f} is the rate constant of filtration of the F-PZO equation (L $h^{-\alpha}$).
- α is the fractional order of time (-).
- Γ is the Gamma function.

2.2.2.2. Pseudo-first order kinetics

For the pseudo-first order kinetics (n=1), the equation (7) can be expressed by the equation (13):

$$\left.\begin{array}{l} \dfrac{dv(t)}{dt} = K_1.(v_m - v(t))^1 \\ v_{t=0} = v(0) = 0 \end{array}\right\} \quad (13)$$

Ordinary solution

Adopting the ordinary solution, the equation (13) can be expressed as the equation (14):

$$\begin{aligned} \int_0^{v(t)} \frac{dv(t)}{(v_m - v(t))} &= \int_0^t K_1 dt \\ Ln\left(\frac{v_m}{v_m - v(t)}\right) &= K_1.t \\ v(t) &= v_m.\left(1 - e^{-K_1.t}\right) \end{aligned} \quad (14)$$

Where:

- K_1 is the rate constant of filtration for the O-PFO equation (h^{-1}).

Fractional solution

Supposed that : $x_t = v_m - v_t$, the equation (14) can be expressed as the equation (15):

$$\left.\begin{array}{l} \dfrac{dx(t)}{dt} = -K_1 x_t \\ x(0) = V_m \end{array}\right\} \quad (15)$$

Adopting the fractional solution, the equation (15) can be expressed as the equation (16):

$$\left.\begin{array}{l} {}_0D_t^{\alpha} x(t) = -K_{1f}.x_t \\ v(0) = v_m \end{array}\right\} \quad (16)$$

Using Laplace's direct and reverse transformation, equation (16) can be expressed as equation (17):

$$\frac{\mathrm{L}}{\mathrm{t}\to\mathrm{S}} \longrightarrow \left.\begin{matrix} \mathrm{S}^{\alpha}x(\mathrm{S}) - \mathrm{S}^{\alpha-1}x(0) = -\mathrm{K}_{1\mathrm{f}}x(\mathrm{S}) \\ v(0) = v_m \end{matrix}\right\}$$

$$x(\mathrm{S}).(\mathrm{S}^{\alpha} + \mathrm{K}_{1\mathrm{f}}) = v_m \mathrm{S}^{\alpha-1}$$

$$x(\mathrm{S}) = \frac{V_m \mathrm{S}^{\alpha-1}}{\mathrm{S}^{\alpha}+\mathrm{K}_{1\mathrm{f}}}$$

$$\frac{\mathrm{L}^{-1}}{\mathrm{S}\to\mathrm{t}} \longrightarrow x(\mathrm{t}) = v_m \mathrm{t}^{0} \mathrm{E}_{\alpha,1}(-\mathrm{K}_{1\mathrm{f}}\mathrm{t}^{\alpha})$$

$$v_m - v(t) = v_m \mathrm{E}_{\alpha,1}(-\mathrm{K}_{1\mathrm{f}}\mathrm{t}^{\alpha})$$

$$v(t) = v_m[1 - \mathrm{E}_{\alpha}(-\mathrm{K}_{1\mathrm{f}}\mathrm{t}^{\alpha})]$$

$$v(t) = v_m \left[1 - \sum_{n=0}^{\infty} \frac{(-1)^n . \mathrm{K}_{1\mathrm{f}}^{\mathrm{n}} . \mathrm{t}^{\alpha\,\mathrm{n}}}{\Gamma(\alpha\,\mathrm{n}+1)}\right] \quad (17)$$

Where:

- K_{1f} is the rate constant of filtration for the F-PFO equation ($h^{-\alpha}$).

2.2.2.3. Pseudo-second order kinetics

For the pseudo-second order kinetics (n=2), the equation (7) can be expressed by the equation (18):

$$\left.\begin{matrix} \frac{dv(t)}{dt} = K_2.(v_m - v(t))^2 \\ v_{t=0} = v(0) = 0 \end{matrix}\right\} \quad (18)$$

<u>Ordinary solution</u>

Adopting the ordinary solution, the equation (18) can be expressed as the equation (19):

$$\int_0^{v(t)} \frac{dv(t)}{(v_m - v(t))^2} = \int_0^t K_2.dt$$

$$\left(\frac{1}{v_m - v(t)}\right) - \left(\frac{1}{v_m}\right) = K_2.t$$

$$v(t) = \frac{v_m^2.K_2.t}{1 + v_m..K_2.t} \quad (19)$$

Where:

- K_2 is the rate constant of filtration for the O-PSO equation ($L^{-1}\ h^{-1}$).

Fractional solution

Supposed that : $x_t = \frac{1}{v_m - v_t}$, the equation (18) can be expressed as the equation (20):

$$\left.\begin{array}{c} \frac{dx(t)}{dt} = K_2 \\ x(0) = \frac{1}{v_m} \end{array}\right\} \quad (20)$$

Adopting the fractional solution, the equation (20) can be expressed as the equation (21):

$$\left.\begin{array}{c} {}_0D_t^{\alpha} x(t) = K_{2f} \\ x(0) = \frac{1}{v_m} \end{array}\right\} \quad (21)$$

Using Laplace's direct and reverse transformation, equation (21) can be expressed as equation (22):

$$\frac{L}{t \to S} \longrightarrow \left.\begin{array}{c} S^{\alpha}.x(S) - S^{\alpha-1}.x(0) = \frac{K_{2f}}{S} \\ x(0) = \frac{1}{v_m} \end{array}\right\}$$

$$x(S) = \frac{S^{\alpha-1}}{v_m.S^{\alpha}} + \frac{K_{2f}}{S.S^{\alpha}} = \frac{1}{v_m}.\frac{1}{S} + K_{2f}\frac{1}{S^{\alpha+1}}$$

$$\frac{L^{-1}}{S \to t} \longrightarrow x(t) = \frac{1}{v_m} + K_{2f}.\frac{t^{\alpha}}{\Gamma(\alpha+1)}$$

$$\frac{1}{V_m - V_t} = \frac{1}{V_m} + K_{2f}\frac{t^{\alpha}}{\Gamma(\alpha+1)}$$

$$\frac{1}{v_m - v_t} = \frac{\Gamma(\alpha+1) + v_m K_{2f} t^{\alpha}}{v_m.\Gamma(\alpha+1)}$$

$$v(t) = v_m\left[1 - \frac{\Gamma(\alpha+1)}{\Gamma(\alpha+1) + v_m.K_{2f}.t^{\alpha}}\right] \quad (22)$$

Where:

- K_{2f} is the rate constant of filtration for the F-PSO equation ($L^{-1}\ h^{-\alpha}$).

2.2.2.4. Pseudo-nth order kinetics

For the pseudo-nth order kinetics (n=n), the equation (7) can be expressed by the equation (23):

$$\left.\begin{aligned} \frac{dv(t)}{dt} &= K_n.(v_m - v(t))^n \\ v_{t=0} &= v(0) = 0 \end{aligned}\right\} \quad (23)$$

Ordinary solution

Adopting the ordinary solution, the equation (23) can be expressed as the equation (24):

$$\int_{v_m}^{v_m - v_t} \frac{d(v_m - v_t)}{(v_m - v_t)^n} = -K_n \int_0^t dt$$

$$\frac{1}{(n-1)}\left[\frac{1}{(v_m - v_t)^{n-1}} - \frac{1}{{v_m}^{n-1}}\right] = K_n\, t$$

$$\left[\frac{1}{(v_m - v_t)^{n-1}} - \frac{1}{{v_m}^{n-1}}\right] = (n-1)K_n\, t$$

$$\frac{1}{(v_m - v_t)^{n-1}} = \frac{\left((n-1)\,{v_m}^{n-1}K_n\, t\right)+1}{{v_m}^{n-1}}$$

$$(v_m - v_t)^{n-1} = \frac{{v_m}^{n-1}}{((n-1){v_m}^{n-1}K_n\, t)+1}$$

$$(v_m - v_t) = \left[\frac{{v_m}^{n-1}}{((n-1){v_m}^{n-1}K_n\, t)+1}\right]^{\frac{1}{n-1}}$$

$$(v_m - v) = \frac{v_m}{[((n-1){v_m}^{n-1}K_n\, t)+1]^{\frac{1}{n-1}}}$$

$$v(t) = v_m\left[1 - \frac{1}{[((n-1)({v_m}^{n-1}).K_n\, .t)+1]^{\frac{1}{n-1}}}\right] \quad (24)$$

Where:

- K_n is the rate constant of filtration of the O-PNO equation ($L^{1-n}\, h^{-1}$).

Fractional solution

Supposed that :$x_t = \frac{1}{(v_m - v_t)^{n-1}}$, the equation (23) can be expressed as equation (25):

$$\left.\begin{aligned} \frac{dx(t)}{dt} &= (n-1)K_n \\ v(0) &= \frac{1}{{v_m}^{n-1}} \end{aligned}\right\} \quad (25)$$

Using Laplace's direct and reverse transformation, equation (25) can be expressed as equation (26):

$$\frac{\text{EDF}}{(\alpha)} \longrightarrow \left.\begin{matrix} {}_{0}D_{t}^{\alpha}x(t) = (n-1)K_{nf} \\ v(0) = \frac{1}{{v_m}^{n-1}} \end{matrix}\right\}$$

$$\frac{L}{t\to S} \longrightarrow \left.\begin{matrix} S^{\alpha}x(S) - S^{\alpha-1}x(0) = \frac{(n-1)K_{nf}}{S} \\ v(0) = \frac{1}{{v_m}^{n-1}} \end{matrix}\right\}$$

$$x(S) = \frac{S^{\alpha-1}}{{v_m}^{n-1}S^{\alpha}} + \frac{(n-1)K_{nf}}{S\,S^{\alpha}}$$

$$x(S) = \frac{1}{{v_m}^{n-1}}.\frac{1}{S} + \frac{(n-1)K_{nf}}{S^{\alpha+1}}$$

$$\frac{L^{-1}}{S\to t} \longrightarrow x(t) = \frac{1}{{v_m}^{n-1}} + \frac{(n-1)K_{nf}t^{\alpha}}{\Gamma(\alpha+1)}$$

$$x(t) = \frac{\left[\Gamma(\alpha+1)+(n-1)K_{nf}{v_m}^{n-1}t^{\alpha}\right]}{\Gamma(\alpha+1).{v_m}^{n-1}}$$

$$(v_m - v_t)^{n-1} = \frac{\Gamma(\alpha+1).{v_m}^{n-1}}{[\Gamma(\alpha+1)+(n-1)K_{nf}\,{v_m}^{n-1}t^{\alpha}]}$$

$$(v_m - v_t) = \frac{\Gamma^{\frac{1}{n-1}}(\alpha+1).v_m}{[\Gamma(\alpha+1)+(n-1)K_{nf}{v_m}^{n-1}t^{\alpha}]^{\frac{1}{n-1}}}$$

$$v(t) = v_m\left[1 - \left[\frac{\Gamma(\alpha+1)}{[\Gamma(\alpha+1)+(n-1).K_{nf}.{v_m}^{n-1}.t^{\alpha}]}\right]^{\frac{1}{n-1}}\right] \qquad (26)$$

Where:

- K_{nf} is the rate constant of filtration for the F-PNO equation ($L^{1-n}\,h^{-\alpha}$).

The established ordinary and fractional dimensional models are summarized in the Table 2.4.

Table 2.4. The ordinary and fractional dimensional models developed in this work.

Solution type	Pseudo Order	Formula	Equation
Ordinary	0	$v(t) = K_0.t$	(10)
	1	$v(t) = v_m\left(1 - e^{-K_1.t}\right)$	(14)
	2	$v(t) = \frac{v_m^2.K_2.t}{1 + v_m.K_2.t}$	(19)
	n	$v(t) = v_m\left[1 - \frac{1}{\left[\left((n-1).v_m^{n-1}.K_n.t\right)\right]^{\frac{1}{n-1}}}\right]$	(24)
Fractional	0	$v(t) = \frac{K_{0f}.t^{\alpha}}{\Gamma(\alpha+1)}$	(12)
	1	$v(t) = v_m\left[1 - \sum_{n=0}^{\infty}\frac{(-1)^n.{K_{1f}}^n.t^{\alpha.n}}{\Gamma(\alpha.n+1)}\right]$	(17)
	2	$v(t) = v_m\left[1 - \frac{\Gamma(\alpha+1)}{\Gamma(\alpha+1) + v_m.K_{2f}.t^{\alpha}}\right]$	(22)
	n	$v(t) = v_m\left[1 - \left[\frac{\Gamma(\alpha+1)}{\Gamma(\alpha+1) + (n-1).v_m^{n-1}.K_{nf}.t^{\alpha}}\right]^{\frac{1}{n-1}}\right]$	(26)

2.2.3. Transformation to dimensionless models

There are several significant advantages to describe the RO process using dimensionless models, including: simplify the parametric representation, reducing the number of variables and enabling cross-scales experiments. The dimensional models, presented in Table 2.4, were transformed to dimensionless models according to the equations (27) and (28), respectively:

$$V = \frac{v(t)}{v_m} \tag{27}$$

$$\tau = \frac{t}{t_m} \tag{28}$$

Where:

- V is the dimensionless cumulative volume of the filtrate (-).
- τ is the dimensionless filtration time (-).
- t_m is the maximum filtration time (h).

2.2.3.1. Pseudo-zero order kinetics

Ordinary model

By replacing the equations (27) and (28) in the equation (10), we obtain the equation (29):

$$V.v_m = K_0.t_m.\tau \tag{29}$$

Assuming that $\left(K_0.\frac{t_m}{v_m} \right) = k_0$, the equation (29) can be written as the equation (30):

$$V = k_0.\tau \tag{30}$$

Where:

- k_0 *is* the constants of O-PZO model(-).

Fractional model

By replacing the equations (27) and (28) in the equation (12), we obtain the equation (31):

$$V = \frac{\left(\frac{K_{0f}.{t_m}^{\alpha}}{v_m} \right).\tau^{\alpha}}{\Gamma(\alpha+1)} \tag{31}$$

Assuming that $\left(\frac{K_{0f}.{t_m}^{\alpha}}{v_m} \right) = k_{0f}$, the equation (31) can be written as the equation (32):

$$V = \frac{k_{0f}.\tau^{\alpha}}{\Gamma(\alpha+1)} \tag{32}$$

Where:

- k_{0f} is the constant of F-PZO model (-).
- α is the fractional order.

2.2.3.2. Pseudo-first order kinetics

Ordinary model

By replacing the equations (27) and (28) in the equation (14), we obtain the equation (33):

$$V = \left(1 - e^{-K_1.t_m.\tau}\right) \tag{33}$$

Assuming that $\left(K_1.t_m\right) = k_1$, the equation (33) can be written as the equation (34):

$$V = 1 - e^{-k_1.\tau} \tag{34}$$

Where :

- k_1 is the constants of O-PFO model (-).

Fractional model

By replacing the equations (27) and (28) in the equation (17), we obtain the equation (35):

$$V = \left[1 - \sum_{n=0}^{\infty} \frac{(-1)^n.\ (\mathrm{K_{1f}}.\mathrm{t_m}^{\alpha})^{\mathrm{n}}.\tau^{\alpha\,\mathrm{n}}}{\Gamma(\alpha\,\mathrm{n}+1)}\right] \tag{35}$$

Assuming that $(\mathrm{K_{1f}}.\mathrm{t_m}^{\alpha}) = \mathrm{k_{1f}}$ and adopting the simplified form, the equation (35) can be written as the equation (36):

$$V = 1 - Exp\left(-k_{1.f}.\tau^{\alpha}\right) \tag{36}$$

Where:

- k_{1f} is the constant of F-PFO model (-).

2.2.3.3. Pseudo-second order kinetics

Ordinary model

By replacing the equations (27) and (28) in the equation (19), we obtain the equation (37):

$$V = \frac{\left(v_m.K_2.t_m\right).\tau}{1 + \left(v_m.K_2.t_m\right).\tau} \tag{37}$$

Assuming that $(v_m.K_2.t_m)=k_2$, the equation (37) can be written as the equation (38):

$$V=\frac{k_2.\tau}{1+k_2.\tau} \tag{38}$$

Where:

- k_2 is the constants of O-PSO model (-).

Fractional model

By replacing the equations (27) and (28) in the equation (22), we obtain the equation (39):

$$V=\left[1-\frac{\Gamma(\alpha+1)}{\Gamma(\alpha+1)+(v_m.K_{2f}.t_m{}^{\alpha}).\ \tau^{\alpha}}\right] \tag{39}$$

Assuming that $(v_m.K_{2f}.t_m{}^{\alpha})=k_{2f}$, the equation (39) can be written as the equation (40):

$$V=\frac{k_{2f}.\ \tau^{\alpha}}{\Gamma(\alpha+1)+k_{2f}.\ \tau^{\alpha}} \tag{40}$$

Where:

- k_{2f} is the constant of F-PSO model (-).

2.2.3.4. Pseudo-nth order kinetics

Ordinary model

By replacing the equations (27) and (28) in the equation (24), we obtain the equation (41):

$$V=\left[1-\frac{1}{\left[\left((n-1)\left((v_m{}^{n-1})K_n.t_m\right).\tau\right)+1\right]^{\frac{1}{n-1}}}\right] \tag{41}$$

Assuming that $\left(K_n t_m v_m{}^{n-1}\right)=k_n$, the equation (41) can be written as the equation (42):

$$V=1-\frac{1}{\left[\left((n-1).k_n.\tau\right)+1\right]^{\frac{1}{1-n}}} \tag{42}$$

Where:

- k_n is the constants of O-PNO model (-).

Fractional models

By replacing the equations (27) and (28) in the equation (26), we obtain the equation (43):

$$V = \left[1 - \left[\frac{\Gamma(\alpha+1)}{[\Gamma(\alpha+1)+(n-1).(K_{nf}.({v_m}^{n-1}).{t_m}^{\alpha}).\tau^{\alpha}]}\right]^{\frac{1}{n-1}}\right] \quad (43)$$

Assuming that $(K_{nf}.({v_m}^{n-1}).{t_m}^{\alpha}) = k_{nf}$, the equation (43) can be written as the equation (44):

$$\mathbf{V = 1 - \left[\frac{\Gamma(\alpha+1)}{[\Gamma(\alpha+1)+(n-1).k_{nf}.\tau^{\alpha}]}\right]^{\frac{1}{n-1}}} \quad (44)$$

Where:

- k_{nf} is the constant of F-PNO model (-).

The ordinary dimensionless models (ODM) and the fractional dimensionless models (FDM) are presented in Table 2.5.

Table 2.5. The ordinary and fractional dimensionless models developed in this work.

Classification		Model code	Formula	Equation
ODM	0	O-PZO	$V = k_0.\tau$	(30)
	1	O-PFO	$V = 1 - Exp(-k_1.\tau)$	(34)
	2	O-PSO	$V = \frac{k_2.\tau}{1+k_2.\tau}$	(38)
	n	O-PNO	$V = 1 - \left[\frac{1}{1+(n-1).k_n.\tau}\right]^{\frac{1}{1-n}}$	(42)
FDM	0	F-PZO	$V = \frac{k_{0.f}}{\Gamma(\alpha+1)}.\tau^{\alpha}$	(36)
	1	F-PFO	$V = 1 - Exp\left(-k_{1.f}.\tau^{\alpha}\right)$	(32)
	2	F-PSO	$V = \frac{k_{2.f}.\tau^{\alpha}}{\Gamma(\alpha+1)+k_{2.f}.\tau^{\alpha}}$	(40)
	n	F-PNO	$V = 1 - \left[\frac{\Gamma(\alpha+1)}{\Gamma(\alpha+1)+(n-1).k_{n.f}.\tau^{\alpha}}\right]^{\frac{1}{n-1}}$	(44)

II.3. Solving of the dimensionless models

The resolution of the developed ODM and FDM, presented in Table 2.5, and the determination of its optimal kinetic constants (n, α, k_n and k_{nf}) have been conducted by setting up an establishment a MATLAB software program.

For each model, the kinetic constants (n, α, k_n, and k_{nf}) were optimized using an algorithm that calculates the objective function by determining the Mean Absolute Relative Error (MARE) values.

This algorithm was implemented in a MATLAB program, for each compartment (alimentation, permeate, and rejection) of the DWRO desalination system, according to the following steps:

a. Importing the experimental data presented in Excel files using the ***xlsread*** function to form a matrix containing the experimental values.
b. Initializing an approximation of adjustable parameters by the ***ga***functions which use genetic algorithms to minimize the objective function (MARE).

$$\text{MARE}\% = \frac{100}{N}\sum_{i=1}^{N}\left|\frac{\left(y^{\exp}(i)-y^{\text{cal}}(i)\right)}{\left(y^{\exp}(i)\right)}\right| \quad (45)$$

c. Refining the initial approximations of the adjustable parameters by MATLAB's ***lsqcurvefit*** function, this uses the non-linear least squares method, setting the use of the Levenberg-Marquardt algorithm as a calculation option.
d. Calculation of the objective function (ERAM) using a function comprising experimental and calculated data of dimensionless cumulative volume.

II.4. Evaluation of the models accuracy by statistical criteria

The applied models accuracy was assessed by the statistical criteria which quantify the error between the model results and the experimental values.

The statistical criteria, used in this work, include the root mean squared error (RMSE) [Adda *et al*., 2020], the average absolute relative deviation (AARD) [Jouyban *et al*., 2002], the coefficient of determination (R^2) [Soleimani *et al*., 2018], the mean absolute error (MAE) [Soleimani *et al*., 2018], the sum of squares regression (SSR) [Coker, 1995]and the sum of squares error (SSE) [Coker, 1995], as follows:

$$RMSE = \sqrt{\frac{\sum_{i=1}^{N}\left(y_{i,\exp} - y_{i,cal}\right)^2}{N}} \tag{46}$$

$$AARD = \frac{1}{N-Z}\sum_{i=1}^{n}\left(\left|\frac{y_{i,cal} - y_{i,\exp}}{y_{i,\exp}}\right|\right)\times 100\% \tag{47}$$

$$R^2 = 1 - \frac{\sum_{i=1}^{N}\left(y_{i,\exp} - y_{i,cal}\right)^2}{\sum_{i=1}^{N}\left(y_{i,\exp} - \bar{y}\right)^2} \tag{48}$$

$$MAE = \frac{1}{n}\sum_{i=1}^{n}\left|y_{i,\exp} - y_{i,cal}\right| \tag{49}$$

$$SSR = \sum_{i=1}^{N}\left(y_{i,cal} - \bar{y}\right)^2 \tag{50}$$

$$SSE = \sum_{i=1}^{N}\left(y_{i,\exp} - y_{i,cal}\right)^2 \tag{51}$$

3. Results and discussions

3. Results and discussions

3.1. Models' reliability and accuracy

The model's reliability and accuracy present the deadliest step in this study using the statistical criteria and the ability of the model's regression. The kinetic constants and the statistical criteria of the developed ordinary dimensionless models (ODM) and fractional dimensionless models (FDM) were established for alimentation, permeate and rejection of the RO desalination process.

In this study, three steps have been followed to select the best model, among the established models, that can be used to fit the experimental data for the three compartment (alimentation, permeate and rejection) of RO desalination process. The first step is the optimization of the kinetic constants of models. The second step is the calculation of the dimensionless cumulative volume by the established models. The third step is the evaluation of the models accuracy.

The optimization of kinetic constants has been established by software MATLAB. For the ordinary models with pseudo-orders 0, 1 and 2, the models constants (k_i) have been determined, while for the ordinary model with pseudo-n^{th} order, the pseudo-order (n) and the model constant (k_i) have been determined. For the fractional models with pseudo-orders 0, 1 and 2, the models constants (k_{if}) and fractional orders of time (α) were determined, while for the ordinary model with pseudo-n^{th} order, the pseudo-order (n), the fractional order of time (α) and the model constant (k_{if}) were determined.
The calculation of the dimensionless cumulative volume was carried out using ordinary dimensionless models (ODM) and fractional dimensionless models (FDM) with the optimized values of the kinetic constants for the three compartment of RO process.
The accuracy of the ordinary and fractional models, established for the alimentation, permeate and rejection was evaluated using the following statistical criteria: R^2, RMSE, AARD, MAE, SSR and SSE. Through the calculated values of these statistical criteria, the best model can be determined. Another method used to analyze the accuracy of ordinary and fractional models is linear regression between experimental and calculated values of dimensionless cumulative volume.

3.1.1. Alimentation compartment

3.1.1.1. Optimization of the kinetic constants of models

The optimized values of the kinetic constants (n, α, k_i and k_f) of ordinary and fractional dimensionless models for the calculated cumulative volume of alimentation (V_A^{cal}) are shown in Table 3.1.

Table 3.1. The kinetic constants of ODM and FDM for the calculated cumulative volume of alimentation (V_A^{cal}).

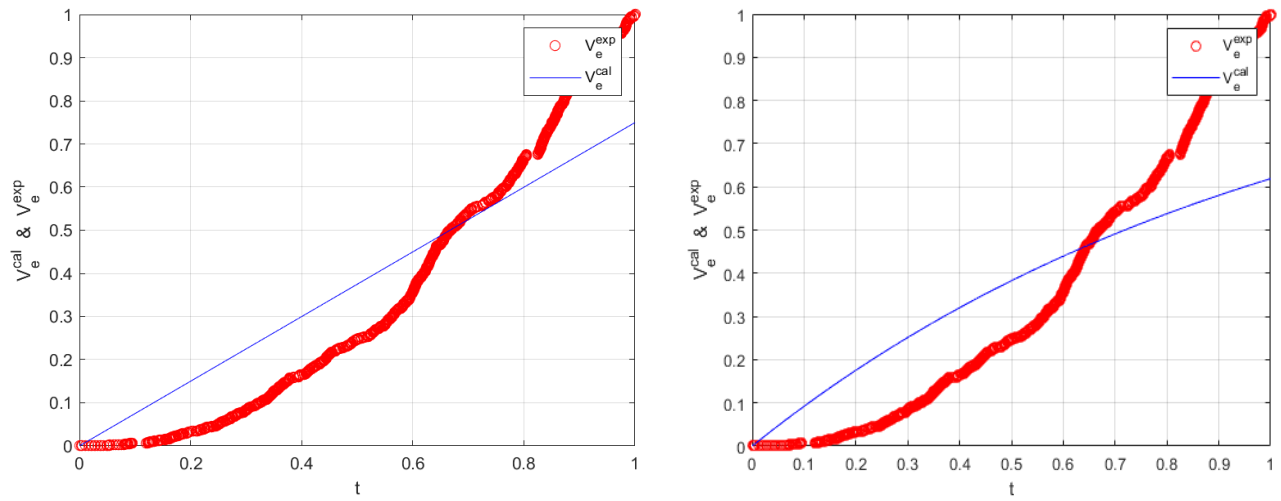
Classification	Kinetic constants									
	n(-)	*α (-)*	k_0(-)	k_1(-)	k_2(-)	k_n(-)	k_{0f}(-)	k_{1f} (-)	k_{2f} (-)	k_{nf} (-)
O-PZO	0	1	0.75	---	---	---	---	---	---	---
O-PFO	1	1	---	0.96	---	---	---	---	---	---
O-PSO	2	1	---	---	-43.001	---	---	---	---	---
O-PNO	0.18	1	---	---	---	0.78	---	---	---	---
F-PZO	0	2.0132	---	---	---	---	2.10	---	---	---
F-PFO	1	3.0352	---	---	---	---	---	2.31	---	---
F-PSO	2	4.1253	---	---	---	---	---	---	1.62E2	---
F-PNO	0.15	2.1693	---	---	---	---	---	---	---	2.74

From the Table 3.1, it can be noted that the optimized values of the pseudo-orders *n* for the O-PNO and F-PNO models were small which its values are 0.18 and 0.15 respectively. Also, the optimized values of the fractional order *α*, of the F-PNO models, were ranging from 2.0132 to 2.1693. Table 3.1 shows that, for the FDM models, there is direct proportionality between the optimized fractional order values *α* [2.0132 - 4.1253] and the optimized pseudo-order values *n* [0 - 2].

3.1.1.2. Calcul of dimensionless cumulative volume of alimentation

Figure 3.1 present the calculated and the experimental values of dimensionless cumulative volume of alimentation (V_A^{cal}, V_A^{exp}) plotted as function of the dimensionless filtration time (τ).

(a) **(b)**



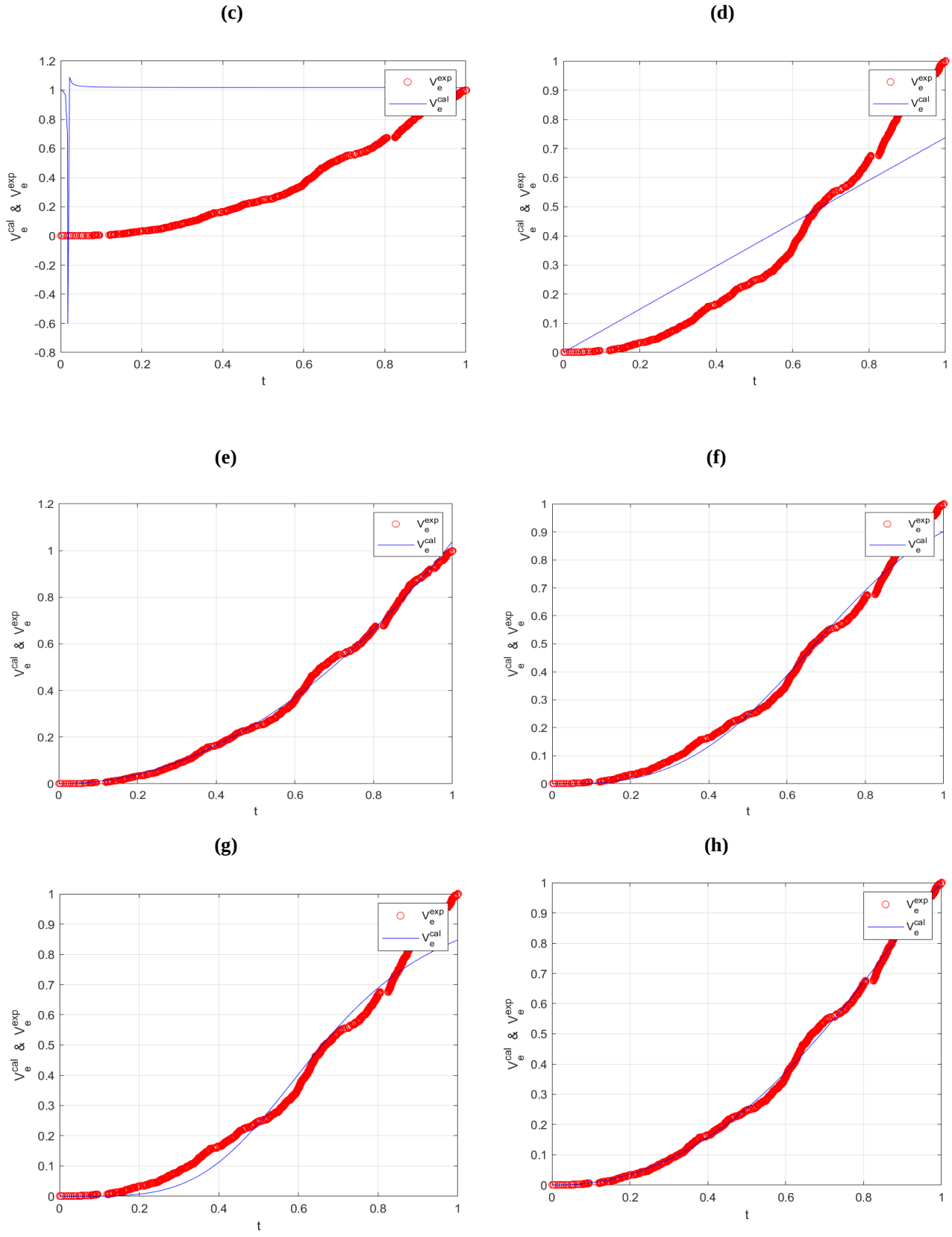


Figure 3.1. The calculated and the experimental values of dimensionless cumulative volume of alimentation ($V_A{}^{cal}$, $V_A{}^{exp}$) plotted as function of dimensionless filtration time (τ): (a) O-PZO model, (b) O-PFO model, (c) O-PSO model, (d) O-PNO model, (e) F-PZO model, (f) F-PFO model, (g) F-PSO model, (h) F-PNO model.

Through a preliminary examination based on visual observation of the various graphical curves shown in Figure 3.1, it can be seen that the (a), (b), (c) and (d) curves show a large divergence between the experimental and calculated values, while the (f) and (g) curves show a medium divergence, but the (e) and (h) curves show convergence between the experimental and calculated values. To validate these initial observations and determine the best mathematical model capable of representing the experimental values, statistical criteria should be used.

3.1.1.3. Evaluation of the models accuracy by statistical criteria

The statistical criteria values (R^2, RMSE, AARD, MAE, SSR and SSE) those have been used to evaluate the ordinary and fractional dimensionless models of alimentation are presented in Table 3.2.

Table 3.2. The statistical criteria of ODM and FDM for the calculated cumulative volume of alimentation (V_A^{cal}).

Classification	**Statistical criteria**					
	R^2	RMSE	AARD	MAE	SSR	SSE
O-PZO	0.8305	11.907	418.57	0.1062	218.961	36.297
O-PFO	0.7074	15.646	527.31	0.1364	216.336	62.670
O-PSO	-5.4171	73.269	2.90E5	0.6728	1371.128	1374.289
O-PNO	0.8284	11.978	413.73	0.1064	217.853	36.729
F-PZO	0.9968	1.619	13.96	0.0121	214.165	0.671
F-PFO	0.9894	2.976	19.21	0.0242	214.310	2.267
F-PSO	0.9739	4.668	30.56	0.0385	214.741	5.578
F-PNO	**0.9975**	**1.452**	**8.03**	**0.0109**	**214.158**	**0.540**

Based on the results presented in Table 3.2, it can be seen that the fractional dimensionless models (FDM) gave the best values of statistical criteria, compared to the other ordinary dimensionless models (ODM). This accuracy can be reflected with high value of R^2 (0.9975) and with lowers values of RMSE (1.452), AARD (8.03), MAE (0.0109), SSR (214.158) and SSE (0.54) for the F-PNO model of alimentation.

To determine the best linear regression, the experimental values are plotted against the calculated values by the ordinary and fractional models. Figure 3.2 (h) argue the previous results, such as the scatter plot of the calculated values, by the fractional model (F-PNO), versus the experimental values of the dimensionless cumulative volume for alimentation were established the best regression.

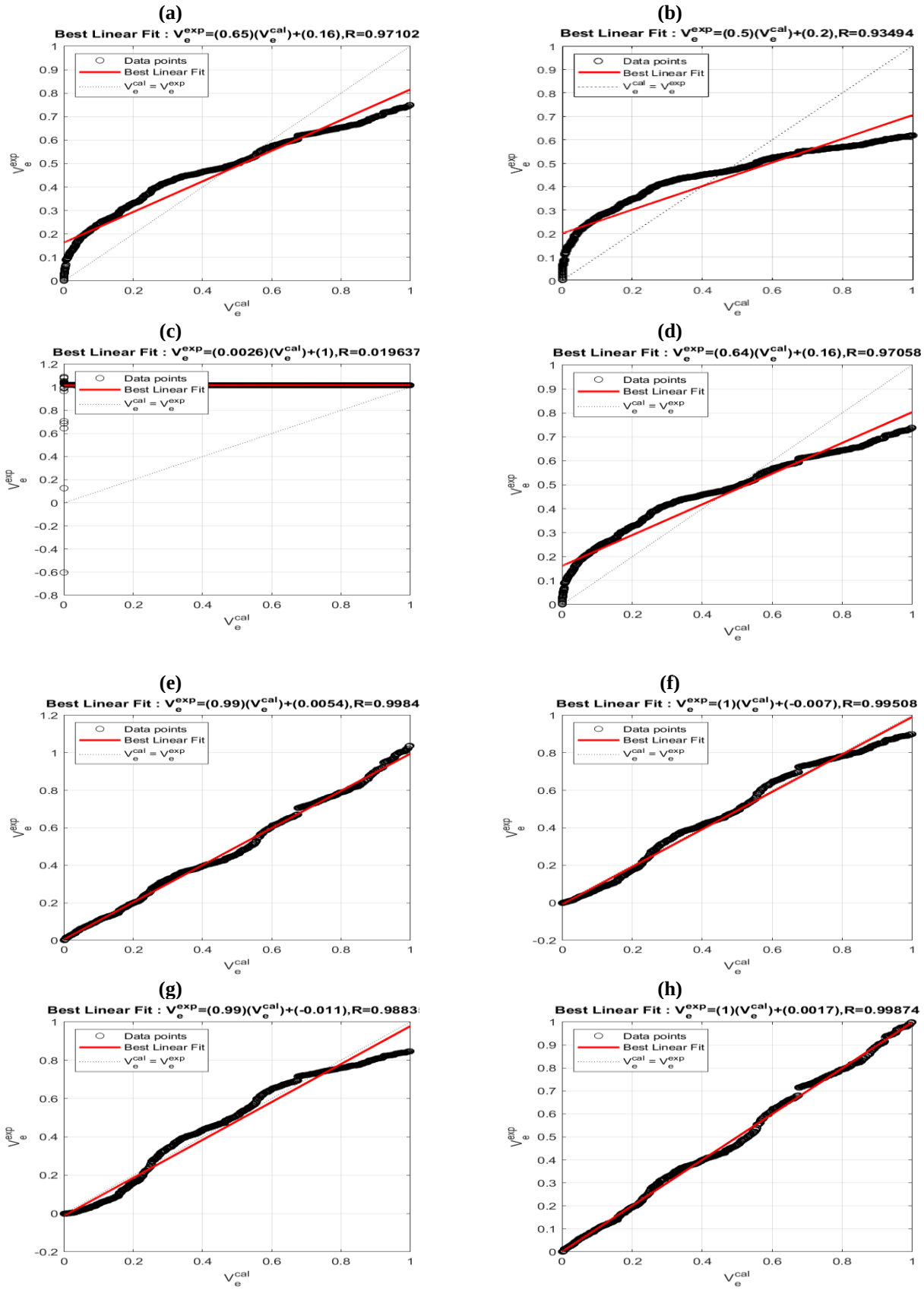


Figure 3.2. Scatter plot of the calculated values ((V_A^{cal}), by the ODM and FDM, versus the experimental values (V_A^{exp}) of dimensionless cumulative volume for alimentation: (a) O-PZO model, (b) O-PFO model, (c) O-PSO model, (d) O-PNO model, (e) F-PZO model**,** (f) F-PFO model**,** (g) F-PSO model**,** (h) F-PNO model.

3.1.2. Permeate compartment

3.1.2.1. Optimization of the kinetic constants of models

The optimized values of the kinetic constants (n, α, k_i and k_f) of ordinary and fractional dimensionless models for the calculated cumulative volume of permeate (V_P^{cal}) are shown in Table 3.3.

Table 3.3. The kinetic constants of ODM and FDM for the calculated cumulative volume of permeate (V_P^{cal}).

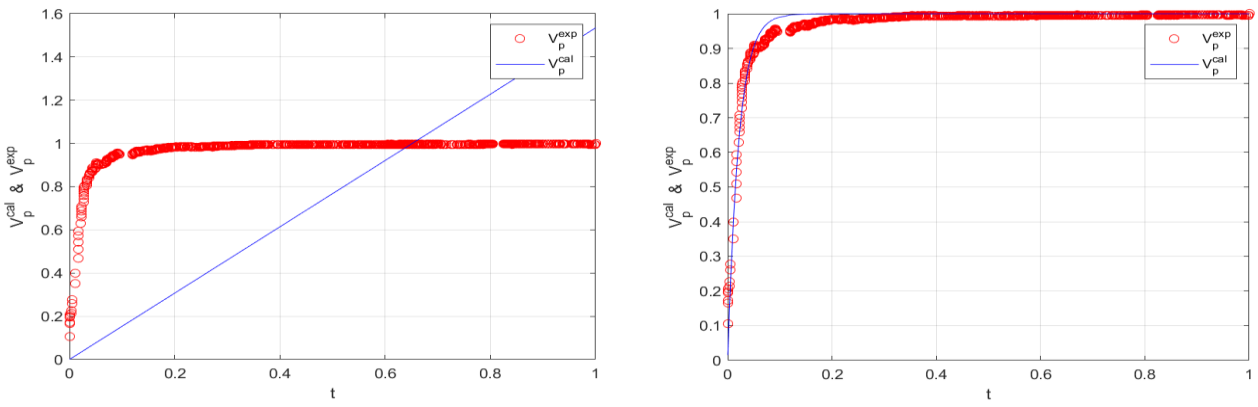
Classification	Kinetic constants									
	n(-)	*α (-)*	k_0(-)	k_1(-)	k_2(-)	k_n(-)	k_{0f}(-)	k_{1f} (-)	k_{2f} (-)	k_{nf} (-)
O-PZO	0	1	1.53	---	---	---	---	---	---	---
O-PFO	1	1	---	46.90	---	---	---	---	---	---
O-PSO	2	1	---	---	181.69	---	---	---	---	---
O-PNO	1.84	1	---	---	---	148.24	---	---	---	---
F-PZO	0	0.0551	---	---	---		1.00	---	---	---
F-PFO	1	0.6443	---	---	---	---	---	13.52	---	---
F-PSO	2	1.2883	---	---	---		---		3.74E2	---
F-PNO	1.59	1.0425	---	---	---	---	---	---	---	92.28

From the Table 3.3, it can be noted that the optimized values of the pseudo-orders *n* for the O-PNO and F-PNO models were close to 2 which its values were 1.84 and 1.59 respectively. Also, the optimized values of the fractional order *α*, of the F-PNO models, were ranging from 0.0551 to 1.2883. Table 3.3 shows that, for the FDM models, there is a direct proportionality between the optimized fractional order values α [0.0551-1.2883] and the optimized pseudo-order values *n* [0-2].

3.1.2.2. Calcul of dimensionless cumulative volume of permeate

Figure 3.3 present the calculated and the experimental values of dimensionless cumulative volume of permeate (V_P^{cal}, V_P^{exp}) plotted as function of the dimensionless filtration time (τ).

(a) **(b)**



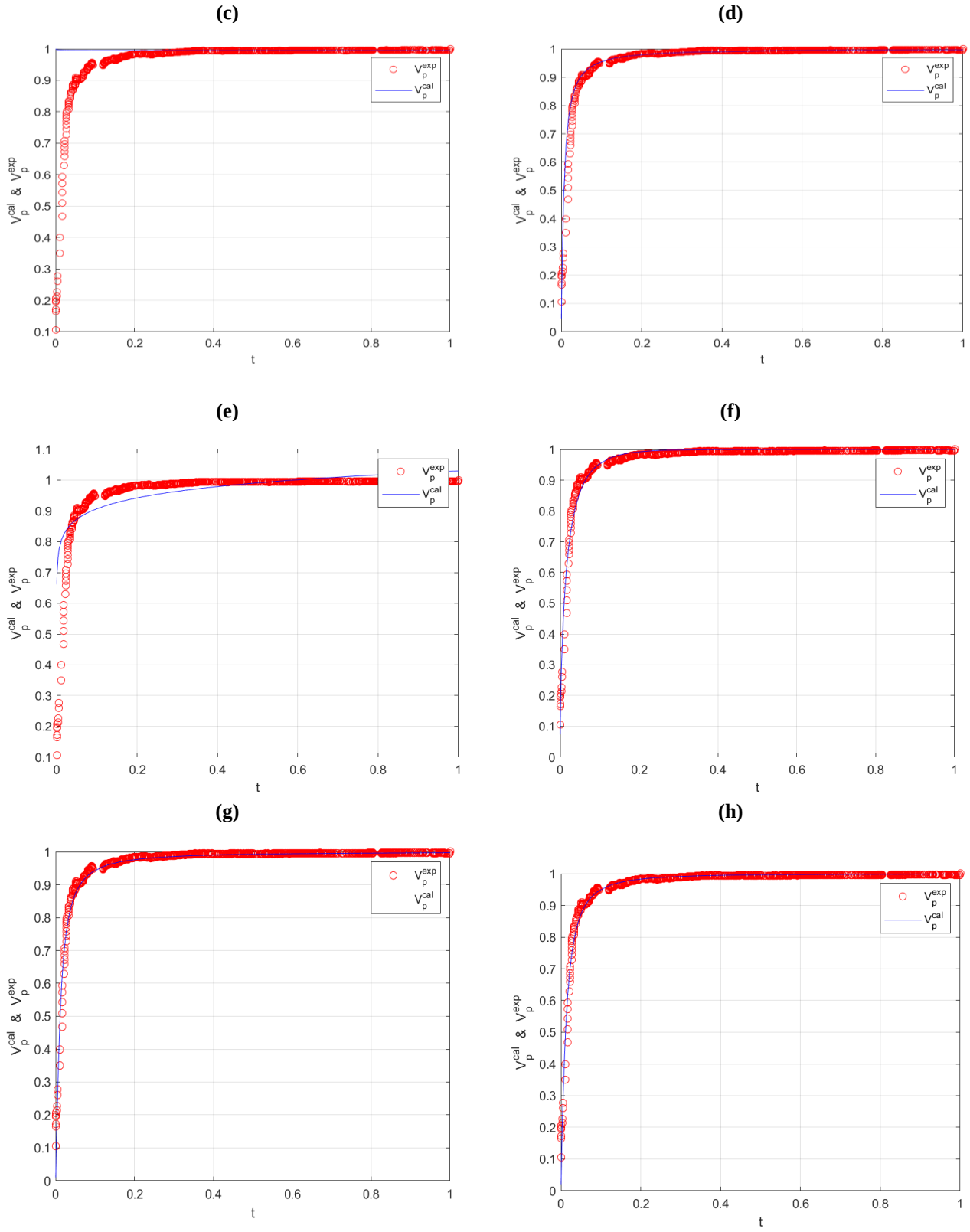


Figure 3.3. The calculated and the experimental values of dimensionless cumulative volume of permeate (V_P^{cal}, V_P^{exp}) plotted as function of dimensionless filtration time (τ): (a) O-PZO model, (b) O-PFO model, (c) O-PSO model, (d) O-PNO model, (e) F-PZO model, (f) F-PFO model, (g) F-PSO model, (h) F-PNO model.

Through a preliminary examination based on visual observation of the various graphical curves shown in Figure 3.3, it can be seen that the (a), (c) and (e) curves show a large divergence between the experimental and calculated values, while the (b) and (d) curves show a medium divergence, but the (f), (g) and (h) curves show convergence between the experimental and calculated values. To validate these initial observations and determine the best mathematical model capable of representing the experimental values, statistical criteria should be used.

3.1.2.3. Evaluation of the models accuracy by statistical criteria

The statistical criteria values (R^2, RMSE, AARD, MAE, SSR and SSE) those have been used to evaluate the ordinary and fractional dimensionless models of permeate are presented in Table 3.4.

Table 3.4. The statistical criteria of ODM and FDM for the calculated cumulative volume of permeate (V_P^{cal}).

Classification	Statistical criteria					
	R^2	RMSE	AARD	MAE	SSR	SSE
O-PZO	-45.9140	42.341	36.78	0.3551	99.730	458.939
O-PFO	0.9395	1.520	1.20	0.0096	9.945	0.591
O-PSO	-0.0456	6.321	2.94	0.0131	10.140	10.229
O-PNO	0.9309	1.624	0.62	0.0035	9.783	0.676
F-PZO	0.4893	4.418	3.35	0.0232	9.782	4.996
F-PFO	0.9645	1.160	0.88	0.0072	9.850	0.348
F-PSO	0.9698	1.070	0.58	0.0035	9.799	0.295
F-PNO	0.9750	0.976	0.53	0.0032	9.786	0.244

Based on the results presented in Table 3.4, it is evident that the fractional dimensionless models (FDM) gave the best values of statistical criteria, compared to the other ordinary dimensionless models (ODM). This accuracy can be reflected with high value of R^2 (0.975) and with lowers values of RMSE (0.976), AARD (0.53), and MAE (0.0032) for the F-PNO model of permeate.

To determine the best linear regression, the experimental values are plotted against the calculated values by the ordinary and fractional models. Figure 3.4 (h) argue the previous results, such as the scatter plot of the calculated values, by the fractional model (F-PNO), versus the experimental values of the dimensionless cumulative volume for permeate were established the best regression.

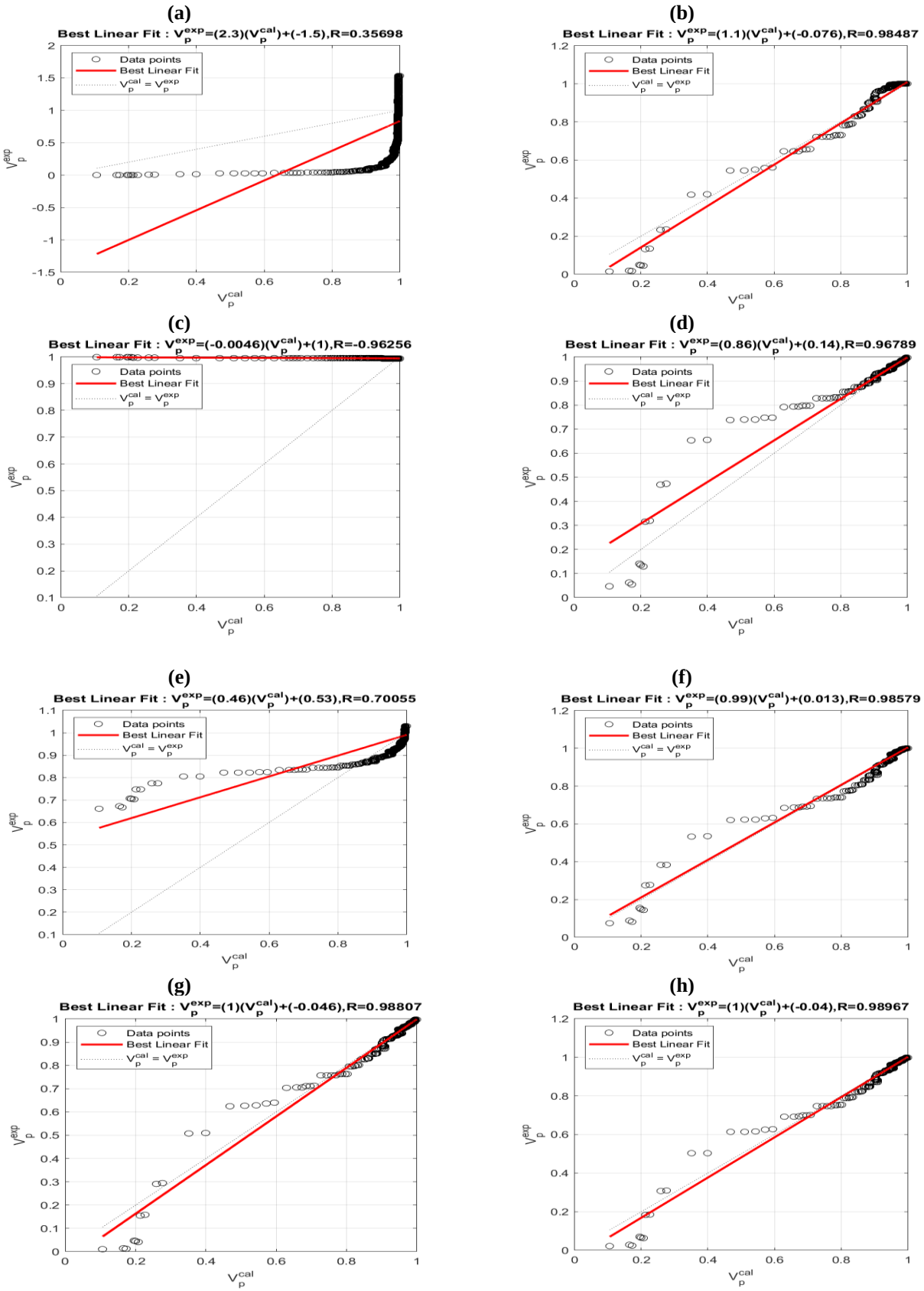


Figure 3.4. Scatter plot of the calculated values (V_P^{cal}), by the ODM and FDM, versus the experimental values (V_P^{exp}) of dimensionless cumulative volume for permeate: (a) O-PZO model, (b) O-PFO model, (c) O-PSO model, (d) O-PNO model, (e) F-PZO model, (f) F-PFO model, (g) F-PSO model, (h) F-PNO model.

3.1.3. Rejection compartment

3.1.3.1. Optimization of the kinetic constants of models

The optimized values of the kinetic constants (n, α, k_i and k_f) of ordinary and fractional dimensionless models for the calculated cumulative volume of rejection (V_R^{cal}) are shown in Table 3.5.

Table 3.5. The kinetic constants of ODM and FDM for the calculated cumulative volume of rejection (V_R^{cal}).

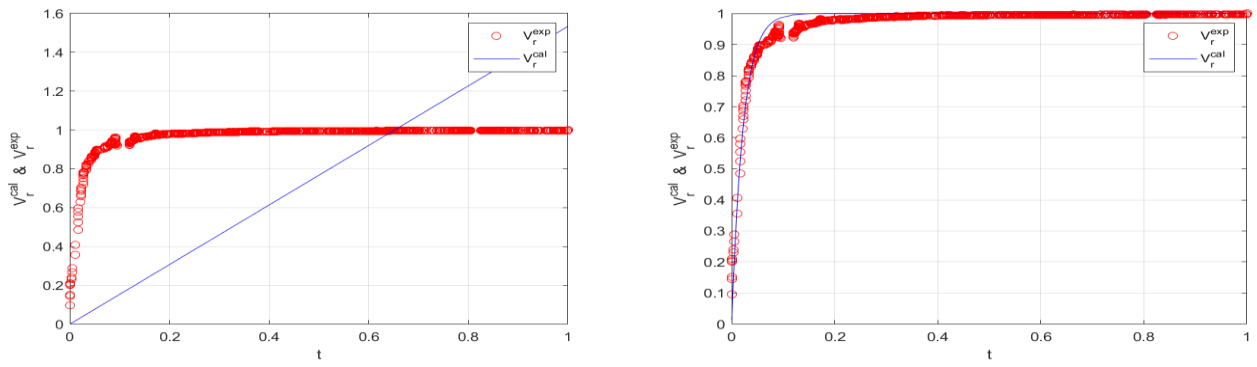
Classification	Kinetic constants									
	n(-)	*α (-)*	*k_0(-)*	*k_1(-)*	*k_2(-)*	*k_n(-)*	*k_{0f}(-)*	*k_{1f} (-)*	*k_{2f} (-)*	*k_{nf} (-)*
O-PZO	0	1	1.54	---	---	---	---	---	---	---
O-PFO	1	1	---	44.92	---	---	---	---	---	---
O-PSO	2	1	---		190.74		---	---	---	---
O-PNO	1.79	1	---	---	---	107.15	---	---	---	---
F-PZO	0	0.0577	---	---	---	---	1.00	---	---	---
F-PFO	1	0.5987	---	---	---	---	---	11.24	---	---
F-PSO	2	1.2166	---	---	---	---	---	---	270.09	---
F-PNO	1.50	0.9206	---	---	---	---	---	---	---	50.94

From the Table 3.5, it can be noted that the optimized values of the pseudo-orders *n* for the O-PNO and F-PNO models were close to 2 which its values were 1.79 and 1.50 respectively. Also, the optimized values of the fractional order *α*, of the F-PNO models, were ranging from 0.0557 to 1.2166. Table 3.5 shows that, for the FDM models, there is a proportionality between the fractional order values α [0.0557-1.2166] and the pseudo-order values n [0-2].

3.1.3.2. Calcul of dimensionless cumulative volume of rejection

Figure 3.5 present the calculated and the experimental values of dimensionless cumulative volume of rejection (V_R^{cal}, V_R^{exp}) plotted as function of the dimensionless filtration time (τ).

(a) **(b)**



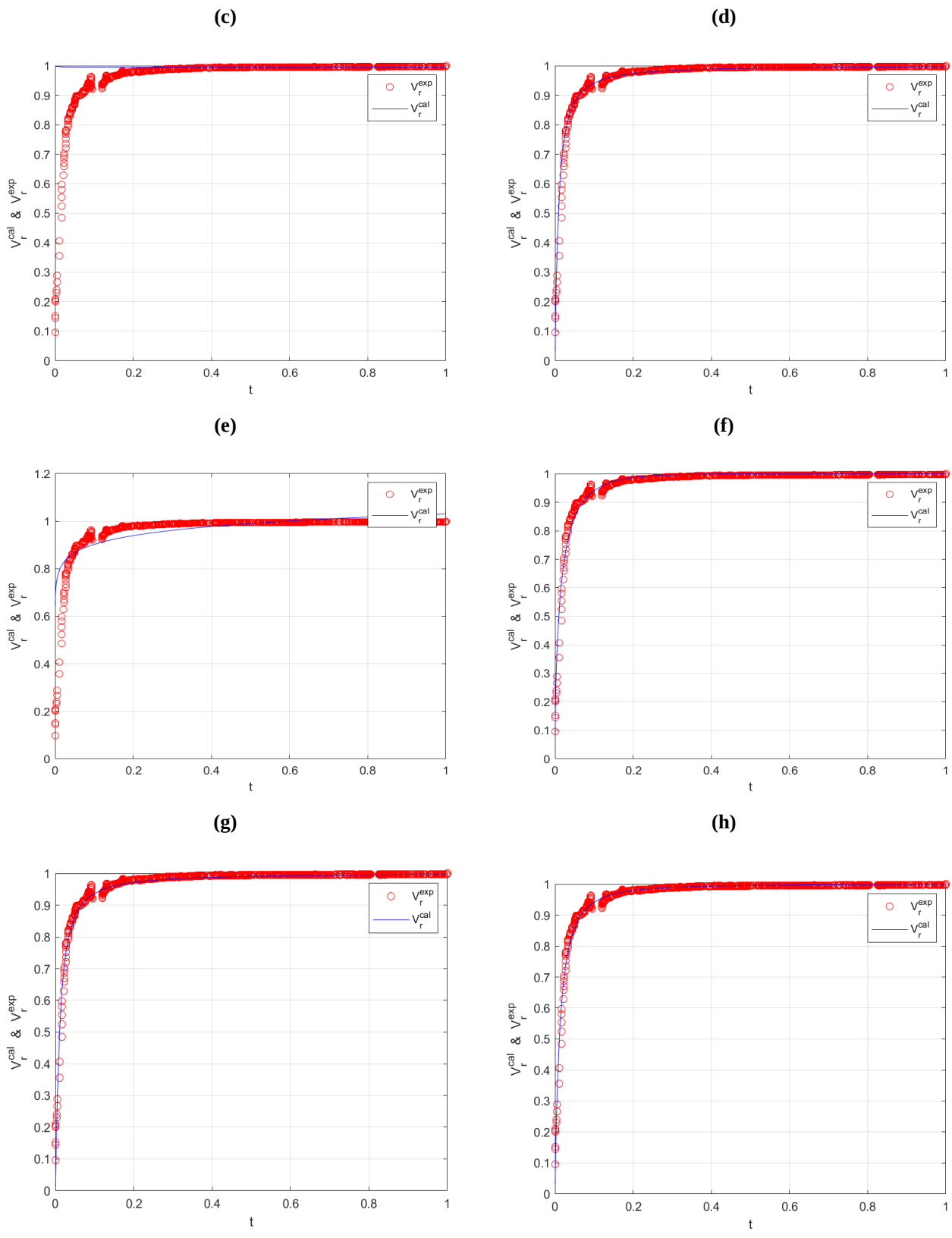


Figure 3.5. The calculated and the experimental values of dimensionless cumulative volume of rejection (V_R^{cal}, V_R^{exp}) plotted as function of dimensionless filtration time (τ): (a) O-PZO model, (b) O-PFO model, (c) O-PSO model, (d) O-PNO model, (e) F-PZO model, (f) F-PFO model, (g) F-PSO model, (h) F-PNO model.

Through a preliminary examination based on visual observation of the various graphical curves shown in Figure 3.5, it can be seen that the (a), (c) and (e) curves show a large divergence between the experimental and calculated values, while the (b) curve show a medium divergence, but the and (d), (f), (g) and (h) curves show convergence between the experimental and calculated values. To validate these initial observations and determine the best mathematical model capable of representing the experimental values, statistical criteria should be used.

3.1.2.3. Evaluation of the models accuracy by statistical criteria

The values of the statistical criteria (R^2, RMSE, AARD, MAE, SSR and SSE) those have been used to evaluate the ordinary and fractional dimensionless models of rejection are presented in Table 3.6.

Table 3.6. The statistical criteria of ODM and FDM for the calculated cumulative volume of rejection (V_R^{cal}).

Classification	Statistical criteria					
	R^2	RMSE	AARD	MAE	SSR	SSE
O-PZO	-44.5200	42.139	36.75	0.3538	99.072	454.584
O-PFO	0.9280	1.675	1.28	0.0103	10.174	0.719
O-PSO	-0.0524	6.408	3.13	0.0144	10.425	10.510
O-PNO	0.9671	1.133	0.62	0.0040	9.997	0.328
F-PZO	0.5212	4.322	3.34	0.0230	9.986	4.781
F-PFO	0.9705	1.072	0.78	0.0064	10.034	0.294
F-PSO	0.9718	1.047	0.73	0.0049	10.026	0.281
F-PNO	**0.9801**	**0.880**	**0.45**	**0.0026**	**9.998**	**0.198**

Based on the results presented in Table 3.6, it is evident that the fractional dimensionless models (FDM) gave the best values of statistical criteria, compared to the other ordinary dimensionless models (ODM).

This accuracy can be reflected with high value of R^2 (0.975) and with lowers values of RMSE (0.976), AARD (0.53), and MAE (0.0032) for the F-PNO model of rejection.

To determine the best linear regression, the experimental values are plotted against the calculated values by the ordinary and fractional models. Figure 3.6 (h) argue the previous results, such as the scatter plot of the calculated values, by the fractional model (F-PNO), versus the experimental values of the dimensionless cumulative volume for rejection were established the best regression.

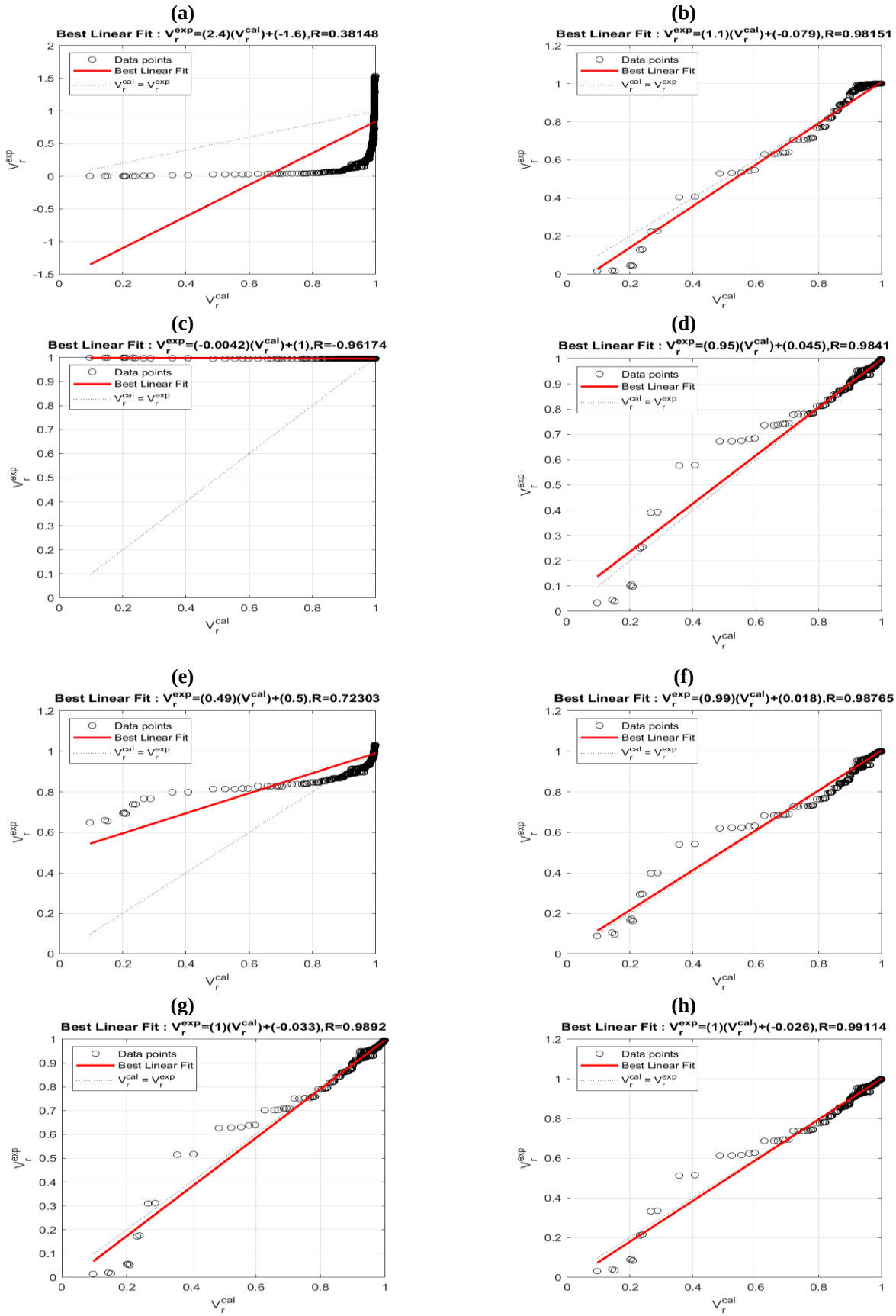


Figure 3.6. Scatter plot of the calculated values (V_R^{cal}), by the ODM and FDM, versus the experimental values (V_R^{exp}) of dimensionless cumulative volume for rejection: (a) O-PZO model, (b) O-PFO model, (c) O-PSO model, (d) O-PNO model, (e) F-PZO model, (f) F-PFO model, (g) F-PSO model, (h) F-PNO model.

3.2. Comparison between the fractional dimensionless models and others models

A comparison was established between the proposed fractional models (F-PNO) and other models in the literature (Table 3.7) according to the number and values of statistical criteria, the number of experimental data points and the number of compartments of the studied process, where several points were recorded.

In this study, three compartments were modeled (alimentation, permeate and rejection) while only one compartment was modeled for the others studies, which give comprehensiveness to this study.
Also, five statistical criteria (R^2, AARD, RSME SSR and SSE) were used in this study, in contrast, a maximum of two statistical criteria have been used in previous studies, which gives strength and robustness to the proposed models in this study.
In addition, the number of experimental points used in the previous studies to evaluate the model accuracy was very small compared to the experimental data used in this study (2561 points), which gives high accuracy to the fractional models proposed in this work.

From all these comparisons, it is obvious that this study conducted on fractional modelling of RO desalination process was based on solid foundations that enabled it to present the best and expressive models. Such as, the proposed fractional models (F-PNO) provide an accurate result and a perfect consistency to the experimental data, against the literature models, with an excellent R^2 values (0.9975, 0.9750, and 0.9801) and with lowers AARD, RMSE, SSR and SSE for the three compartments of RO process desalination: alimentation, permeate and rejection, respectively.

Table 3.7. Comparison between the proposed fractional dimensionless models (FDM) and others models in the literature.

Process	Application	Compartment	Type of membrane	Number of data points	Type of model	R^2	RMSE	AARD	MAE	SSR	SSE	Reference
RO	Treatment of Ground water	Alimentation	Polyamide (ROGA® - HR 8.5")	2561	F-PNO	0.9975	1.452	8.03	0.0109	214.158	0.540	This work
		Permeate	Polyamide (ROGA® - HR 8.5")	2561	F-PNO	0.9750	0.976	0.53	0.0032	9.786	0.244	
		Rejection	Polyamide (ROGA® - HR 8.5")	2561	F-PNO	0.9801	0.880	0.45	0.0026	9.998	0.198	
MF	Retention of organic compound	Retentate	Polycarbonate track-etched (PCTE)	< 15	Fractional pseudo n^{th} order	0,9989	0.0091	-----	0.0064	-----	-----	(Mesli *et al*., 2022)
NF/RO	Removal of NaCl from water	Permeate	PolyamideBW30LE400	<07	Complete pore blocking	0 ,9500	0,0270	-----	-----	-----	-----	(Bchiti *et al*., 2022)
			Polyamide (NF270)	<07	Complete pore blocking	0,9500	0,0250	-----	-----	-----	-----	
			Polyamide (NF90)	<07	Complete pore blocking	0,9600	0,0290	-----	-----	-----	-----	
MF	Retention of collagen protein	Retentate	High-density polyethylene	<20	Cake filtration intermediate blockage	0,9900	-----	-----	-----	1.913E-4	6.525E-4	(Heidari *et al*., 2021)
MF	Retention of organic molecules	Retentate	Polycarbonate track-etched	<15	Ordinary pseudo n^{th} order	0,9970	0.0171	-----	0.2141	-----	-----	(Adda et al., 2020)
NF/RO	Treatment of wastewater	Permeate	Aromatic polyamide composite	<60	Normalized intermediate blocking	0,9910	-----	-----	-----	-----	-----	(Tong *et al*., 2020)
MF	Retention of colloidal and organic compounds	Retentate	Micro-fluidic Mimic	<600	Complete pore blocking	0,9768	-----	-----	-----	-----	-----	(Debnath *et al*., 2019)
DF	Purification of several monoclonal antibodies compounds	Rejection	Cellulose (XOHC)	<500	Cake-adsorption fouling	0,8600	-----	-----	-----	-----	-----	(Goldrick *et al*., 2017)
MF	Separation of bovine serum albumin protein solution	Permeate	Polyethylene	<31	Cake filtration intermediate blocking	-----	-----	-----	-----	-----	1.9982	(Heidari *et al*., 2017)
MF	Separation of mixture Oil/Water	Permeate and Rejection	Polyvinylidene fluoride	<60	Intermediate blocking	0,9896	-----	-----	-----	-----	-----	(Fouladitajar *et al*., 2013)
				<60	Genetic programming	0,9999	-----	-----	-----	-----	-----	

Conclusion
&
Recommendation

Conclusion & Recommendation

The aim of this work was to study the usefulness of fractional modelling for the performance monitoring of water filtration system which is based on membrane separation technique. This study was considered as contribution to resolving the performance prediction problem, for water purification by a membrane, which it is affected by the various phenomena that have a memory effect. The results of this study will contribute to propose new models improving the design and efficiency of the filtration by membrane.

To achieve this objective, a comparative study has been established between fractional and ordinary modelling of matter transport for an industrial RO desalination unit to produce ultrapure water for pharmaceutical application. This contribution was devoted to establishing, from the pseudo-n^{th} order equation (PNO), ordinary and fractional dimensionless models to predict the cumulative volumes for the three compartments (feed, permeate and rejection) of the RO unit.

This study revealed valuable and promising results that are considered a beginning for developing successful membrane transport models for the monitoring performance of reverse osmosis desalination.
As such, a direct proportionality between the fractional order (α) values and the pseudo-order (n) values has been proven through the results obtained for the fractional models.
In addition, the fractional dimensionless models (FDM) with optimal kinetic constants (n, α, k_n and k_{nf}) provided an accurate result and a perfect consistency with the experimental data of the RO desalination process.
The statistical criteria were perfect with high values of R^2 (0.9975, 0.9750 and 0.9801) and with lower values of AARD (8.03, 0.53 and 0.45, RMSE (1.452, 0.976 and 0.880), MAE, SSR and SSE for alimentation, permeate and rejection, respectively.

The proposed fractional models were able to better predict the cumulative volumes of the three compartments of reverse osmosis desalination unit, which they will contribute to improve the performance monitoring.

Therefore, the fractional modelling can effectively serve as an alternative to classical (ordinary) modelling thanks to the fractional order of time (α). The fractional models can better represent the

anomalous kinetic, caused by the memory effect, of matter transport during reverse osmosis desalination process.

As a perspective to continue this study, we recommend to apply the fractional calculus approach with other mathematical models to give the best description of the experimental and the operational data for the RO desalination process.

References

References

- **Abel N.H. (1881)**. Solution de quelques problèmes á l'aide d'intégrales définies. In Oeuvres Complètes de Niels Henrik Abel; Sylow, L., Lie, S., Eds.; CUP: Cambridge, UK.
- **Abid M.F., Zablouk M.A., Abid-Alameer A.M. (2012)**. Experimental study of dye removal from industrial wastewater by membrane technologies of reverse osmosis and nanofiltration; Iranian Journal of Environmental Health Science & Engineering, 9(1), 17-17.
- **Adda A., Hanini S., Abbas M., Sediri M. (2020)**. Novel adsorption model of filtration process in polycarbonate track-etched membrane: Comparative study; Environmental Engineering Research, 25(4), 479-487.
- **Ahmed M.A., Amin S., Mohamed A.A. (2023)**. Fouling in reverse osmosis membranes: monitoring, characterization, mitigation strategies and future directions; Heliyon, 9, e14908.
- **Ahmed, F., Hashaikeh, R., Diabat, A., Hilal, N. (2019)**. Mathematical and optimization modelling in desalination: State-of-the-art and future direction; Desalination, 469, 114092.
- **Al-Bastaki N.M., Abbas A (1999).** Modeling an industrial reverse osmosis unit; Desalination, 126, 33-39.
- **Albo J., Hagiwara H., Yanagishita H., Ito K., Tsuru T. (2014)**. Structural characterization of thin-film polyamide reverse osmosis membranes, Ind. Eng. Chem. Res., 53, 1442-1451.
- **Al-Obaidi M.A., Alsarayreh A.A., Al-Hroub A.M., Alsadaie S., Mujtaba I.M (2018)**. Performance analysis of a medium-sized industrial reverse osmosis brackish water desalination plant, Desalination 443, 272–284.
- **Alsarayreh A.A., Al-Obaidi M.A., Al-Hroub A.M., Patel R., and Mujtaba I.M. (2020)**. Evaluation and minimization of energy consumption in a medium-scale reverse osmosis brackish water desalination plant, Journal of Cleaner Production, 248, 119220.
- **An D., Kim N.H., Choi J.H. (2015)**. Practical options for selecting data-driven or physics-based prognostics algorithms with reviews, Reliability Engineering & System Safety, 133, 223-236.
- **Anderson J.E., Hoffman 8.J., Peters, C.R. (1972)**. Factors influencing reverse osmosis rejection of organic solutes from aqueous solution, Journal of Physical Chemistry, 76 (26), 4006-4011.
- **Ang W.L., Mohammad A.W. (2015)**. 12 - Mathematical modeling of membrane operations for water treatment; Advances in Membrane Technologies for Water Treatment.

- **Annane K. (2015)**. Extraction et transport des ions de cadium (II) par membranes d'affinité dans des dispositifs microfluidiques ; Thèse de doctorat, Université de Mouloud Mammeri.Tizi-Ouzou. Algérie.
- **Antoniuk D., McCutchan J.W. (1973)**. Desalting Irrigation Field Drainage Water by Reverse Osmosis; Desalination Report No. 54, Firebaugh, California, UCLA-ENG-7368, California Water Resources Center, August.
- **Antony A., Low J.H., Gray S., Childress A.E., Le-Clech P., Leslie G. (2011)**. Scale formation and control in high pressure membrane water treatment systems: A review ; Journal of Membrane Science, 383, 1– 16.
- **Antony A., Low J.H., Gray S., Childress A.E., Le-Clech P., Leslie G. (2011)**. Scale formation and control in high pressure membrane water treatment systems: A review ; Journal of Membrane Science, 383, 1– 16.
- **Atangana A., Secer A. (2013).** A Note on Fractional Order Derivatives and Table of Fractional Derivatives of Some Special Functions, Hindawi Publishing Corporation Abstract and Applied Analysis, Article ID 279681, 8 pages.
- **Azizi A., Abouda L., Hanini S., Moussaoui M. (2022)**. Empirical correlation with dimensionless parameters for following the kinetic separation performance via reverse osmosis desalination process of groundwater, Global NEST Journal, 24(4), 638-661.
- **Baker R.W. (2004).** Membrane Technology and Applications, 2nd edition, John Wiley & Sons, Ltd.
- **Bchiti M., Igouzal M., El-Ghzizel S., El Midaoui A. (2022)**. Modeling pore blocking of nanofiltration and reverse osmosis membranes during NaCl removal, Bulgarian Chemical Communications, 54(3), 199-204.
- **Bechold H. (1907)**. Kolloidstudien mit der Filterationes-methode; Z. Physik. Chem., 60, 257-318.
- **Belhamiti O., Absar B. (2017)**. A numerical study of fractional order reverse osmosis desalination model using legendre wavelet approximation, Iranian Journal of Mathematical Chemistry, 8(4), 345-364.
- **Bhattacharyya D., Williams M. (1992).** Theory - Reverse Osmosis, in Membrane Handbook, W. Ho.
- **Blanchard G., Maunaye M., Martin G. (1984)**. Removal of heavy metals from waters by means of natural zeolites, Water Research, 18(12), 501-1507.
- **Boltzmann L. (1874)**. Theory of elastic after effect [Zur Theorie der elastischen Nachwirkung] Sitz. Kais. Akad. Wissenhaft Wien Math. Nat.;70:275–306.

- **Boltzmann L. (1876).** Theory of elastic after effect [Zur Theorie der elastischen Nachwirkung] [(accessed on 12 April 2021)]; Ann. Der Phys. Und Chem. Erganz. VII. 7:624–654.
- **Brousse C., Chapurlat R., Quentin J.P. (1976).** New membranes for reverse osmosis I. Characteristics of the base polymer: sulphonated polysulphones; Desalination, 18, 137–153.
- **Burghoff, H.G., Lee, K.L., Pusch, W. (1980).** Characterization of Transport Across Cellulose Acetate Membranes in the presence of strong solute-membrane interactions. Journal of Applied Polymer Science, 25, 323-347.
- **Cadotte J., Petersen R., Larson R., Erickson E. (1980).** A new thin-film composite seawater reverse osmosis membrane; Desalination, 32, 25–31.
- **Cannon C.R., Cantor P.A (1971)**. Mixed Esters of Cellulose; U.S. Patent Application, No. 3 (585),126-156.
- **Chamgoué A.C., Ngueuteu G.S.M., Yamapi R., Woafo P. (2018).** Memory effect in a self-sustained birhythmic biological system, Chaos, Solitons & Fractals 109, 160–169.
- **Chen Z., Ito K., Yanagishita H., Oshima N., Suzuki R., Kobayashi Y. (2011).** Correlation study between free-volume holes and molecular separations of composite membranes for reverse osmosis processes by means of variable-energy positron annihilation techniques, J. Phys. Chem. C, 115, 18055-18060.
- **Coker A.K. (1995).** Fortran Programs for Chemical Process Design, Analysis, and Simulation- CHAPTER 1 - Numerical Computation, 1-102, Gulf Publishing Company, Houston, Texas, USA.
- **Creber S.A., Vrouwenvelder J.S., van Loosdrecht M.C.M., Johns M.L. (2010).** Chemical cleaning of biofouling in reverse osmosis membranes evaluated using magnetic resonance imaging, Journal of Membrane Science, 362, 202-210.
- **Cunningham A.B., Lennox J.E., Ross R.J. (2011).** The Biofilms Hypertextbook: Introduction to Biofilms; Montana State University – Center for Biofilm Engineering, USA.
- **De Souza Matias G., Bissaro C.A., Matos Jorge L.M., Rossoni D.F. (2018).** The fractional calculus in studies on drying: A new kinetic semi-empirical model for drying, The Journal of Food Process Engineering, 42(1), e12955.
- **Debnath N., Kumar A., Thundat T., Sadrzadeh M. (2019).** Investigating fouling at the pore-scale using a microfluidic membrane mimic filtration system, Scientific Reports, 9, 10587.
- **Del Rio-Chanona E.A., Ahmed N.R., Wagner J., Lu Y., Zhang D., Jing K. (2019).** Comparison of physics-based and data-driven modelling techniques for dynamic

optimisation of fed-batch bioprocesses; Biotechnology and bioengineering; 116 (11), 2971-2982.

- **Dickson J.M. (1988).** Fundamentals Aspects of Reverse Osmosis. In B.S. Parekh (Ed.). Reverse Osmosis Technology- Applications for high-purity-water Production. New York: Marcel Dekker, Ch. 1, pp. 1-51.
- **Dimitriou E., Boutikos P., Mohamed E.S., Koziel S., Papadakis G. (2017).** Theoretical performance prediction of a reverse osmosis desalination membrane element under variable operating conditions, Desalination, 419, 70-78.
- **Du M., Wang Z., Hu, H. (2013).** Measuring memory with the order of fractional derivative; Sci Rep, 3, 3431.
- **Duke M.C., O'Brien-Abraham J., Milne N., Zhua B., Lin L.Y.S., Diniz da Costa J.C. (2009).** Seawater desalination performance of MFI type membranes made by secondary growth, Sep. Purif. Technol. 68, 343–350.
- **Dutrochet R.J.H. (1828)**. Nouvelles recherches sur l'endosmose et l'exosmose, suivies de l'application expérimentale de ces actions physiques à la solution du problème de l'irritabilité végétale et à la détermination de la cause de l'ascension des tiges et de la descente des racines ; libraire de l'académie royale de médecine.
- **Dytnerskii Yu. N., Polyakov G.V., Lukavyi L.S. (1972).** Tero. Osn. Khim. Tekhnol. (in Russian), 6 (4), 72.
- **Eisenman G. (1962).** Cation selective glass electrodes and their mode of operation, Biophysics Journal, 2, 259.
- **El-Gazar E.F., Zahra W.K., Hassan H., Rabia S.I. (2021).** Fractional modeling for enhancing the thermal performance of conventional solar still using hybrid nanofluid: energy and exergy analysis, Desalination, 503, 114847.
- **Feria-Díaz J.J., Correa-Mahecha F., López-Méndez M.C., Rodríguez-Miranda J.P, Barrera-Rojas J. (2021).** Recent desalination technologies by hybridization and integration with reverse osmosis: a review, Water, 13(10), 1369.
- **Fick A. (1855)**. Ueber Diffusion ; Annalen der Physik, 170(1), 59-86.
- **Flemming H.C., (1997)**. Reverse osmosis membrane biofouling; Experimental Thermal and Fluid Science, 14, 382-391.
- **Fouladitajar A., Ashtiani F. Z., Okhovat A., Dabir B. (2013).** Membrane fouling in microfiltration of oil-in-water emulsions, a comparison between constant pressure blocking laws and genetic programming (GP) model; Desalination, 329, 41-49.

- **Friesen V.C., Leitoles D.P., Gonçalves G., Lenzi E.K., Lenzi M.K. (2015).** Modeling heavy metal sorption kinetics using fractional calculus; Hindawi-Mathematical Problems in Engineering, 11, 1-8.
- **Fritzmann C., Löwenberg J., Wintgens T., Melin T. (2007).** State-of-the-art of reverse osmosis desalination; Desalination, 216(1-3), 1-76.
- **Gabelich C.J., Chen W.R., Yun T.I., Coffey B.M., "Mel" Suffet I.H. (2005).** The role of dissolved aluminum in silica chemistry for membrane processes; Desalination, 180, 307–319.
- **Glater J. (1998).** The early history of reverse osmosis membrane development; Desalination, 117, 297-309.
- **Goh P.S., Liang Y.Y., Ismail A.F. (2021).** Energy Efficient Seawater Desalination: Strategies and Opportunities; Energy Technol., 9, 2100008.
- **Goldrick S., Joseph A., Mollet M., Turner R., Gruber D., Farid S.S., Titchener-Hooker N.J. (2017).** Predicting performance of constant flow depth filtration using constant pressure filtration data; Journal of Membrane Sciences, 531, 138-147.
- **Gómez-Aguilar J.F., Razo-Hernández R., Granados-Lieberman D. (2014)**. A physical interpretation of fractional calculus in observables terms: analysis of the fractional time constant and the transitory response; Revista Mexicana de F´ısica 60, 32–38.
- **Graham T. (1854)**. The Bakerian lecture: on osmotic force; Phil. Trans. R. Soc. 144, 177-228.
- **Gu B., Adjiman C.S., Xu X.Y. (2021)**. Correlations for Concentration Polarization and Pressure Drop in Spacer-Filled RO Membrane Modules Based on CFD Simulations; Membranes, 11, 338.
- **Gupta A.K., Ray S.S. (2014).** Wavelet Methods for Solving Fractional Order Differential Equations; Hindawi Publishing Corporation Mathematical Problems in Engineering, Article ID 140453, 11 pages.
- **Hagihara H., Ito K., Oshima N., Yabuuchi A., Suda H., Yanagishita H. (2014).** Depth profiling of the free-volume holes in cellulose triacetate hollow-fiber membranes for reverse osmosis by means of variable-energy positron annihilation lifetime spectroscopy; Desalination, 344, 86-89.
- **Haluch V., Zanoelo E.F., Hermes C.J.L. (2017)**. Experimental evaluation and semi-empirical modeling of a small-capacity reverse osmosis desalination unit; Chemical Engineering Research and Design, 122, 243-253.

- **Hamlaoui M.L., Kherrat R., Marrakchi M., Jaffrezic-Renault N., Walcarius A. (2002).** Development of an ammonium ISFET sensor with a polymeric membrane including zeolite; Materials Science and Engineering, 21 (1-2), 25-28.
- **Hardy G.H., Littlewood J.E. (1928).** Some properties of fractional integrals I.; Math. Z., 27, 565–606.
- **Hardy G.H., Littlewood J.E. (1932).** Some properties of fractional integrals II.; Math. Z., 34, 403–439.
- **Hassler G.L. (1949)**. The seas as a source of freshwater; UCLA Department of Engineering, Research Report, University of California, Los Angeles, Los Angeles.
- **Hassler G.L. (1950)**. The use of molecular oil films in a pressure method for obtaining irrigation water from the sea; unpublished Report, August 1950, Gift to UCLA Engineering Library, July 1954, University of California, Los Angeles, Los Angeles.
- **Heidari S., Etemadi H., Yegani R. (2021).** A comprehensive analysis of membrane fouling in microfiltration of complex linear macromolecules based on theoretical modeling and FESEM images; Journal of Chemical Technology & Biotechnology, 96(2), 360-373.
- **Heidari S., Jafarzadeh Y., Samarin M. S., Yegani R. (2017).** Study on the fouling behavior of HDPE/PE-g-MA/EVA blend membrane fabricated via thermally induced phase separation method; Polyolefins Journal, 4(2), 235-251.
- **Henthorne L., Boysen B. (2015)**. State-of-the-art of reverse osmosis desalination pretreatment; Desalination, 356, 129-139.
- **Hermans P.H., Bredée H.L. (1935).** Zur kenntnis der filtrationsgesetze ; Recueil des Travaux Chimiques des Pays-Bas, 54(9), 680-700.
- **Hermia J. (1982).** Constant pressure blocking filtration laws; Institution of Chemical Engineers, 60, 183–187.
- **Ho C.C., Zydney A.L. (2000).** A combined pore blockage and cake filtration model for protein fouling during microfiltration; Journal of Colloid and Interface Science, 232(2), 389-399.
- **Hoang T., Stevens G., Kentish S. (2010).** The effect of feed pH on the performance of a reverse osmosis membrane; Desalination, 261, 99–103,
- **Hoek E.M.V., Allred J., Knoell T., Jeong B.H. (2008).** Modeling the effects of fouling on full-scale reverse osmosis processes; Journal of Membrane Science, 314, 33-49.
- **Horvath A.G. (1931).** Water softening; Unite States Patent Office, 1, 825, 631.
- **Ibrahim, G.P.S., Isloor, A. M., & Farnood, R. (2020).** Fundamentals and basics of reverse osmosis. Current Trends and Future Developments on (Bio-) Membranes, 141–163.

- **Jamal K., Khan M.A., Kamil M. (2004).** Mathematical modeling of reverse osmosis systems; Desalination, 160(1), 29-42.
- **Jeong S., Naidu G., Vollprecht R., Leiknes T.O., Vigneswaran S. (2016).** In-depth analyses of organic matters in a full-scale seawater desalination plant and an autopsy of reverse osmosis membrane; Separation and Purification Technology, 162, 171-179.
- **Jiang S., Li Y., Ladewig B.P. (2017).** A review of reverse osmosis membrane fouling and control strategies; Science of the Total Environment 595, 567–583.
- **Johnson J.S., McCutchan J.W., Bennion D.N. (1969).** Three and One-Half Years Experience with Reverse Osmosis at Coalinga, California, Report #69-45, UCLA School of Engineering and Applied Science, Los angeles, California, July.
- **Jonsson G. (1980).** Overview of theories for water and solute transport in UF/RO membranes; Desalination, 35, 21-38.
- **Jonsson G., Boesen, C. (1975).** Water and Solute Transport Through Cellulose Acetate Reverse Osmosis Membranes; Desalination, 17, 145.
- **Jouyban A., Chan H.K., Foster N.R. (2002).** Mathematical representation of solute solubility in supercritical carbon dioxide using empirical expressions ; The Journal of supercritical fluids, 24 (1), 19-35.
- **Ju Y., Hong S. (2014).** Nano-colloidal fouling mechanisms in seawater reverse osmosis process evaluated by cake resistance simulator-modified fouling index nanofiltration; Desalination, 343, 88-96.
- **Kahdim A.S., Ismail S., Jassim A. A. (2003).** Modeling of reverse osmosis systems; Desalination, 158, 323-329.
- **Kashchenko N.M., Nikitin M.A. (2014).** Simulation of anomalous-diffusion effects for drainage systems; Mathematical Models and Computer Simulations, 6, 337-341.
- **Kedem O., Katchalsky A. (1958).** Thermodynamic analysis of the permeability of biological membranes to non-electrolytes; Biochimica et Biophysica ACta, 27, 229-246.
- **Khalil R., Al Horani M., Yousef A., Sababheh M. (2014)**. A new definition of fractional derivative; Journal of Computational and Applied Mathematics, 264, 65–70.
- **Khorshidi B., Thundat T., Fleck B.A., Sadrzadeh M. A. (2016)**. Novel approach toward fabrication of high performance thin film composite polyamide membranes; Scientific Reports. 6, 22069.
- **Kim Y., Elimelech M., Shon H.K., Hong S. (2014).** Combined organic and colloidal fouling in forward osmosis: fouling reversibility and the role of applied pressure; Journal of Membrane Science, 460, 206-212.

- **Kim T.S., Park S.H., Park D., Lee J.H., Kang S. (2019).** Surface immobilization of chlorhexidine on a reverse osmosis membrane for in-situ biofouling control; Journal of Membrane Science, 576, 17–25.
- **King W.M., Cantor P.A., Schoellenback L.W., Cannon C.R. (1970).** High-retention reverse-osmosis desalination membranes from cellulose acetate, in: A.F. Turbak (Ed.), Membranes from Cellulose Derivatives, Inter science Publisher,New York.
- **Košuti´c K., Kaštelan-Kunst L., Kunst B. (2000).** Porosity of some commercial reverse osmosis and nanofiltration polyamide thin-film composite membranes; Journal of Membrane Science, 168, 101–108.
- **Kumano A. (2013).** Advances in Water Desalination, First Edition. Edited by Noam Lior. © John Wiley & Sons.
- **Kumar D., Singh J., Tanwar K., Baleanu D. (2019).** A new fractional exothermic reactions model having constant heat source in porous media with power, exponential and Mittag-Leffler laws; International Journal of Heat and Mass Transfer, 138, 1222-1227.
- **Lagergren S. (1898).** Zur Theorie der sogenannten Adsorption gelöster Stoffe, Bihang till Kongl; Svenskavetenskaps-akademiens handlingar, 24(4), 1-39.
- **Laurent H. (1884).** Sur le calcul des dérivées à indices quelconques ; Nouv. Ann. Mathématiques J. Des Candidats Aux Écoles Polytech. Norm., 3, 240–252.
- **Lee J. G., Ghaffour N. (2019).** Predicting the performance of large-scale forward osmosis module using spatial variation model: Effect of operating parameters including temperature; Desalination, 469, 114095.
- **Lee J.M., Ha J.H., Song I.H. (2017).** Enhanced fouling resistance of surface-modified alumina membranes by controlling humic acid and negatively charged-organosilane concentrations; Desalination Water Treatement, 88, 16–24.
- **Lee K.P., Arnot T.C., Mattia D. (2011)**. A review of reverse osmosis membrane materials for desalination—Development to date and future potential; Journal of Membrane Science, 370, 1–22.
- **Lee S., Elimelech M. (2006).** Relating organic fouling of reverse osmosis membranes to intermolecular adhesion forces; Environmental Science & Technology, 40(3), 980-987.
- **Lemus-Mondaca R., Nuñez H., Jaques A., Ramírez C., Simpson R. (2021).** The anomalous diffusion model based on a fractional calculus approach applied to describe the rehydration process of dried vegetal food matrices; The Journal of Food Process Engineering, 44(9), e13773.

- **Leyva-Ramos R., Rivera-Utrilla J., Medellin-Castillo N.A., Sanchez-Polo M. (2010).** Kinetic modeling of fluoride adsorption from aqueous solution onto bone char; Chemical Engineering Journal, 158, 458-467.
- **Li C., Chen A., Ye J. (2011).** Numerical approaches to fractional calculus and fractional ordinary differential equation; Journal of Computational Physics, 230, 3352–3368.
- **Ling B., Xie P., Ladner D., Battiato I. (2021).** Dynamic Modeling of Fouling in Reverse Osmosis Membranes; Membranes, 11, 349.
- **Liouville J. (1832).** Mémoire Sur quelques Questions de Géometrie et de Mécanique, et sur un nouveau genre de Calcul pour résoudre ces Questions ; J. L'École Polytech., 13, 1–69.
- **Lipp P., Gimbel R., Frimmel F.H. (1994).** Parameters influencing the rejection properties of FT30 membranes; Journal of Membrane Science, 95, 185–197.
- **Loeb S. (1966).** A composite tubular assembly for reverse osmosis desalination; Desalination, 1, 35–49.
- **Loeb S. and Sourirajan S., (1963)**. Sea Water Demineralization by Means of an Osmotic Membrane, in: Saline Water Conversion – I, Advances in Chemistry; American Chemical Society: Washington, DC, 117-132.
- **Loeb S., Selover E., (1967).** Sixteen months of field experience on the Coalinga pilot plant; Desalination, 2, 75-80.
- **Loeb S., Sourirajan S. (1964).** High Flow Porous Membranes for Separating Water from Saline Solutions; US Patent 3, 132-133.
- **Lonsdale H.K., Merten U., Riley R.L. (1965).** Transport properties of cellulose acetate osmotic membranes; J. Appl. Polym. Sci. 9 1341–1362.
- **Machado J.T., Kiryakova V., Mainardi F. (2011).** Recent history of fractional calculus, Commun Nonlinear Sci Numer Simulat, 16, 1140–1153.
- **Madaeni S.S. (2001).** The effect of surface characteristics on RO membrane performance; Desalination, 139 (1–3), 371.
- **Mahdad A., Laidi M., Hanini S., Hentabli M., Amrane A. (2021a).** A Grey wolf optimizer-based fractional calculus in studies on solar drying; Kemija u industriji, 70(1-2), 39-47.
- **Mahdad A., Laidi M., Hanini S., Hentabli M., Benhelal M. (2021b).** Modelling the drying kinetics of apple (Golab Variety): fractional calculus vs semi-empirical models; Kemija u industriji, 70(5-6), 251-262.
- **Matin A., Khan Z., Zaidi S.M.J., Boyce M.C., (2011).** Biofouling in reverse osmosis membranes for seawater desalination: phenomena and prevention; Desalination, 281, 1-16.

- **Matin A., Rahman, F., Shafi, H.Z., Zubair, S.M. (2019).** Scaling of reverse osmosis membranes used in water desalination: Phenomena, impact, and control; future directions; Desalination, 455, 135–157.
- **Matsuura T., Sourirajan S. (1981).** Reverse Osmosis Transport Through Capillary Pores Under the Influence of Surface Forces"; Industrial and Engineering Chemistry Process Design and Development, 20, 273-282.
- **Merten U., (1966).** Transport Properties of Osmotic Membranes", in Desalination by Reverse Osmosis; Merten, U. (ed),15-54, MIT Press, Cambridge, Mass.
- **Mesli C., Laidi M., Hanini S., Adda A., Moussaoui M., Hentabli M. (2022).** Fractional calculus-based modelling of membrane filtration; Kemija u Industriji, 71(1-2), 1-7.
- **Mirza I.A., Akram M.S., Shah N.A., Akhtar S., Muneer M. (2021).** Study of one dimensional contaminant transport in soils using fractional calculus; Mathematical Methods in the Applied Sciences, 44(8), 6839-6856.
- **Mohammad A.T., Al-Obaidi M.A., Hameed E.M., Basheer B.N., Mujtaba I.M. (2020).** Modelling the chlorophenol removal from wastewater via reverse osmosis process using a multilayer artificial neural network with genetic algorithm; Journal of Water Process Engineering, 33, 100993.
- **Morais W.A., de Almeida A.L.P., Pereira M.R., Fonseca J.L.C. (2008).** Equilibrium and kinetic analysis of methyl orange sorption on chitosan spheres; Carbohydrate Research, 343, 2489-2493.
- **Morais W.A., Fernandes A.L.P., Dantas T.N.C., Pereira M.R., Fonseca J.L.C. (2007).** Sorption studies of a model anionic dye on crosslinked chitosan, Colloids and Surfaces A: Physicochem; Eng. Aspects, 310, 20-31.
- **Myat D.T., Stewart M.B., Mergen M., Zhao O., Orbell J.D., Gray S. (2014)**. Experimental and computational investigations of the interactions between model organic compounds and subsequent membrane fouling; Water Research, 48, 108–118.
- **Nikan O., Machado J.A.T., Golbabai A., Nikazad T. (2020).** Numerical approach for modeling fractal mobile/immobile transport model in porous and fractured media; International Communications in Heat and Mass Transfer, 111, 104443.
- **Ning R.Y., Troyer T.L., Tominello R.S., (2005)**. Chemical control of colloidal fouling of reverse osmosis systems; Desalination, 172, 1-6.
- **Nollet J.A. (1748)**. Lecons de physique experimentale, Hippolyte-Louis Guerin and Louis-Francios Delatour, Paris.

- **Obembe A.D., Abu-Khamsin S.A., Hossain M.E., Mustapha K. (2018).** Analysis of subdiffusion in disordered and fractured media using a Grünwald-Letnikov fractional calculus model; Computational Geosciences, 22(5), 1231-1250.
- **Odabaşı Ç., Dologlu P., Gülmez F., Kuşoğlu G., Çağlar Ö. (2022).** Investigation of the factors affecting reverse osmosis membrane performance using machine-learning techniques; Computers & Chemical Engineering, 159, 107669.
- **Oldham K.B., Spanier J. (1974).** The Fractional Calculus: Theory and Application of Differentiation and Integration to Arbitrary Order, Dover Books on Mathematics, 234 pages, ISBN:978-0486450018 [in English].
- **Ozaki H., Sharma K., Saktaywin W. (2002).** Performance of an ultra-low-pressure reverse osmosis membrane (ULPROM) for separating heavy metal: effects of interference parameters; Desalination, 144, 287–294.
- **Padrino J.C. (2017).** On the self-similar, early-time, anomalous diffusion in random networks-Approach by fractional calculus; International Communications in Heat and Mass Transfer, 89, 134-138.
- **Pakhira R., Ghosh U., Sarkar S. (2018).** Study of Memory Effects in an Inventory Model Using Fractional Calculus; Applied Mathematical Sciences, 12(17), 797-824.
- **Park C., Kim H., Hong S., Choi S.I. (2006).** Variation and prediction of membrane fouling index under various feed water characteristics; Journal of Membrane Science, 284, 248-254.
- **Pfeffer W. (1877)**. Osmotische Untersuchungen: Studien Zur Zellmechanik. Verlag von Wilhelm Engelmann in Leipzig, Germany. Osmotic Investigations: Studies on Cell Mechanics, Van Nostrand Reinhold Company. New York (1985).
- **Piekutin J. (2021).** The Identification of Fouling in Reverse Osmosis in the Treatment of Water with Petroleum Substances; Water, 13, 1092.
- **Puti´c L., Alnouri S., Stijepovi´c V., Staji´c-Troši´c J., Gruji´c A., Stijepovi´c M. (2021).** A universal transportation model for reverse osmosis systems; Computers and Chemical Engineering, 148, 107264.
- **Qin J.J., Oo M.H., Coniglio B. (2005).** Relationship between feed pH and permeate pH in reverse osmosis with town water as feed; Desalination 177, 267-272.
- **Qrenawi L.I., Abuhabib A.A. (2020).** A review on sources, types, mechanisms, characteristics, impacts and control strategies of fouling in RO membrane systems; Desalination and Water Treatment, 208, 4369.
- **Rahaman M.S., Thérien-Aubin H., Ben-Sasson M., Ober C.K., Nielsen M., Elimelech M. (2014).** Control of biofouling on reverse osmosis polyamide membranes modified with

biocidal nanoparticles and antifouling polymer brushes; Journal of Materials Chemistry B, 2(12), 1724-1732.

- **Ramírez C., Astorga V., Nuñez H., Jaques A., Simpson R. (2017).** Anomalous diffusion based on fractional calculus approach applied to drying analysis of apple slices: The effects of relative humidity and temperature: The Journal of Food Process Engineering, 40(5), e12549.
- **Reid C.E. (1958)**. Osmotic membranes for demineralization of saline water; Proc. Symposium on saline water conversion, National Academy of Sciences, National Research Council and Office of Saline Research, Washington, D.C., 238
- **Reid C.E., Breton E.J. (1959).** Water and ion flow across cellulosic membranes; Journal of Applied Polymer Science, 1(2), 133-143.
- **Richter J.W., Hoehn H.H. (1971).** Permselective, aromatic, nitrogen-containing polymeric membranes. EI Du Pont de Nemours and Co., U.S. Patent 3, 567-632
- **Riemann B. (1876).** Versuch einer allgemeinen Auffassung der Integration und Differentiation. In Gessamelte Mathematische Werke; Dedekind, R., Weber, H., Eds.; Druck und Verlag: Leipzig, Germany.
- **Riley R.L., Lonsdale H.K., Lyons C.R., Merten U. (1967).** Preparation of ultrathin reverse osmosis membranes and the attainment of theoretical salt rejection; Journal of Applied Polymer Science, 11, 2143-2158.
- **Ross B. (1974).** Fractional Calculus and Its Applications: Proceedings of the International Conference held at the University of New Haven, June 1974 (Lecture Notes in Mathematics 457), 1975, 392 pages, ISBN-10:354007161X, ISBN-13:978-3540071617 [in English].
- **Ruth B.F., Montillar G.H., Montonna R.E. (1933).** Studies in filtration - I. Critical analysis of filtration theory; Industrial and Engineering Chemistry, 25(1), 76-82.
- **Samko S. G., Kilbas A.A., Marichev O.I. (1987).** Integrals and Derivatives of Fractional Order and Some of Their Applications, Nauka i Tekhnika, Minsk, 1987, 688 pages, with 1421 Refs., UDK 517.3 [In Russian].
- **Shao S.L., Fu W.W., Li X.J., Shi D.T., Jiang Y., Li J.Y., Gong T.J., Li X. (2019).** Membrane fouling by the aggregations formed from oppositely charged organic foulants; Water Research, 159, 95–101.
- **Sherwood T.K., Brian P.L.T., Fisher R.E. (1967).** Desalination by reverse osmosis; Ind. Eng. Chem. Fundam. 6, 2-12
- **Shields C. (1979).** Five year's experience with reverse osmosis systems using Du Pont "Permasep" permeators; Desalination, 28(3), 157–179.

- **Soleimani R., Dehaghani A.H.S., Shoushtari N.A., Yaghoubi P., Bahadori A. (2018).** Toward an intelligent approach for predicting surface tension of binary mixtures containing ionic liquids; Korean Journal of Chemical Engineering, 35(7), 1556-1569.
- **Solomatine D.P., Ostfeld A. (2008).** Data-driven modelling: some past experiences and new approaches; Journal of Hydroinformatics; 10(1), 3-22.
- **Soltanieh M., Gill W.N. (1981).** Review of reverse osmosis membranes and transport models. Chemical Engineering Communications, Vol. 12, pp. 279-363.
- **Sourirajan S. (1970).** Reverse Osmosis, New York: Academic Press.
- **Sourirajan S., Matsuura T. (1985).** Reverse Osmosis and Ultrafiltration Process Principles. Ottawa, Canada: National Research Council of Canada Publications.
- **Speight L.W., McCutchan J.W. (1979).** Reverse Osmosis Desalination Plant Design and System Optimization Based on the Facility at Firebaugh, California, UCLA-SEAS Report No. UCLA-ENG-7982, School of Engineering and Applied Science, Los Angeles, California.
- **Spiegler K.S., Kedem O. (1966).** Thermodynamics of hyperfiltration (RO): Criteria for efficient membranes; Desalination, 1, 311-326.
- **Subramani S., Panda R (2014).** Statistical regression and modelling analysis for reverse osmosis desalination process; Desalination, 351, 120–127.
- **Tang C.Y., Chong T.H., Fane A.G. (2011).** Colloidal interactions and fouling of NF and RO membranes: a review; Advance in. Colloid and Interface Science, 164,126-143.
- **Tarasov V.E. (2018).** Generalized Memory: Fractional Calculus Approach; Fractal and Fractional, 2(4), 23.
- **Tien C., Ramarao B.V., Yasarl R. (2014).** A blocking model for membrane filtration; Chemical Engineering Science, 111, 421-431.
- **Tong X., Wu Y.H., Wang Y.H., Bai Y., Zhao X.H., Luo L.W., Mao Y., Ikuno N., Hu H.Y. (2020).** Simulating and predicting the flux change of reverse osmosis membranes over time during wastewater reclamation caused by organic fouling; Environment International, 140, 105744.
- **Traube M. (1867)**. Experimente zur Theorie der Zellbildung und Endosmose. Arch. Anat. Physiol. Wiss. Med., 87-165.
- **Tseng R.L., Wu P.H., Wu F.C., Juang R.S. (2014).** A convenient method to determine kinetic parameters of adsorption processes by nonlinear regression of pseudo-nth-order equation; Chemical Engineering Journal, 237, 153-161.
- **Van de Lisdonk C.A.C., van Paassen J.A.M., Schippers J.C. (2000).** Monitoring scaling in nanofiltration and reverse osmosis membrane systems, Desalination, 132 101–108.

- **Van Wagner E.M., Sagle A.C., Sharma M.M., Freeman B.D. (2009).** Effect of cross-flow testing conditions, including feed pH and continuous feed filtration, on commercial reverse osmosis membrane performance; Journal of Membrane Science, 345, 97–109.
- **Van't Hoff J.H. (1887).** The role of osmotic pressure in the analogy between solutions and gases; Zeitschrift für physikalische Chemie, 1, 481-508.
- **Wang J., Armstrong M.D., Grzebyk K., Vickers R., Coronell O. (2021).** Effect of Feed Water pH on the Partitioning of Alkali Metal Salts from Aqueous Phase into the Polyamide Active Layers of Reverse Osmosis Membranes; Environmental Science & Technology, 55, 3250-3259.
- **Wang L., Cao T., Dykstra J.E., Porada S., Biesheuvel P. M., Elimelech M. (2021a)**. Salt and Water Transport in Reverse Osmosis Membranes: Beyond the Solution-Diffusion Model; Environmental Science & Technology, 55 (24), 16665-16675.
- **Wang Z.G., Cao J., Meng F.G. (2015).** Interactions between proteinlike and humic-like components in dissolved organic matter revealed by fluorescence quenching; Water Research, 68, 404–413.
- **Westmoreland, J.C. (1968)**. Spirally wrapped reverse osmosis membrane cell; US 3, 367-504.
- **Xie R.J., Tan E.K., Puah A.N. (2009).** Oxidation-reduction potential in saline water reverse osmosis membrane desalination and its potential use for system control; Desalination and Water Treatment, 3, 193–203.
- **Xu H., Xiao K., Yu J., Huang B., Wang X., Liang S., Wei C., Wen X., Huang X. (2020).** A Simple method to identify the dominant fouling mechanisms during membrane filtration based on piecewise multiple linear regressions; Membrane, 10(8), 171.
- **Yokoyama F., Nakajima M., Ichikawa S. (2022).** Analysis of Calcium Sulfate Scaling Phenomena on Reverse Osmosis Membranes by Scaling-Based Flux Model; Membranes, 12, 894.
- **Yu W., Yang Y., Graham N., (2016).** Evaluation of ferrate as a coagulant aid/oxidant pretreatment for mitigating submerged ultrafiltration membrane fouling in drinking water treatment; Chemical Engineering Journal, 298, 234–242.
- **Zarzo D., Prats D (2018).** Desalination and energy consumption. What can we expect in the near future?; Desalination, 427, 1-9.
- **Zhai S., Gui D., Huang P., Feng X. (2015).** A novel high-order ADI method for 3D fractional convection–diffusion equations; International Communications in Heat and Mass Transfer, 66, 212-217.

- **Zheng L.B., Yu D.W., Wang G., Yue Z.G., Zhang C., Wang Y.W., Zhang J.Y., Wang J., Liang G.L., Wei Y.S. (2018).** Characteristics and formation mechanism of membrane fouling in a full-scale RO wastewater reclamation process: membrane autopsy and fouling characterization; Journal of Membrane Science, 563, 843–856.
- **Özer A. (2007).** Removal of Pb(II) ions from aqueous solutions by sulphuric acid-treated wheat bran; Journal of Hazardous Materials, 141, 753-761.

Scientific production

Scientific production

Articles:

1. Azizi A., **Abouda L.**, Krika A., Krika F.; Removal of methylene blue from aqueous solutions with hybrid bioprocess: biosorption on modified cork powder and soluble turnip peroxidase; *Global NEST Journal*, Vol 24, No 2, pp 318-324, 2022.
2. Ahmed Azizi, **Lakhdar Abouda**, Hakima Cherifi, Abderrezak Krika, Fouad Krika; Enzymatic regeneration of modified cork with sodium dodecyl through the cationic dye removal from aqueous solution; *Desalination and Water Treatment*; 265, 157–163, 2022.
3. Azizi A., **Abouda L.**, Hanini S., and Moussaoui M.; Empirical correlation with dimensionless parameters for following the kinetic separation performance via reverse osmosis desalination process of groundwater; *Global NEST Journal*, Vol 24, No 4, pp 638-661, 2022.
4. **Abouda L.,** Azizi A., Hanini S., Moussaoui M., Cherifi H. and Laidi M.; Fractional modelling of the reverse osmosis process used for dam water desalination; *Global NEST Journal*, Vol 25, No 8, pp 17-26, 2023.

International communications:

1. Azizi Ahmed, **Abouda Lakhdar**, Hanini Salah, Neuronal networks for simulation and prediction the performance of cellulose acetate reverse osmosis membranes during groundwater desalination upstream of a pharmaceutical plant; *The first international seminar on material synthesis and environmental monitoring ISMSEM*; University of Ouargla; 2022.
2. **L. Abouda,** A. Azizi, S. Hanini, M. Moussaoui; Mathematical modelling of reverse osmosis process using differential equations; 2nd International Conference on the 'Evolution of Contemporary Mathematics and their Impact in Sciences and Technology'; University of Constantine; 2023.
3. **L. Abouda,** A. Azizi, S. Hanini and M. Moussaoui; Monitoring of reverse osmosis performance used for dam water desalination plant by empirical correlation with dimensionless parameters; International Conference on Sustainable Water Treatment Technologies and Environment SUST_WATER2023, UDES,Algeria, 27-28thNovember 2023.